Spring 5-15-2020

Effects of agonistic anti-CD137 antibody on chikungunya virus infection and B cell responses

Jun Hong
Washington University in St. Louis

WASHINGTON UNIVERSITY IN ST. LOUIS

Division of Biology and Biomedical Sciences

Immunology

Dissertation Examination Committee:
Michael S. Diamond, Chair
Paul M. Allen
Adrianus "Jacco" Boon
Anthony R. French
Deborah J. Lenschow

Effects of Agonistic Anti-CD137 Antibody on Chikungunya Virus Infection and B Cell

Responses

By

Jun Pyu Hong

A dissertation presented to
The Graduate School
of Washington University in
partial fulfillment of the
requirements for the degree
of Doctor of Philosophy

May 2020

St. Louis, Missouri

Table of Contents

List of figures

List of abbreviations

ACK	Ammonium-chloride-potassium
ANOVA	Analysis of variance
BCR	B cell receptor
Brdu	5-bromo-2'-deoxyuridine
CHIKV	Chikungunya virus
CR	Complement receptor
DC	Dendritic cell
DLN	Draining lymph node
DMEM	Dulbecco's modified Eagle's medium
DNA	Deoxyribonucleic acid
dpi	Days post-infection
ELISA	Enzyme-linked immunosorbent assay
FBS	Fetal bovine serum
FDC	Follicular dendritic cell
FFU	Focus forming units
GC	Germinal center
HA	Hemagglutinin
HEL	Hen egg lysozyme
IFN	Interferon
i.m.	Intramuscular
i.p.	Intraperitoneal
LLPC	Long-lived plasma cell
MAYV	Mayaro virus
MBC	Memory B cell
mAb	Monoclonal antibody
MZ	Marginal zone
NK	Natural killer cell
NKT	Natural killer T cell
NP	4-hydroxy-3-nitrophenylacetyl
OD	Optical density
PAMP	Pathogen associated molecular patterns
PBS	Phosphate-buffered saline
PFA	Paraformaldehyde
PFU	Plaque forming units
PNA	Peanut agglutinin
qRT-PCR	Quantitative reverse transcription polymerase chain reaction
RNA	Ribonucleic acid
scRNAseq	Single cell RNA sequencing
TD	T cell-dependent
Tfh	Follicular helper T cell
Tfr	Follicular regulatory T cell
TI	T cell-independent
VLP	Virus-like particle
WT	Wild-type

Jun Pyu Hong

Washington University in St. Louis

May 2020

ABSTRACT OF DISSERTATION

Effects of agonistic anti-CD137 antibody on chikungunya virus infection and B cell responses

By

Jun Pyu Hong

Doctor of Philosophy in Biology and Biomedical Sciences

(Immunology)

Washington University in St. Louis, 2020

Professor Michael Diamond, Chair

CD137, a member of the tumor necrosis factor receptor superfamily of cell surface proteins, acts as a costimulatory receptor on T cells, natural killer cells, B cell subsets, and some dendritic cells. Agonistic anti-CD137 monoclonal antibody (MAb) therapy has been combined with other chemotherapeutic agents in human cancer trials. Based on its ability to promote tumor clearance, we hypothesized that anti-CD137 MAb might activate immune responses and resolve chronic viral infections. We evaluated anti-CD137 MAb therapy in a mouse infection model of chikungunya virus (CHIKV), an alphavirus that causes chronic polyarthritis in humans and is associated with reservoirs of CHIKV RNA that are not cleared efficiently by adaptive immune responses. Analysis of viral tropism revealed that CHIKV RNA was present preferentially in splenic B cells and follicular dendritic cells during the persistent phase of infection, and animals lacking B cells did not develop persistent CHIKV infection in lymphoid tissue. Anti-CD137 MAb treatment resulted in T cell-dependent clearance of CHIKV RNA in lymphoid tissue, although this effect was not observed in musculoskeletal tissue. The clearance of CHIKV RNA from lymphoid tissue by anti-CD137 MAb was associated with reductions in the numbers of

germinal center B cells and follicular dendritic cells. Similar results were observed with anti-CD137 MAb treatment of mice infected with Mayaro virus, a related arthritogenic alphavirus. Thus, anti-CD137 MAb treatment promotes resolution of chronic alphavirus infection in lymphoid tissues by reducing the numbers of target cells for infection and persistence.

As a result of agonistic anti-CD137 MAb treatment, antibody responses to multiple T cell-dependent antigens including infectious virus, recombinant viral proteins, and conjugated haptens but not to a T cell-independent antigen or at homeostasis were impaired. These effects were not due to enhanced apoptosis or impaired proliferation of B cells but instead correlated with changes in lymphoid follicle structure and GC B cell dispersal, and were mediated by CD137 signaling in $CD4^+$ and $CD8^+$ T cells. Our experiments in mice suggest that agonistic anti-CD137 mAbs used in cancer and autoimmunity therapy may cause GC collapse and impair long-term antibody and B cell memory responses.

Chapter 1: Introduction

Introduction

Tumor Necrosis Factor Receptor Superfamily

The members of tumor necrosis factor receptor superfamily (TNFRSF) include proteins with extracellular cysteine-rich domains (CRD) and share high-level homology with the archetypical member, TNFR1. Most TNFRSFs are expressed in the immune cells, where their signaling plays crucial roles in proliferation and protective functions in immune cells in response to pathogens. In addition to their role in host defense, the role of TNFRSFs in organogenesis has also been identified (Bodmer et al., 2002; Botchkareva et al., 1999; Kong et al., 1999). The extracellular CRDs are involved in the formation of disulfide bonds and confer an elongated shape of the receptors, which is characterized by a twisted ladder of disulfide bridges (Bodmer et al., 2002). The cytoplasmic domains of TNFRSFs function as docking site for signaling adaptor proteins, of which two classes exist: TNF receptor-associated factors (TRAF) and "death domain" (DD) molecules. The selective binding of signaling adaptors via DD or TRAF binding motif of TNFRSFs trigger caspase activation and cell death or NF-κB and other cellular pathways, respectively.

Discovery of CD137 and its ligand

CD137, also called 4-1BB or TNFRS member 9 (TNFRSF9), is a costimulatory receptor on T cells, natural killer cells, B cell subsets, and some dendritic cells. cDNA of CD137 was cloned and sequenced in 1989 as an inducible gene from stimulated T cells (Kwon and Weissman, 1989). Murine CD137 encodes a polypeptide of 256 amino acids (30-kDa glycoprotein). The ligand for murine CD137 (CD137L), a 34-kDa type II membrane glycoprotein that has homology to TNF, was discovered by constructing soluble forms of CD137 (Goodwin et al.,

1993). CD137L is highly expressed on mature B and macrophage cell lines, activated B cells and dendritic cells (Pollok et al., 1994). CD137L also is inducible in T cells (Goodwin et al., 1993).

CD137-mediated signaling

Trimeric forms of CD137L interact with a trimeric form of CD137, facilitating its intracellular signaling pathway. The cytoplasmic domain of CD137 associates with TRAF 1, 2 and 3 at two TRAF-binding consensus sequences (Arch and Thompson, 1998; Jang et al., 1998; Saoulli et al., 1998; Ye et al., 1999). Three distinct CD137 signaling pathways have been reported: NF-κB-inducing kinase (Jang et al., 1998), p38 mitogen-activated protein kinase (Cannons et al., 2000) and c-Jun N-terminal kinase (Cannons et al., 1999). Anti-CD137 monoclonal antibody (mAb)-mediated crosslinking of cell-surface-expressed CD137 molecules triggers internalization into an unidentified endosomal compartment, of which name has been proposed to be "CD137 signalosomes," which could then recruit TRAF molecules (Melero et al., 2008).

Immunological consequences of CD137-mediated signaling

CD137 signaling induced by anti-CD137 mAb enhances proliferation of and interferon (IFN)-γ secretion by NK cells *in vitro*, whereas their cytolytic activity against NK-sensitive tumor cell lines remains unchanged, which suggests that anti-CD137 mAb-mediated signaling can selectively regulate immune functions of NK cells (Wilcox et al., 2002c). Anti-CD137 mAb-mediated signaling in activated monocytes increases the expression of TNF-α and IL-8 but decreases the expression of IL-10 at transcript level (Kienzle and von Kempis, 2000). CD137-stimulated monocytes may inhibit antibody responses by promoting B-cell apoptosis (Kienzle and von Kempis, 2000). DCs isolated from mice treated with anti-CD137 mAb can better induce proliferation of antigen-specific T cells when compared to DCs from mice treated with isotype

control mAb (Wilcox et al., 2002a). Anti-CD137 mAb-mediated signaling has been reported to promote apoptosis in neutrophils and eosinophils (Heinisch et al., 2001).

The importance of CD137 signaling in adaptive immune cells has been demonstrated in different disease animal models. Anti-CD137 mAb has been shown to enhance proliferation of and IFN-γ secretion by CD8$^+$ T cells in acute graft versus host disease (GVHD), cardiac and skin allograft rejection, and tumor rejection models (Melero et al., 1997; Shuford et al., 1997). CD137 stimulation enhances survival of T cells by inducing expression of anti-apoptotic proteins such as Bcl-X$_L$ (Starck et al., 2005). Anti-CD137 mAb treatment increases CD4$^+$ T cell-mediated GVHD (Blazar et al., 2001). CD137 stimulation reportedly abrogates the suppressive activities in Treg, although Treg from CD137$^{-/-}$ or WT mice suppress responder T cells to the same extent (Choi et al., 2004).

CD137-deficient mice: the role of CD137 in vivo

CD137$^{-/-}$ mice show no abnormality in the organs upon gross necropsy or histopathologic examination and no abnormality in B cell or T cell development (Kwon et al., 2002). The antibody responses to KLH or vesicular stomatitis virus are normal in these mice (Kwon et al., 2002). In acute viral infection models with some influenza viruses, CD137 signaling is dispensable for normal primary responses of CD8$^+$ T cells but is critical for maintenance of antigen-specific CD8$^+$ T cells and development of memory CD8$^+$ T cells (Bertram et al., 2002; Dawicki and Watts, 2004; Wang et al., 2009). It is worth noting that the CD137 requirement for optimal primary CD8$^+$ T cell responses may depend on different models (Wang et al., 2009). In contrast to previous reports on a positive costimulatory role of CD137 in CD4$^+$ and CD8$^+$ T cells, Lee et. al. show enhanced effector CD4 T cell responses to OVA with adjuvant in CD137$^{-/-}$ mice, although antibody responses are comparable to those in WT animals (Lee et al., 2005).

Adoptively transferred CD137$^{-/-}$ OT-II cells show early clonal expansion compared to WT OT-II cells in WT recipient hosts, and this is not due to intrinsically hyperresponsive properties of CD137$^{-/-}$ OT-II cells (Lee et al., 2005). How the lack of CD137 makes CD4$^+$ T cells hyperresponsive to a protein antigen *in vivo* is not clear. It is possible that CD137 may interact with another yet unidentified inhibitory ligand, similar to HVEM/LIGHT and HVEM/BTLA pairs. Transgenic CD4$^+$ T cells that are adoptively transferred into CD137L-deficient mice show minor defects in primary response but significantly impaired recall responses (Dawicki and Watts, 2004). CD137$^{-/-}$ mice cannot clear subcutaneously injected RMA-S cells, a NK cell-dependent MHCI-deficient tumor (Vinay et al., 2004). These mice have reduced numbers of spleen and liver NK and NKT cells (Vinay et al., 2004). Increased numbers of conventional DCs and plasmacytoid DCs were observed in the spleens of CD137$^{-/-}$ mice, compared to WT animals. CD137 may negatively regulate myelopoiesis by interacting with CD137L on myeloid progenitors and regulating their proliferation (Kwon et al., 2002; Lee et al., 2008). Moreover, CD137 may be required for M cell functional maturation in nasopharyngeal associated lymphoid tissue and Peyer's patch epithelium (Hsieh et al., 2010).

Anti-CD137 antibody as immunotherapy for cancer

CD137-mediated signaling is an intense focus of cancer therapy research. Although I focus on agonistic anti-CD137 mAb here, one of the active areas of research is also on chimeric antigen receptor (CAR) T cells, which are autologous T cells genetically modified to express CARs that consist of antigen-binding domain fused to transmembrane, costimulatory, and CD3ζ domains. One of the largest, promising CAR classes includes CD137 costimulatory domain (Li et al., 2018). The efficacy of anti-CD137 mAb as immunotherapy for cancer is studied as a monotherapy or a combined treatment with other antibodies and/or reagents.

As a monotherapy, anti-CD137 mAb shows efficacy in the murine models of hepatocellular carcinoma, lymphoma, some melanoma, thymoma, and lung, breast and prostate carcinoma (Fisher et al., 2012; Gauttier et al., 2014; Houot et al., 2009; Morales-Kastresana et al., 2013a; Narazaki et al., 2010; Shi and Siemann, 2006). The lymph node biopsies from untreated lymphoma patients show significant percentages of CD137-expressing cells among tumor-infiltrating T cells, suggesting that the target of anti-CD137 mAb is selectively expressed on cells with potential anti-tumor activities (Houot et al., 2009). The anti-CD137 mAb-mediated tumoricidal activities are mediated by NK cells and effector and memory CD8$^+$ T cells and may involve local reductions of myeloid-derived suppressor cells and Tregs in tumor microenvironments (Gauttier et al., 2014; Houot et al., 2009; Narazaki et al., 2010). In mice injected with EG7 lymphoma cells, both the perforin/granzyme and FasL play important roles in tumor rejection following anti-CD137 mAb treatment (Morales-Kastresana et al., 2013b). However, anti-CD137 mAb treatment has a minimal effect on poorly immunogenic tumor cells (Curran et al., 2011; Wei et al., 2013; Westwood et al., 2014).

Several therapies are being investigated combining anti-CD137 mAb with other immunomodulatory antibodies, tumor-targeting antibodies and/or non-antibody reagents that enhance cancer immunity. Immunomodulatory antibodies including anti-PD-1, anti-CTLA-4, anti-PD-L1, anti-OX40, anti-CD40, anti-TIM-3, and anti-CD4 mAb in combination with anti-CD137 mAb show at least some synergistic efficacy (Choi et al., 2007; Guo et al., 2013; Kocak et al., 2006; Morales-Kastresana et al., 2013b; Palazon et al., 2012; Wei et al., 2013; Westwood et al., 2014). Of note, not all combined treatments show synergistic efficacy. The therapeutic efficacy of anti-CD137 mAb is abrogated by anti-PD-1 mAbs in a spontaneous lymphoma model (McKee et al., 2017). Tumor-targeting antibodies that are being studied in combination with anti-

CD137 mAb include anti-epidermal growth factor receptor (cetuximab), anti-HER2 (trastuzumab), and anti-CD20 (rituximab) mAbs (Kohrt et al., 2014; Kohrt et al., 2011; Stagg et al., 2011). Rituximab coated on the lymphoma cells increases the expression of CD137 on NK cells, and subsequent stimulation of CD137 with targeting mAb enhances rituximab-dependent cytotoxicity against the tumor cells (Kohrt et al., 2011). Combinations of anti-CD137 mAb with different immunization strategies are also being investigated. Anti-CD137 mAb combined with tumor lysate-pulsed DC vaccine, hybrids of DC and syngeneic endothelial cells, irradiated tumor cells secreting granulocyte-macrophage colony-stimulating factor, irradiated tumor cells expressing fms-related tyrosine kinase 3 ligand (FVAX), or tumor cells expressing single-chain variable fragment against Herpes virus entry mediator receptor on the cell surface synergistically enhanced tumor regression (Curran et al., 2013; Ito et al., 2004; Ko et al., 2007; Park et al., 2012). In mice that are therapeutically vaccinated with FVAX, anti-CD137 mAb treatment enhances tumor rejection and elicits strong infiltration of KLRG1-expressing $CD4^+$ and $CD8^+$ T cells with a novel phenotype characterized by enhanced, multipotent cytotoxicity and driven by the T-box transcription factor Eomesodermin (Curran et al., 2013; Curran et al., 2011). Other strategies include combinations with proto-oncogen B-Raf inhibitor, IL-12 gene therapy, or oncolytic virus (John et al., 2012; Knight et al., 2013; Xu et al., 2004).

<u>Chikungunya virus</u>

Epidemiology and pathogenesis

Chikungunya virus (CHIKV) is a re-emerging, enveloped Alphavirus in the *Togaviridae* family of positive (+) sense RNA viruses and is transmitted by *Aedes* species mosquitoes. Since the first isolation of CHIKV in Tanzania in 1952 and subsequent outbreaks throughout Africa, India, Southeast Asia and Polynesia (Robinson, 1955; Staples et al., 2009), CHIKV emerged in the

Caribbean in 2013 and has spread throughout Central and South America, affecting more than 1.7 million people (Petersen and Powers, 2016). The symptoms of CHIKV infection include fever, rash, malaise, myalgia and polyarthritis (Simon et al., 2011). Although symptoms can resolve within a few weeks, 30% to 60% of individuals report persistent musculoskeletal pain months to years after initial diagnosis (Rodriguez-Morales et al., 2015; Rodriguez-Morales et al., 2016; Sissoko et al., 2009). Debilitating chronic arthralgia caused by CHIKV infection can result in a stooped and contorted posture, for which "chikungunya" is named in Makonde language.

One of the prospective cohort studies addresses the pathogenesis of CHIKV infection in 49 hospitalized patients from Reunion Island, who are followed from the first day of clinical acute infection until 12 months after infection (Hoarau et al., 2010). Both groups of individuals that eventually recover from acute infection and those who experience chronic relapsing arthralgia 12 months after infection show a strong immune response as demonstrated by a robust activation of DC, NK, $CD4^+$ and $CD8^+$ T cells but relatively weak Th1/Th2 cytokine responses during the acute phase of infection. However, only the individuals with chronic symptoms show increased levels of IFN-α mRNA and IL-12 in peripheral blood mononuclear cells (PBMC) and serum, respectively, for months compared to the individuals who recover. CHIKV RNA and protein have been detected in perivascular synovial macrophages in one chronic patient at 18 months after infection (Hoarau et al., 2010). Persistent viral RNA in cells may act as a pathogen-associated molecular pattern (PAMP) and contribute to CHIKV-induced inflammation and arthritis (Magnusson et al., 2006; McCarthy and Morrison, 2017; Zare et al., 2004).

Murine model of chikungunya virus pathogenesis

The most commonly used experimental animal models of CHIKV are mice and nonhuman primates. Here, I introduce only the murine model, but both the murine and nonhuman primate

models have their advantages for studying different aspects of CHIKV infection. Due to a lack of functional conservation between some mouse and human genes, there are cases where murine models do not fully recapitulate key aspects of human CHIKV disease such as maternal/neonatal transmission, enhanced CHIKV disease in elderly individuals and chronic disease pathogenesis. There are three different murine models of CHIKV: lethal neonatal challenge model, immunocompromised model of lethal disease and CHIKV arthritis/myositis model. Here, I use the third model and describe it in more details.

Tropism of chikungunya virus

In murine model of CHIKV, mice are inoculated subcutaneously in the footpad. During the acute phase of infection, CHIKV is readily detected in skeletal muscle cells, synovial fibroblasts, other nonhematopoietic and hemaotopoietic cells in mice (Hawman et al., 2013; Nair et al., 2017; Young et al., 2019). During the chronic phase, the reservoir of CHIKV in muscle and joint tissues is less clear, although experiments with a Cre recombinase CHIKV strain and reporter mice showed that fibroblasts and skeletal muscle cells harbored persistent viral RNA (Young et al., 2019). Even after infectious virus is cleared from the blood and within tissues, as judged by plaque- or focus-forming assays, CHIKV RNA can be detected in the ipsilateral and contralateral ankles of WT mice for at least 16 weeks after infection and in the spleens for 6 weeks after infection, as judged by quantitative reverse transcription-PCR (qRT-PCR) (Hawman et al., 2013). Viral tropism in lymphoid tissues is not clearly defined, although macrophages and monocytes are a reported reservoir of chronic CHIKV infection in mice and nonhuman primates (Labadie et al., 2010).

Immune responses and chikungunya virus pathogenesis in mice

CHIKV-infected mice exhibit a biphasic pattern of footpad swelling in the ipsilateral feet. The first peak of swelling occurs between 2 and 3 days post-infection (dpi) and is smaller than the second, which occurs between 6 and 7 dpi. The first peak is due to extensive viral replication in the footpad, resulting in cytokine production, tissue edema and some cellular infiltrates. Pattern recognition receptors (PRR) that recognize PAMPs induce type I IFN responses, which are necessary to prevent lethality (Couderc et al., 2008; Schilte et al., 2012). Signaling via PRRs and IFN receptors promotes secretion of pro-inflammatory cytokines, which recruit innate and adaptive immune cells to the site of infection. Macrophages and inflammatory monocytes may have both protective and pathogenic roles in CHIKV disease. Depletion of macrophages using clodronate treatment reduces foot swelling (Gardner et al., 2010), while $CCR2^{-/-}$ mice, which lack monocyte/macrophage infiltration, show enhanced foot swelling and neutrophil-dominated inflammation (Poo et al., 2014a). Depletion of macrophages also increases viremia, suggesting that macrophages promote inflammation while aiding in clearance of virus (Gardner et al., 2010). In mutant mice lacking γδ T cells, which are the most abundant T lymphocytes in the skin and mucosal surfaces, increased numbers of infiltrating inflammatory monocytes at the site of CHIKV infection exacerbate foot swelling and tissue damage (Long et al., 2016). Replication of CHKV in bone reportedly causes osteoclastogenesis and bone loss (Chen et al., 2015).

The second peak of foot swelling is driven by immune-mediated responses and damage associated with the influx of inflammatory cells into the joint and surrounding tissue. Antibody responses are critical in controlling CHIKV infection (Hawman et al., 2016; Hawman et al., 2013; Poo et al., 2014b). Genetic or acquired deficiency of CD4^{+} T cells or MHC class II molecules result in reduced foot swelling without significant effect on viremia (Poo et al., 2014b; Teo et al., 2013). In contrast, genetic or acquired deficiency of CD8^{+} T cells did not affect foot

swelling or viremia (Teo et al., 2013). The minimal role that CD8^{+} T cells seem to have during CHIKV infection warrants further studies. CHIKV-neutralizing antibodies protect mice from persistent viremia and exacerbated inflammation in the feet, as demonstrated by B cell-deficient mice and adoptive transfer of exogenous CHIKV-neutralizing antibodies to Rag1^{-/-} mice (Hawman et al., 2013; Poo et al., 2014b).

B cell response

Depending on the nature of antigens, either T-dependent (TD) or T-independent (TI) B cell response can occur. Antigens of low valency trigger initial cell cycle progression in activated B cells, which then rapidly proliferate in response to cognate T cell-derived signals. For certain antigens, strong signaling via co-receptors such as toll-like receptors (TI type I response) or high degree of multivalency of antigens (TI type II response) can overcome the need for T cell help and result in cell division and subsequent differentiation.

Germinal center reaction

During TD B cell response, encounter of antigen-engaged B cells with cognate T cells is facilitated by upregulation of CCR7 and EBI2 and downregulation of S1PR1 on the B cells and their migration to the interface of the B cell follicle and the T cell zone (Cyster et al., 2014). After T cell help initiates germinal center (GC) formation, the maintenance of GC is regulated by ongoing B-T interactions via ICOSL/ICOS, CD40/CD40L, SLAM and PD-L1/PD-1 (Cannons et al., 2011; Shi et al., 2018). GCs in lymphoid tissues are complex anatomical sites where somatic hypermutation (SHM) and antibody isotype switching, or class-switch recombination (CSR), occurs. GC B cells proliferate extensively and traffic through the light and dark zones as part of an antigen-driven affinity-based clonal selection process (reviewed in (Mesin et al., 2016)). In the light zone, GC B cells recognize cognate antigens and undergo selection with the cytokine-

directed input of follicular helper T cells (Tfh), which themselves are modulated by follicular regulatory T cells (Tfr) (Linterman et al., 2011). GC B cell confinement is mediated by the migration inhibitory receptors S1PR2 and P2RY8 (in human), which signal through heterotrimeric G-proteins containing Gα13 (Muppidi et al., 2014). S1PR2 is uniquely expressed by GC B cells and controls the size of chronic GCs (Green et al., 2011). The ligand for S1PR2 and four other S1PRs is sphingosine-1-phosphate (S1P), which is a metabolic intermediate made by all eukaryotic cell types during sphingolipid metabolism aided by the action of sphingosine kinase 1 and 2 and secreted by some cell type (Schwab and Cyster, 2007). The GC confinement of Tfh may also be mediated by S1PR2 and further augmented by their CXCR5 expression (Moriyama et al., 2014). Early localization of activated T cells at the interface of the B cell-follicle and T zone is guided by EBI2 on T cells, similar to the role of EBI2 on early-activated B cells (Li et al., 2016). Production of its ligand 7α,25-dihydroxycholesterol (7α,25-OHC) by CH25H and CYP7B1 in lymphoid stromal cells may be important to establish 7α,25-OHC gradient required for B cell responses (Yi et al., 2012). EBI2 on T cells guides their localization near CD25-expressing DCs, which may promote distinct cell fate decisions dependent on IL-2 availability (Li et al., 2016). GC B cells without strong affinity for antigens or without T cell help undergo apoptosis. CD40-mediated signaling not only is important for GC maintenance but also influences the fate decisions of GC B cells. The GC reaction culminates in the generation of memory B cells and plasma cells, the latter of which are professional antibody-secreting cells. Some memory B cells and early short-lived plasma cells develop independently of GC (Nutt et al., 2015; Toyama et al., 2002).

Fate decisions in germinal center

Although the exact mechanism of GC B cell fate decisions is not clear, the strength of CD40-mediated signaling seems to be an important factor; the strong CD40 signal leads to plasma cell differentiation, while the weaker CD40 signal leads to memory B cell differentiation or recycling GC cell fate (Ise et al., 2018; Koike et al., 2019). The B cells expressing higher-affinity B cell receptor (BCR) can acquire greater amount of antigen for presentation to Tfh (Victora et al., 2010). Thus, high-affinity GC B cells with greater extent of affinity maturation are selected into the plasma cell compartment, while memory B cell differentiation has more permissive affinity requirements (Phan et al., 2006; Smith et al., 1997). IL-4 and IL-21 secreted by Tfh promote B cell proliferation, CSR, and differentiation into plasma cells or GC B cells (Moens and Tangye, 2014; Vinuesa et al., 2016). BCR signal by engagement of antigens presented by follicular dendritic cells (FDC) as well as CD40 and cytokine receptor signal are integrated in GC B cells to influence their fate decisions, and these signaling pathways seem to be rewired in GC B cells (Luo et al., 2018). It is possible that a small difference in CD40 signal as determined by the extent of T cell contact results in both quantitative and qualitative difference in signaling in GC B cells.

Transcription factors define the identity of a particular cell population. A sequential transition from one stage of cell differentiation state to another, e.g. from naïve B cells to plasma cells, is induced by dynamic regulation of transcription factors. In B cells, Pax5 and Blimp-1 mutually repress each other, forming a double-negative feedback loop, or a toggle switch-like gene regulatory network (Gardner et al., 2000). Pax5 defines B-cell identity from early progenitor B cells to mature B cells. However, expression of almost half of the genes induced by Pax5 is absent or reduced in plasma cells, which do not express Pax5 (Schebesta et al., 2007). Instead, expression of Blimp-1 and Irf4 is increased, which promotes plasma cell status. The

transcriptional program of GC B cells is regulated by their master transcription factor Bcl6. Transcription factors involved in development, activation, maturation, and differentiation of B cells, such as NF-κB, Irf4, Mef2c, Myc, E2A, Ebf1, Obf-1, and Bach2, as well as a Rho-Rac guanine-exchange factor Dock8 are critical in GC initiation and/or maintenance (De Silva and Klein, 2015). Particularly, Bach2, which is downstream of Pax5, can interact with Bcl6 and repress Blimp-1 expression and plasma cell differentiation (Ochiai et al., 2008). SHM is compromised in Bcl6$^{-/-}$ mice, but class-switched memory B cells can still form in these animals in the absence of germinal centers (Toyama et al., 2002). However, both SHM and CSR are abrogated in Bach2$^{-/-}$ mice, raising the question on the role of Bach2 for CSR (Muto et al., 2004). A delay-driven diversity model has been proposed, postulating that Bach2 achieves a time delay in Blimp-1 induction, which inhibits plasma cell differentiation while allowing induction of AID by Pax5 and, therefore, CSR (Muto et al., 2010).

Marginal zone B cells

Lymphoid tissues contain follicular B cells and marginal zone (MZ) B cells, the latter of which express polyreactive BCR, produce natural IgM and IgG antibodies, and protect against blood-borne bacterial infection in a T cell-independent manner (Cerutti et al., 2013; Tanigaki et al., 2002). Several studies have provided some insights into follicular versus MZ B cell fate decision. Transitional T1 B cells enter the spleen and further mature into AA4.1^{+}, recirculating T2 B cells, which express high levels of IgD and CD23 and intermediate levels of CD21 (Allman et al., 2001). Initially dependent only on tonic BCR signals via self-antigens for survival, transitional B cells eventually require both tonic BCR signals and BAFF-mediated survival signals (Cancro, 2009). BAFFR can activate both the canonical and non-canonical NF-κB pathways (Siebenlist et al., 2005). The non-canonical NF-κB pathways through IKKα-mediated targeting of p100 for

cleavage to produce p52, or NF-κB2, support B-cell survival functions mediated by BAFF from transitional to mature B cell stage (Senftleben et al., 2001). In addition to the non-canonical NF-κB pathways, the development of MZ B cells, but not follicular B cells, requires the canonical NF-κB pathways through p50, which can complex with both c-Rel and RelA in B cells (Cariappa et al., 2000). MZ B cells also require the signals mediated by Notch through its ligand DL1, which is expressed mainly on the luminal face of venules in the red pulp of the spleen and some in the marginal zone (Tan et al., 2009). Based on some experiments involving mice with the mutations in or the lack of molecules regulating BCR signaling such as Aiolos, Btk, CD21, CD22 or Igα, the strength of BCR signaling may influence MZ versus follicular B cell development, with weak BCR signaling inducing MZ B cell development and relatively strong BCR signaling follicular B cell development (Cariappa et al., 2001; Kraus et al., 2001; Samardzic et al., 2002). Receptors such as S1PR1 as well as integrins, including LFA1 and α4β1 on MZ B cells, which bind to ICAM1 and VCAM1, respectively, expressed on MZ stromal cells, facilitate the migration and retention of MZ B cells and may also contribute to their maturation and survival (Cinamon et al., 2008; Lu and Cyster, 2002).

Chapter 2: Clearance of Chikungunya virus infection in lymphoid tissues is promoted by treatment with an agonistic anti-CD137 antibody

ABSTRACT

CD137, a member of the tumor necrosis factor receptor superfamily of cell surface proteins, acts as a costimulatory receptor on T cells, natural killer cells, B cell subsets, and some dendritic cells. Agonistic anti-CD137 monoclonal antibody (mAb) therapy has been combined with other chemotherapeutic agents in human cancer trials. Based on its ability to promote tumor clearance, we hypothesized that anti-CD137 mAb might activate immune responses and resolve chronic viral infections. We evaluated anti-CD137 mAb therapy in a mouse infection model of chikungunya virus (CHIKV), an alphavirus that causes chronic polyarthritis in humans, and is associated with reservoirs of CHIKV RNA that are not cleared efficiently by adaptive immune responses. Analysis of viral tropism revealed that CHIKV RNA preferentially was present in splenic B cells and follicular dendritic cells during the persistent phase of infection, and animals lacking B cells did not develop persistent CHIKV infection in lymphoid tissue. Anti-CD137 mAb treatment resulted in a T cell-dependent clearance of CHIKV RNA in lymphoid tissue, although this effect was not observed in musculoskeletal tissue. The clearance of CHIKV RNA from lymphoid tissue by anti-CD137 mAb was associated with reductions in numbers of germinal center B cells and follicular dendritic cells. Similar results were observed with anti-CD137 mAb treatment of mice infected with Mayaro virus (MAYV), a related arthritogenic alphavirus. Thus, anti-CD137 mAb treatment promotes resolution of chronic alphavirus infection in lymphoid tissues by reducing the number of target cells for infection and persistence.

INTRODUCTION

Targeting of CD137 with agonistic monoclonal antibody (mAb) enhances spontaneous and Ab-dependent cell-mediated cytotoxicity by natural killer (NK) cells and proliferation and survival of $CD8^+$ T cells. Anti-CD137 mAb also enhances antigen presentation by promoting costimulatory activity of dendritic cells (DCs) and by inhibiting the functions of regulatory T cells (Tregs) (Yonezawa et al., 2015). Based on preclinical studies demonstrating anti-CD137 mAb as a promising cancer immunotherapy (Cuadros et al., 2005; Ito et al., 2004; Lee et al., 2011; Lee et al., 2004; Wei et al., 2013), clinical trials in humans that combine anti-CD137 mAb with conventional chemotherapies have been initiated for the treatment of metastatic solid tumors, non-small cell lung cancer, melanoma, non-Hodgkin's B cell lymphoma, colorectal cancer, and multiple myeloma (Yonezawa et al., 2015).

Chikungunya virus (CHIKV) is a re-emerging alphavirus of the *Togaviridae* family and is transmitted by *Aedes* species mosquitoes. CHIKV was first isolated in Tanzania in 1952 and historically caused infections in Africa and Asia (Staples et al., 2009). In 2013, CHIKV spread into South and Central America, and an epidemic caused over 1.8 million infections including cases in the United States (Petersen and Powers, 2016). Infected individuals present with fever, rash, malaise, myalgia and polyarthritis (Simon et al., 2011). Although symptoms can resolve within a few weeks, 30 to 60% of individuals report persistent musculoskeletal pain months to years after initial diagnosis (Rodriguez-Morales et al., 2015; Rodriguez-Morales et al., 2016; Sissoko et al., 2009). Indeed, CHIKV RNA and protein have been detected in perivascular synovial macrophages at 18 months after infection (Hoarau et al., 2010). Persistent viral RNA in cells may act as a pathogen-associated molecular pattern (PAMP) and contribute to CHIKV-

induced inflammation and arthritis (Magnusson et al., 2006; McCarthy and Morrison, 2017; Zare et al., 2004).

In murine models of CHIKV, infectious virus is cleared from the blood and most tissues by 7 days post-infection (dpi). However, CHIKV RNA can be detected in musculoskeletal tissues, the spleen, and lymph nodes of immunocompetent mice for months (Hawman et al., 2013). Although combinations of anti-CHIKV monoclonal antibody with CTLA4-Ig, an immunomodulatory drug, controlled CHIKV arthritis in mice (Miner et al., 2017), neither antiviral antibody alone nor in combination with CTLA4-Ig cleared CHIKV RNA from sites of persistence when administered after infection. Based on studies in cancer models, we hypothesized that an agonistic anti-CD137 mAb could activate immune responses that resolve chronic viral infections. Here, we evaluated the activity of anti-CD137 mAb in a model of CHIKV arthritis in immunocompetent C57BL/6 mice. Treatment with an agonistic anti-CD137 mAb promoted clearance of persistent CHIKV RNA in the spleen and draining lymph node (DLN), and this effect required the presence of $CD4^+$ and $CD8^+$ T cells. However, clearance was not observed in musculoskeletal tissues. Viral RNA tropism studies revealed that B cells and follicular dendritic cells (FDCs) harbored much of the CHIKV RNA in lymphoid tissues. Unexpectedly, anti-CD137 mAb treatment resulted in reduced numbers of germinal center B cells and FDCs compared with isotype control mAb-treated animals. Thus, anti-CD137 mAb treatment cleared viral RNA in the spleen through either direct killing or indirect effects by T cells. As similar results were seen in mice with a second emerging alphavirus, Mayaro virus (MAYV), anti-CD137 mAb treatment resolves chronic alphavirus infection in lymphoid tissues by reducing the number of germinal center B cells and FDCs, which are the primary viral reservoirs in these tissues.

MATERIALS AND METHODS

Viruses and cells. A recombinant CHIKV La Reunion OPY1 strain was provided by S. Higgs (Kansas State University) and generated from *in vitro* transcribed cDNA as described (Tsetsarkin et al., 2006). The resultant virus was propagated once in C6/36 *Aedes albopictus* cells and titrated using Vero cells as described (Pal et al., 2013). CHIKV SL15649 was generated in BHK21 cells from *in vitro* transcribed cDNA as described (Morrison et al., 2011). The MAYV BeH407 strain was provided by the World Reference Center for Arboviruses (S. Weaver, K. Plante, and R. Tesh) and propagated in Vero cells.

Animal studies. All animal experiments were performed in accordance and with approval of Washington University and University of Colorado School of Medicine Institutional Animal Care and Use Committee guidelines. C57BL/6J (catalog# 000664), B6.129S2-Ighm^{tm1Cgn}/J (catalog# 002288; abbreviated mMT) and B6.129P2-Tcrb^{tm1Mom} Tcrd^{tm1Mom}/J (catalog# 002121; abbreviated TCRbd$^{-/-}$) were purchased from Jackson Laboratories. CD137$^{-/-}$ mice (Kwon et al., 2002) were obtained as a gift from Michael Croft (La Jolla Institute for Immunology). MD4 mice (Mason et al., 1992) in a mMT B cell-deficient genetic background were generated at the University of Colorado by crossing the MD4 transgene (Jackson Laboratories; catalog# 002595) onto the mMT B cell-deficient background. At 4 weeks of age, male mice anesthesized with ketamine hydrochloride (80 mg/kg) and xylazine (15 mg/kg) were inoculated subcutaneously in the left rear footpad with 10^3 focus-forming units (FFU) of CHIKV or MAYV in 10 ml of PBS. Foot swelling was measured daily with digital calipers (54-100-004-2, Fowler). At the termination of experiments, mice were euthanized and perfused via intracardiac injection with PBS. Tissues were harvested and stored at -80°C.

Quantitative reverse transcription PCR (qRT-PCR). Viral RNA was extracted from tissue homogenates using the RNeasy Mini Kit (74182, Qiagen). To extract viral RNA from paraformaldehyde (PFA) fixed cells, the RNeasy kit for purification of total RNA from formalin-fixed, paraffin-embedded tissue sections (73504, Qiagen) was used according to the manufacturer's protocol. qRT-PCR was performed using the TaqMan RNA-to-CT 1-Step Kit (Applied Biosystems) with a CHIKV E1- or MAYV E2-specific primer/probe set (Bellini et al., 2012; Long et al., 2011). The extracted RNA was compared to a standard curve generated from RNA extracted from a CHIKV or MAYV stock to determine FFU equivalents. To quantify CHIKV genomic and subgenomic RNA levels in the spleen, random primed cDNA was used as a template for CHIKV sequence-specific forward (CHIKV2444, 5'-TTTGCGTGCCACTCTGG-3') and CHIKV sequence-specific reverse (CHIKV2524, 5'-CGGGTCACCACAAAGTACAA-3') primers and a CHIKV sequence-specific TaqMan probe (CHIKV2467, 5'FAM- ACTTGCTTTGATCGCCTTGGTGAGA-3') to amplify a region of the nsP2 gene. The same random primed cDNA also was used as a template for CHIKV sequence-specific forward (CHIKV10239, 5'-CGGCGTCTACCCATTTAT GT-3') and CHIKV sequence-specific reverse (CHIKV10363, 5'-CCCTG TATGCTGATGCAAATTC-3') primers and a CHIKV sequence-specific TaqMan probe (CHIKV10290, 5'-FAM-AAACACGCAGTTGAGCGAA GCAC-MGB-3') that amplified a region in the E1 gene. A standard curve composed of 10-fold dilutions from 10^7 to 10^0 copies of CHIKV positive-strand genomic RNA, synthesized *in vitro* and spiked into RNA from BHK21 cells was used to determine the nsP1 and E1 gene copy number and confirm that the two assays amplified with similar efficiencies. To determine the relative abundance of the subgenomic RNA compared with

full-length genomic RNA, the data were expressed as a ratio of the E1 to nsP2 gene copy number.

Antibodies and cell depletions. Anti-CD137 mAb (clone 2A, rat Ig2a mAb) has been described previously (Wilcox et al., 2002b). Antibody was purified from hybridoma supernatants by protein G affinity chromatography by a commercial vendor (BioXCell). Anti-CD4 (clone GK1.5), anti-CD8 (clone YTS169.4), anti-NK1.1 (clone PK136), anti-Ly6G (clone 1A8), anti-CD40L (clone MR-1), rat IgG2b isotype control (clone LTF-2) for CD4$^+$ and CD8$^+$ T cell depletion, mouse IgG2a (clone C1.18.4) for NK and B cell depletion, rat IgG2a isotype control (clone 2A3) for neutrophil depletion and polyclonal Armenian hamster IgG for CD40L blockade were purchased from BioXCell. Anti-CD20 (clone 5D2) was obtained from Genentech. Mice were administered 400 mg of anti-CD137 or rat Ig2a isotype control mAb (clone 2A3, BioXCell) via intraperitoneal (i.p.) route at 2 dpi. For cell depletion studies, mice were administered 300 mg of anti-CD4 mAb, 500 mg of anti-CD8 mAb, or 200 mg of anti-NK1.1 mAb on 2 dpi and every 4 days thereafter until 14 dpi or 500 mg of anti-Ly6G antibody on 2 dpi and every 2 days thereafter until 14 dpi. For B cell depletion, mice were administered 200 mg of anti-CD20 mAb on 2 dpi. For CD40L block, mice were administered 500 mg of anti-CD40L mAb on 2 dpi and every 3 days thereafter until 14 dpi.

RNA in situ hybridization (ISH). Uninfected and infected mice were sacrificed and perfused extensively via intracardiac injection of PBS. The spleen was dissected and fixed in 1% PFA in PBS for 2 h at room temperature and transferred to 10% sucrose in PBS at 4°C. After incubation overnight, tissues were placed in 30% sucrose in PBS at 4°C overnight and frozen in Tissue Tek Compound (catalog # 4583, Sakura) at -80°C. Tissues were cut in 10 µm sections. Viral RNA ISH was performed using RNAscope 2.5 (Advanced Cell Diagnostics) according to

the manufacturer's instructions. The probe targeting CHIKV RNA was designed and synthesized by Advanced Cell Diagnostics (catalog # 479501). All samples were visualized using a Nikon Eclipse microscope with a QICAM 12-bit camera (QImaging) and processed with QCapture software.

Immune cell analysis. Ipsilateral feet from CHIKV-infected mice were skinned and incubated for 2 h at 37°C in 10 ml of digestion buffer (2.5 mg/ml collagenase (Sigma) and 10 mg/mL DNase I (Sigma) in RPMI 1640 medium containing 10% fetal bovine serum (FBS)). The cell suspension was passed through a 70 mm cell strainer. After centrifugation, cells were washed with 1% FBS in Hank's Balanced Salt Solution, followed by another round of centrifugation and washing. Cells were resuspended in washing buffer (5% FBS in PBS) at 5 x 10^6 cells/ml and incubated with 2.5 mg of anti-mouse CD16/32 antibody (101302, Biolegend) per 10^6 cells for 20 min on ice. Cells then were stained with BV605-conjugated anti-CD45 (103140, Biolegend), FITC-conjugated anti-CD3ε (11-0031-85, Invitrogen), PE-conjugated anti-CD4 (553049, BD), PerCP-Cy5.5-conjugated anti-CD8α (100734, Biolegend), PE-Cy7-conjugated anti-NK1.1 (108714, Biolegend), APC-Cy7-conjugated anti-CD19 (115530, Biolegend), Brilliant Violet 421-conjugated anti-Ly6C (562727, BD), Alexa 700-conjugated anti-Ly6G (127622, Biolegend) antibody. Subsequently, cells were fixed and permeabilized with eBioscience FoxP3/Transcription Factor Staining kit and incubated with Alexa 647-conjugated anti-FoxP3 (126408, Biolegend) antibody.

Spleens from CHIKV-infected mice were minced and incubated for 30 min at 37°C in 2 ml digestion buffer (1 mg/ml collagenase (Sigma) and 100 mg/mL DNase I (Sigma) in Dulbecco's modified Eagle's medium containing 2% FBS) in a 24-well plate. The cell suspension was passed through a 100 mm cell strainer. After rinsing with 10% FBS, 5 mM

EDTA in DMEM, erythrocytes were lysed with 1 ml of ACK Lysing Buffer (Gibco) for 2 min. Cells were washed with DMEM and centrifuged, followed by rinsing with washing buffer (2% FBS, 5mM EDTA in PBS). After centrifugation, cells were resuspended in washing buffer at 5 x 10^8 cells/ml and incubated with 2.5 mg of anti-mouse CD16/32 antibody (101302, Biolegend) per 10^8 cells for 20 min on ice. Then, cells were stained with BV605-conjugated anti-CD45 (103140, Biolegend), PE-Cy7-conjugated anti-CD3 (100320, Biolegend), APC-Cy7-conjugated anti-CD19 (115530, Biolegend), PerCP-Cy5.5-conjugated anti-CD11c (117328, Biolegend), FITC-conjugated anti-CD21/35 (553818, BD Biosciences), Brilliant Violet 421-conjugated anti-CD54 (564704, BD), PE-conjugated anti-CD95 (554258, BD Biosciences) antibody and biotin-conjugated PNA (B-1075, Vector). To confirm CD137 expression, cells were stained with biotin-conjugated anti-CD137 (106104, Biolegend). Cells then were washed and incubated with Alexa647-conjugated streptavidin (S32357, Invitrogen). Subsequently, cells were fixed with BD FACS Lysing Solution, processed on a LSR Fortessa X-20 (BD Biosciences) flow cytometer, and analyzed using BD FACSDiva and FlowJo software. For fluorescence-activated cell sorting, a BD FACS Aria II was used.

Serum anti-CHIKV IgG ELISA assay. MaxiSorp 96-well flat-bottom ELISA plates (Thermo Fisher) were coated with 2 μg/ml of CHIKV E2 protein (a gift of Melissa Barrow (Washington University in St. Louis)) (Pal et al., 2013) overnight at 4°C. Plates were washed with ELISA wash buffer (PBS, 0.05% Tween 20) and blocked with blocking buffer (PBS, 5% FBS) for 4 h at 37°C. Sera from CHIKV-infected mice were added in 3-fold dilutions starting with a 1/100 dilution. After incubating for 1 h at room temperature, plates were washed with ELISA wash buffer. Plates were incubated with biotinylated anti-IgG (115-065-062, Jackson ImmunoResearch) for 1 h at room temperature. After washing, plates were incubated with

streptavidin-conjugated HRP (SA-5004, Vector Laboratories) for 30 min at room temperature. After washing sequentially with ELISA buffer and PBS, substrate solution (Thermo Fisher) was added. The reaction was quenched with 2N H_2SO_4. The plates were read using a Synergy H1 Hybrid Reader (BioTek). Optical density (OD) value of naïve serum was subtracted from OD values of samples, and non-linear regression curves were calculated for each sample. 50% binding point was defined as the dilution to have a half-maximal optical density.

Statistical analysis. All data were analyzed with GraphPad Prism software. For viral RNA analysis and immune cell analysis, data were analyzed by the Mann-Whitney test, Kruskal-Wallis ANOVA with Dunn's post-test, or two-way ANOVA with Sidak post-test. *P* values of less than 0.05 indicated statistically significant differences.

RESULTS

Anti-CD137 mAb treatment reduces CHIKV RNA levels in lymphoid but not musculoskeletal tissues. We hypothesized that agonistic anti-CD137 mAb might stimulate the immune system to clear chronic viral infections, analogous to its ability to reduce tumor burden (Yonezawa et al., 2015). To test this idea, we used a murine model of CHIKV infection. Four week-old wild-type C57BL/6 male mice inoculated subcutaneously with CHIKV in the foot develop a biphasic pattern of joint swelling with persistent viral RNA present in the musculoskeletal tissues of the ipsilateral and contralateral feet, the spleen, and the DLN (**Fig 2.1** and (Hawman et al., 2013)); this viral RNA is maintained although infectious virus cannot be recovered after 7 dpi in immunocompetent mice (Poo et al., 2014b). CHIKV-infected mice treated therapeutically with agonistic anti-CD137 mAb at 2 dpi developed increased foot swelling from 7 to 10 dpi compared with isotype control mAb-treated animals (**Fig 2.1A**). Associated with this, at 7 dpi, we observed increased numbers of CD8$^+$ T cells (3.3-fold, $P <$ 0.01) and Ly6G$^+$ neutrophils (3.0-fold, $P <$ 0.01) in the joints of anti-CD137 mAb-treated mice compared with isotype control mAb-treated animals (**Fig 2.1B**).

Despite the changes in foot swelling induced by anti-CD137 mAb treatment, no differences in viral RNA levels were observed in the ipsilateral or contralateral feet at 7, 14 or 28 dpi (**Fig 2.1C-E**). Similarly, the amount of CHIKV RNA in ipsilateral or contralateral feet did not change compared with isotype control mAb-treated animals at 14 dpi when mice were treated with anti-CD137 mAb at day 0, the same time as virus inoculation (**Fig 2.1H-J**).

Although anti-CD137 mAb treatment at 0 or 2 dpi failed to clear CHIKV RNA in musculoskeletal tissues, we observed reduced viral RNA levels in the spleen at 7 dpi compared with isotype control mAb (**Fig 2.1F**). At 14 and 28 dpi, anti-CD137 mAb-treated mice showed greater reductions in CHIKV RNA in the spleen (~130 to 220-fold, $P <$ 0.0001) compared with

isotype control mAb treated animals. In most (7 of 10) animals treated with a single dose of anti-CD137 at 2 dpi, viral RNA was not detected in the spleen at 28 dpi (**Fig 2.1F**). Reduced levels (110-fold, *P* < 0.0001) of CHIKV RNA also were observed at 14 dpi in the DLN after anti-CD137 mAb treatment (**Fig 2.1G**). However, at 28 dpi, CHIKV RNA in the DLN was absent in most anti-CD137 and isotype control mAb-treated animals (**Fig 2.1G**). When mice were treated with anti-CD137 mAb at 0 dpi, the amount of CHIKV RNA in the spleen and DLN at 14 dpi also was substantially reduced (140 to 7,000-fold, *P* < 0.05) compared with isotype control mAb-treated animals (**Fig 2.1K-L**). We confirmed the specificity of the effect; treatment of CHIKV-infected CD137$^{-/-}$ mice with agonistic anti-CD137 mAb at 2 dpi did not reduce viral RNA levels in the spleen (**Fig 2.1M**).

Effect of anti-CD137 mAb on CHIKV tropism in the spleen. To begin to elucidate how anti-CD137 mAb treatment promoted clearance of CHIKV RNA in the spleen, we explored the cellular tropism of the virus in this tissue, which has remained undefined. Initially, we performed viral RNA *in situ* hybridization (ISH) on spleens from CHIKV-infected mice treated with anti-CD137 or isotype control mAb. At 7 dpi, much of the viral RNA was present in the center of lymphoid follicles of anti-CD137 or isotype control mAb-treated animals (**Fig 2.2A-B**). To define the cell types harboring CHIKV RNA, we sorted splenocyte subsets at 7 and 14 dpi by flow cytometry and performed qRT-PCR; cells were fixed with paraformaldehyde prior to sorting because of containment issues, as infectious CHIKV is a biosafety level 3 agent. At 7 and 14 dpi, follicular dendritic cells (FDCs) and germinal center B cells contained the highest relative levels of CHIKV RNA on a per cell basis in the spleens of isotype control mAb-treated animals (**Fig 2.2C**). When anti-CD137 mAb treatment was administered at 2 dpi, CHIKV RNA preferentially was cleared from FDCs at 7 dpi and not appreciably detected in any splenocyte

subsets at 14 dpi. During productive CHIKV infection, the subgenomic mRNA segment encoding the structural proteins (C-E3-E2-6K-E1) is preferentially transcribed compared to the genomic RNA (Carrasco et al., 2018). This results in more copies of structural proteins, such as E1, than the non-structural proteins. As a surrogate assay for detecting infectious virus in the spleen, we measured the ratio of subgenomic (E1 RNA) to genomic (nsP2 RNA) RNA by qRT-PCR. At least up through 14 dpi, the ratio of E1 RNA compared to nsP2 RNA was greater than 1 (**Fig 2.2D-F**), suggesting active infection.

In addition to altering CHIKV persistence in the spleen, we speculated that anti-CD137 mAb treatment might impact specific immune cell populations after infection. Anti-CD137 mAb treatment did not diminish the total number of leukocytes in the spleen (**Fig 2.3A**), and we even observed a small increase (1.6-fold increase, $P < 0.01$) in the number $CD3^+$ T cells at 14 dpi. (**Fig 2.3B**). However, we did observe a small decrease (1.4-fold decrease, $P < 0.01$) in the number of $CD19^+$ B cells (**Fig 2.3C**) and markedly reduced (up to ~40-fold, $P < 0.01$) numbers of PNA^+CD95^+ or $GL7^+CD95^+$ germinal center B cells and $CD45^-CD54^+CD21/35^+$ FDCs at 7 and 14 dpi (**Fig 2.3D-G**). To test whether inhibition of germinal center development affected antiviral antibody responses, we measured anti-CHIKV IgG levels in the serum of infected mice at 30 dpi. Consistent with the reduced numbers of germinal center B cells, we observed lower (32-fold, $P < 0.001$) levels of anti-CHIKV IgG in anti-CD137 mAb-treated than isotype control mAb-treated animals (**Fig 2.3H**).

B cells are required for persistence of CHIKV RNA in the spleen. Since splenic germinal center B cells and FDCs showed the highest quantities of viral RNA on a per cell basis after CHIKV infection, we further evaluated the contribution of these cells to persistence of CHIKV RNA in the spleen. Initially, at 2 dpi we treated isotype control mAb-treated mice with

an anti-CD40L-blocking mAb, which inhibits engagement of CD40L on B cells with its receptor

CD40 on T helper cells and results in impaired germinal center formation (Baumjohann et al.,

2013). As expected, administration of CD40L-blocking mAb reduced the number of germinal

center B cells and FDCs at 14 dpi by 108- and 7-fold, respectively (**Fig 2.4A-D**). This depletion

was associated with an approximately 5-fold reduction in CHIKV RNA in the spleen, although

the difference did not attain statistical significance (**Fig 2.4E,** *comparison of black circles*). In

comparison, treatment with anti-CD137 mAb in combination with CD40L-blocking mAb or the

block isotype control mAb reduced viral RNA levels in the spleen compared with treatment with

isotype control mAb in combination with CD40L-blocking mAb (123-fold, $P < 0.05$) or block

isotype control mAb (660-fold, $P < 0.001$), respectively (**Fig 2.4E**, *comparison of black and red*

circles on the left-side or right-side, respectively). Collectively, these experiments show that

although germinal center B cells and FDCs contain high levels of CHIKV RNA in the spleens of

isotype control mAb-treated mice, other cell populations contribute to the persistence of CHIKV

RNA.

Based on these data, we speculated that non-germinal center B cells also harbored

CHIKV RNA in the spleen. Indeed, when we depleted all $CD20^+$ B cells using an anti-CD20

mAb at 2 dpi we observed a 75-fold reduction ($P < 0.001$) in CHIKV RNA in the spleen at 14

dpi (**Fig 2.4F-G**; *comparison of black circles*). To corroborate these data, mMT (B cell-deficient)

mice were inoculated with CHIKV and treated with anti-CD137 mAb at 2 dpi. Viral RNA levels

at 7 dpi in the spleens of mMT mice were lower than WT mice with anti-CD137 mAb treatment

(87-fold, $P < 0.001$) or without it (299-fold, $P < 0.001$), respectively (**Fig 2.1D and Fig 2.4H**).

However, the levels of viral RNA in the spleens of anti-CD137 mAb-treated and isotype control

mAb-treated mMT mice at 7 dpi were similar. At 14 dpi, almost no CHIKV RNA was detected in the spleen of these mice with or without anti-CD137 mAb treatment (**Fig 2.4H**).

Antigen in the form of immune complexes can be captured by cells expressing Fc-g or complement receptors, or antigen can be directly captured by B cell receptors. We next tested whether CHIKV-specific antibody was required for the persistence of viral RNA in the spleen. To assess this, we used transgenic MD4 mice in a mMT background; these mice have B cell receptors specific only for hen egg lysozyme (HEL) (**Fig 2.4I**) (Mason et al., 1992). At 14 dpi, viral RNA was detected in the spleens of MD4 mice, albeit at substantially lower levels than WT mice, whereas almost no viral RNA was measured from the spleens of mMT mice (**Fig 2.4J**). Thus, the antigen-specificity of B cells contributes to persistence of CHIKV RNA in the mouse spleen.

T cells are required for anti-CD137-mediated clearance of CHIKV in the spleen. We hypothesized that agonistic anti-CD137 mAb cleared CHIKV RNA in lymphoid tissues by activating $CD137^+$ immune cells with effector activity (Yonezawa et al., 2015). We detected CD137 expression by flow cytometry on splenic $CD4^+$ and $CD8^+$ T cells, NK cells and NKT cells in CHIKV-infected mice at 2 dpi (**Fig 2.5**). To define the cells responsible for anti-CD137 mAb-mediated clearance of CHIKV RNA, we performed anti-CD137 mAb treatment experiments in mice depleted of NK cells, $CD8^+$ T cells, $CD4^+$ T cells, or neutrophils. Administration of anti-CD137 mAb in NK cell, $CD8^+$ T cell, or $CD4^+$ T cell depleted mice resulted in diminished CHIKV RNA levels in the spleen at 14 dpi, although the reduction was only 2 to 5-fold less than with control non-depleting mAbs (**Fig 2.6A-F**). Ab-mediated depletion of both $CD4^+$ and $CD8^+$ T cells resulted in 9-fold less of a clearance effect by anti-CD137 mAb (**Fig 2.6G-H**). Similarly, Ab-mediated triple depletion of $CD4^+$ and $CD8^+$ T cells as well as NK

cells resulted in 21-fold less clearance by anti-CD137 mAb (**Fig 2.6I-J**). In comparison, depletion of neutrophils did not affect anti-CD137 mAb-mediated clearance of CHIKV RNA in the spleen at 14 dpi (**Fig 2.6K-L**). Consistent with a dominant role for CD3$^+$ cells in mediating clearance of CHIKV RNA in the spleen, the effect of anti-CD137 mAb was abolished completely in TCRβδ$^{-/-}$ mice, which lack all T cell and NKT cell subsets (**Fig 2.6M**).

Anti-CD137 mAb treatment reduces Mayaro virus RNA levels. We assessed the effect anti-CD137 mAb on a second alphavirus, MAYV, to determine whether the clearance phenotype was specific to CHIKV. In contrast to that observed with CHIKV-infected mice, treatment with anti-CD137 mAb reduced (8-fold, *P* < 0.0001) viral RNA level in the ipsilateral foot of MAYV-infected mice at 14 dpi (**Fig 2.7A**), although viral RNA levels in the contralateral foot of anti-CD137 and isotype control mAb-treated mice were similar (**Fig 2.7B**). Similar to CHIKV-infected mice, anti-CD137 mAb treatment resulted in markedly reduced MAYV RNA levels in the spleen (241-fold, *P* < 0.0001) and DLN (5,962-fold, *P* < 0.001) at 14 dpi (**Fig 2.7C-D**). Thus, anti-CD137 mAb-mediated clearance of viral RNA in lymphoid tissues occurred in the context of multiple alphavirus infections in mice, whereas reduction of viral RNA in musculoskeletal tissues was virus type-specific.

DISCUSSION

In this study, we observed that agonistic anti-CD137 mAb administered at 2 dpi cleared CHIKV RNA in the spleen and DLN by 28 dpi although viral RNA in musculoskeletal tissues of the foot persisted. In a parallel model of infection with MAYV, a second arthritogenic alphavirus, anti-CD137 mAb treatment also reduced MAYV RNA levels in the spleen and DLN by 14 dpi. However, in the MAYV model, a partial clearance effect was observed in the ipsilateral but not contralateral foot. Based on our cell sorting and tropism data, in the spleen, germinal center B cells and FDCs were associated with the highest levels of viral RNA on a per cell basis at 7 and 14 dpi. Flow cytometric analysis revealed that anti-CD137 mAb treatment reduced the number of germinal center B cells and FDCs, and this was associated with diminished anti-CHIKV IgG responses. Inhibition of germinal center formation by anti-CD137 mAb has been reported in mice immunized with sheep red blood cells or keyhole limpet hemocyanin (Sun et al., 2005). When B cells were depleted using anti-CD20 mAb, CHIKV RNA in the spleen also was reduced at 14 dpi. Together, these data suggest a key role for B cells in maintaining persistent CHIKV RNA in the spleen. Consistent with these results mMT mice lacking B cells had almost no detectable viral RNA in the spleen at 14 dpi, and MD4 transgenic mice, which have B cells specific for HEL, also had less CHIKV RNA in the spleen at 14 dpi. These data suggest that antigen-specific B cells are responsible for the persistence of CHIKV RNA in mouse spleen. Anti-CD137 mAb-mediated clearance of CHIKV RNA in the spleen was diminished in anti-NK 1.1, anti-CD4, and anti-CD8 treated mice and abrogated in TCR$\beta\delta^{-/-}$ mice, which lack CD4$^+$ and CD8$^+$ T cells, NKT cells, and gd T cells in the spleen. Thus, anti-CD137 mAb-mediated clearance of CHIKV in lymphoid tissues is dependent primarily on T cells.

The basis of CHIKV RNA persistence in musculoskeletal tissues of infected animals remains a long-standing question in the field. Although anti-CD137 mAb treatment had marked effects in lymphoid tissues, it did not significantly alter CHIKV RNA levels in the ipsilateral or the contralateral feet at 7, 14, or 28 dpi. The lack of CHIKV RNA clearance in the musculoskeletal tissues after anti-CD137 mAb treatment may be due to the distinct viral tropism in these tissues. During the acute phase of infection, CHIKV is readily detected in skeletal muscle cells, synovial fibroblasts, and other non-hematopoietic cells in mice (Nair et al., 2017; Young et al., 2019). During the chronic phase, the reservoir of CHIKV in muscle and joint tissues is less clear, although experiments with a Cre-recombinase CHIKV strain and reporter mice showed fibroblasts and skeletal muscle cells harbor persistent viral RNA (Young et al., 2019). In contrast to our observations in the CHIKV model, agonistic anti-CD137 mAb treatment reduced viral RNA levels in the ipsilateral foot in the MAYV model. Although further study is warranted, the cellular tropism of MAYV may differ with respect to CHIKV, as has been reported for other arthritogenic alphaviruses, such that additional infected cell types can be cleared by anti-CD137 activated T cells (Suhrbier and La Linn, 2004).

Our experiments showed that in the spleen, germinal center B cells and FDCs are associated with high levels of CHIKV RNA at 7 and 14 dpi. Although viral RNA was readily detected, we did not recover infectious CHIKV from lymphoid tissues at these time points, as judged by plaque or focusing forming assays. Notwithstanding these data, we did observe higher E1:nsP2 RNA ratios consistent with productive CHIKV infection. Additionally, B cells may capture CHIKV immune complexes via surface complement and Fc-g receptors and transport it to FDCs in the B cell follicles (Cinamon et al., 2008; Heinen et al., 1986). Marginal zone B cells continuously shuttle between marginal zone and follicular areas, which can facilitate antigen

transport (Cinamon et al., 2008). Alternatively, immune complexes taken up by subcapsular sinus or marginal zone macrophages can be transferred to complement receptor 2 (CR2)-expressing B cells, which then transport the immune complexes to CR2-expressing FDCs (Batista and Harwood, 2009).

FDCs are believed to retain opsonized antigen for extended periods time periods and present it to cognate B cells to form germinal centers (Hanna and Szakal, 1968). As an example, human FDCs isolated from patients retain HIV for prolonged periods of time within non-degradative cycling compartments (Heesters et al., 2015). Clearance of CHIKV RNA in the spleen after anti-CD137 mAb treatment correlated with reductions in the number of germinal center B cells and FDCs. Moreover, the level of viral RNA in the spleen was reduced in mMT or MD4 transgenic mice lacking CHIKV-specific B cells and Abs. Based on our tropism analysis, blocking studies with anti-CD40L mAb, depletion studies with anti-CD20 mAb and infection experiments in mMT B cell-deficient mice, it appears that multiple subtypes of B cells and FDCs retain much of the CHIKV RNA in lymphoid tissues during the subacute and chronic phases of infection.

Anti-tumor mechanisms of anti-CD137 mAb activity are thought to depend on direct killing by $CD8^+$ T cells and NK cells, enhanced proliferation and cytokine secretion by tumor-specific T cells, and Ab-dependent cell-mediated cytotoxicity by NK cells at tumor sites (Yonezawa et al., 2015). In a mouse B cell lymphoma model, depletion of $CD8^+$ T cells or NK cells abrogated the anti-tumor effect of anti-CD137 mAb (Houot et al., 2009). Although the anti-tumor effect of anti-CD137 mAb is mediated through engagement of $CD8^+$ T cells in most preclinical tumor models, the role of $CD4^+$ T cells is less clear. Depletion of $CD4^+$ T cells improved the therapeutic efficacy of anti-CD137 mAb in a mouse B cell lymphoma model

(Houot et al., 2009), whereas CD4$^+$ T cells were required for anti-CD137 mAb-induced anti-tumor immunity in a mouse mastocytoma model (Melero et al., 1997). Based on our cell depletion experiments, anti-CD137 mAb-mediated clearance of persistent CHIKV RNA was dependent only partially on NK cells, CD4$^+$ and CD8$^+$ T cells. However, anti-CD137 mAb-mediated clearance of CHIKV RNA was abrogated in TCRβδ$^{-/-}$ mice. Immune cell subsets other than conventional CD4$^+$ or CD8$^+$ T cells such as NKT cells that are absent in these mice could contribute to anti-CD137 mAb-mediated clearance of CHIKV RNA in the spleen. Because B cells are a major reservoir of persistent CHIKV RNA in the spleen, we hypothesize that anti-CD137 mAb clears persistent CHIKV RNA in the spleen and DLN by targeting B cells. Further study is necessary to define how activation by anti-CD137 mAb induces T cells and possibly NKT cells to lyse and/or prevent expansion of B cells, and whether any of this process is antigen-specific.

Our study helps to elucidate the basis for retention of CHIKV RNA in secondary lymphoid tissues. The clearance of CHIKV RNA coincided with a reduction in B cells and FDCs that was mediated by anti-CD137 mAb treatment and T cells. These effects on germinal center formation may be relevant for infections and vaccinations that occur in patients treated with agonistic anti-CD137 mAb therapies for cancers. Although further study is warranted, treatment with anti-CD137 mAbs might blunt humoral response to newly-administered vaccines or infection with pathogens.

Figure 2.1
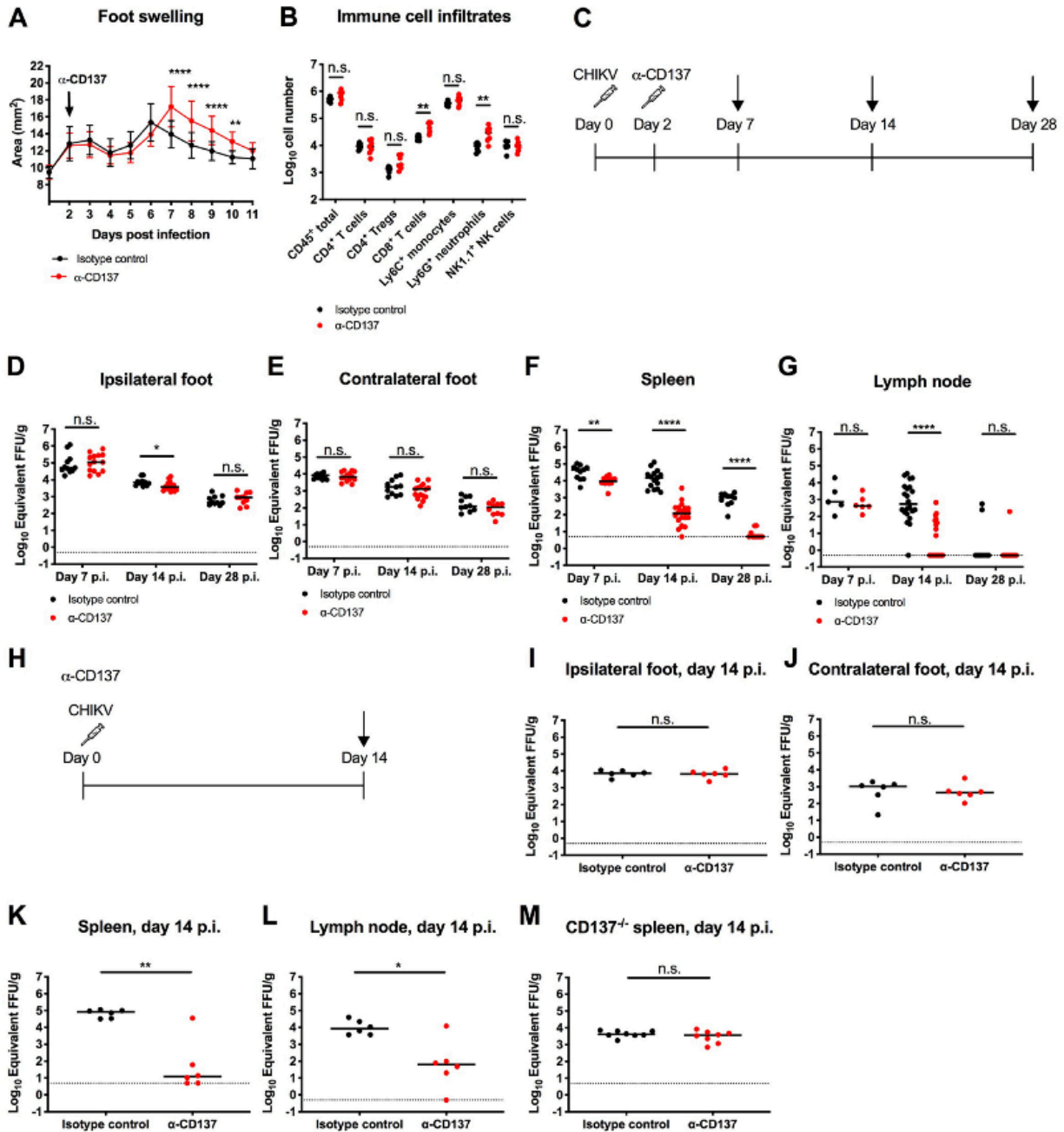
Figure 2.1. Anti-CD137 mAb treatment increases footpad swelling but reduces viral RNA level in the spleen and DLN. Four-week-old WT C57BL/6 male mice were inoculated with 10^3 FFU of CHIKV-LR at day 0. At 2 dpi, 400 mg of agonistic anti-CD137 or isotype control mAb

was administered via an i.p. route. (**A**) Foot swelling was measured with digital calipers (15-18 mice per group). Each symbol represents a mean value of each group, and bars indicate standard deviation (two-way ANOVA with Sidak post-test; **, $P < 0.01$; ****, $P < 0.0001$). (**B**) Ipsilateral feet were harvested at 7 dpi and processed for flow cytometry to quantify immune cell infiltrates. (**C**) Experimental scheme for panels **D-G**. Ipsilateral (**D**) and contralateral (**E**) feet, spleen (**F**), and DLN (**G**) were harvested at 7, 14, and 28 dpi. Viral RNA was measured from tissue homogenates by qRT-PCR. (**H**) Experimental scheme of panels **I-L**. At the same time as virus inoculation, 400 mg of agonistic anti-CD137 mAb or isotype control was administered i.p. Ipsilateral (**I**) and contralateral (**J**) foot, spleen (**K**) and DLN (**L**) were harvested at 14 dpi, and viral RNA was measured from tissue homogenates by qRT-PCR. (**M**) Four-week-old CD137$^{-/-}$ C57BL/6 mice were inoculated with 10^3 FFU of CHIKV-LR at day 0. At 2 dpi, 400 mg of agonistic anti-CD137 or isotype control mAb was administered via an i.p. route. Spleens were harvested on 14 dpi. Viral RNA was measured from tissue homogenates by qRT-PCR. Each symbol represents an individual mouse, and bars indicate median values. Data in panels **B, D-G, and I-M** are pooled from 2 or 3 experiments (Mann-Whitney test: *, $P < 0.05$; **, $P < 0.01$; ****, $P < 0.0001$; n.s., not significant).

Figure 2.2
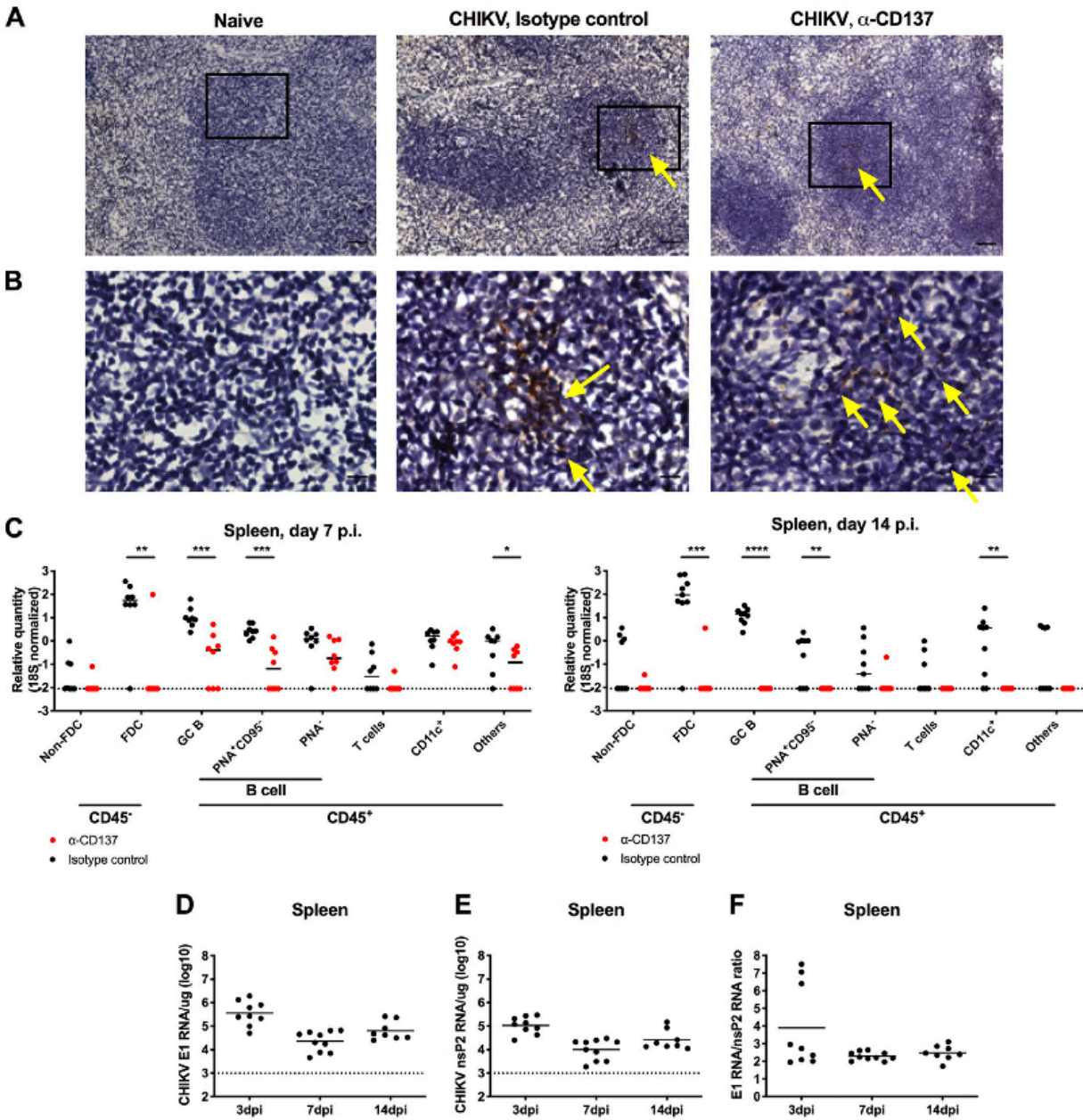
Figure 2.2. Germinal center B cells and FDCs harbor CHIKV viral RNA. Four-week-old

WT C57BL/6 male mice were inoculated with 10^3 FFU of CHIKV-LR. At 2 dpi, 400 mg of

agonistic anti-CD137 or isotype control mAb was administered via an i.p. route. (**A**) Spleens

were harvested at 7 dpi, and viral RNA (brown) was visualized by ISH. Tissue sections were

counterstained with Gill's haematoxylin. Scale bar (50 mm). (**B**) Inset of panel **A** (black boxes)

visualized with higher magnification. Scale bar (10 mm). Yellow arrows indicate CHIKV RNA. (**C**) Spleens were harvested at 7 dpi (left panel) and 14 dpi (right panel), and bulk cells were fixed with paraformaldehyde and sorted using flow cytometry. Viral RNA in each sorted cell subset was measured by qRT-PCR and normalized to 18S. (**D-F**) Four-week-old WT C57BL/6 male mice were inoculated with 10^3 PFU of CHIKV SL15649. Spleens were harvested at 3, 7, and 14 dpi, and CHIKV E1 (**D**) and nsP2 (**E**) RNA was measured from tissue homogenates by qRT-PCR. (**F**) The ratio of E1 RNA to nsP2 RNA was calculated. Data in this Figure are pooled from 2 experiments. Each symbol represents one mouse, and bars indicate median values (Mann-Whitney test: *, $P < 0.05$; **, $P < 0.01$; ***, $P < 0.001$; ****, $P < 0.0001$).

Figure 2.3
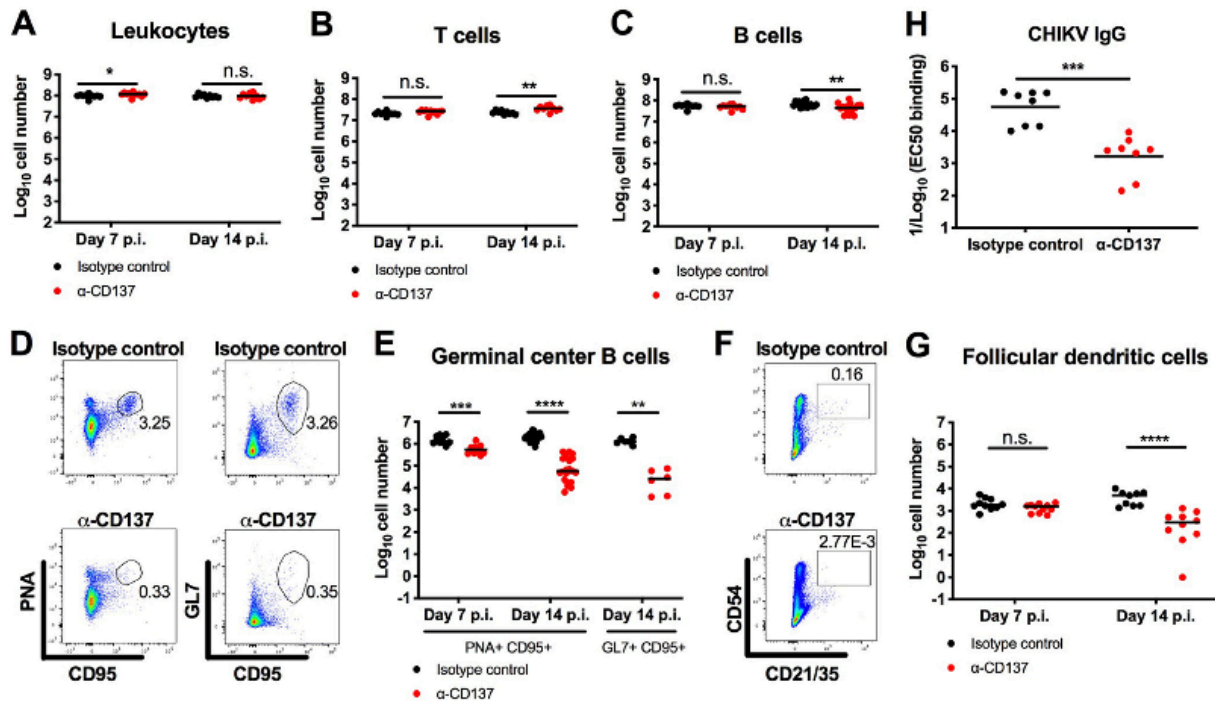
Figure 2.3. Anti-CD137 mAb treatment reduces the number of germinal center B cells and FDCs. Four-week-old WT C57BL/6 male mice were inoculated with 10^3 FFU of CHIKV-LR. At 2 dpi, 400 mg of agonistic anti-CD137 or isotype control mAb was administered via an i.p. route. The number of total $CD45^+$ leukocytes (**A**), $CD3^+$ T cells (**B**), $CD19^+$ B cells (**C**), PNA^+CD95^+ or $GL7^+CD95^+$ germinal center B cells (**D-E**) and $CD45^-CD54^+CD21/35^+$ FDCs (**F-G**) in the spleen at 14 dpi was analyzed by flow cytometry. Representative flow cytometry dot plots of (**D**) germinal center B cells and (**F**) FDCs are shown. (**H**) Serum was harvested at 30 dpi, and anti-CHIKV IgG titer was measured by ELISA. Each symbol represents an individual mouse, and bars indicate median values. Data in this Figure were pooled from 2 to 3 experiments (Mann-Whitney test: *, $P < 0.05$; **, $P < 0.01$; ***, $P < 0.001$; ****, $P < 0.0001$; n.s., not significant).

Figure 2.4
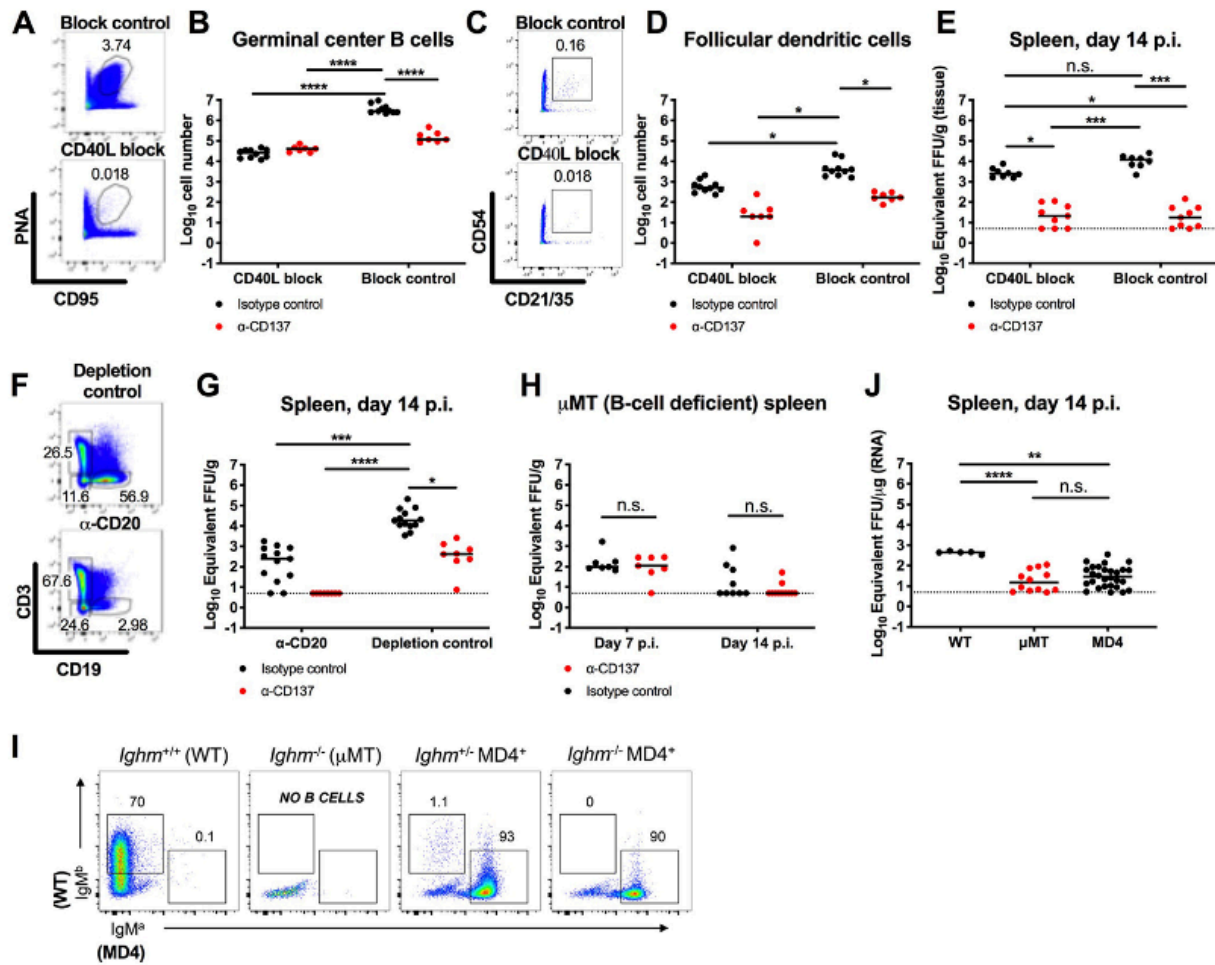
Figure 2.4. B cells are required for persistence of CHIKV RNA in the spleen. (**A-G**) Four-week-old WT C57BL/6 male mice were inoculated with 10^3 FFU of CHIKV-LR. At 2 dpi, 400 mg of agonistic anti-CD137 or isotype control mAb in combination with CD40L-blocking or isotype (block) control mAb (**A-E**) or anti-CD20 depleting or depletion isotype control mAb (**F-G**) was administered via an i.p. route. Spleens were harvested at 14 dpi, and the number of PNA$^+$CD95$^+$ germinal center B cells (**A-B**) and CD45$^-$CD54$^+$CD21/35$^+$ FDCs (**C-D**) was determined after flow cytometry. Representative flow cytometry dot plots of germinal center B cells (**A**), FDCs (**C**) and CD19$^+$ B cells (**F**) are shown. (**E and G**) Viral RNA was measured from tissue homogenates by qRT-PCR. (**H-J**) 4-week-old mMT mice (**H**) or MD4 transgenic mice in

a mMT background (**I-J**) were inoculated with 10^3 FFU of CHIKV-LR. (**H**) At 2 dpi, 400 mg of agonistic anti-CD137 or isotype control mAb was administered. Spleens were harvested at 7 or 14 dpi, and viral RNA was measured. Each symbol (**H and J**) represents an individual mouse, and bars indicate median values (Kruskal-Wallis ANOVA with Dunn's post-test: *, $P < 0.05$; **, $P < 0.01$; ***, $P < 0.001$; ****, $P < 0.0001$; n.s., not significant). (**I**) At 14 dpi, the spleen was removed and processed for flow cytometry. Splenocytes were gated on $B220^+CD19^+$ for B cells. Representative flow plots from each genotype are shown. WT B cells are IgM^{b+}, and HEL-specific (MD4) B cells are IgM^{a+}. MD4 B cells were also confirmed by staining with HEL (data not shown). Data in this figure are pooled from 2 to 4 experiments.

Figure 2.5
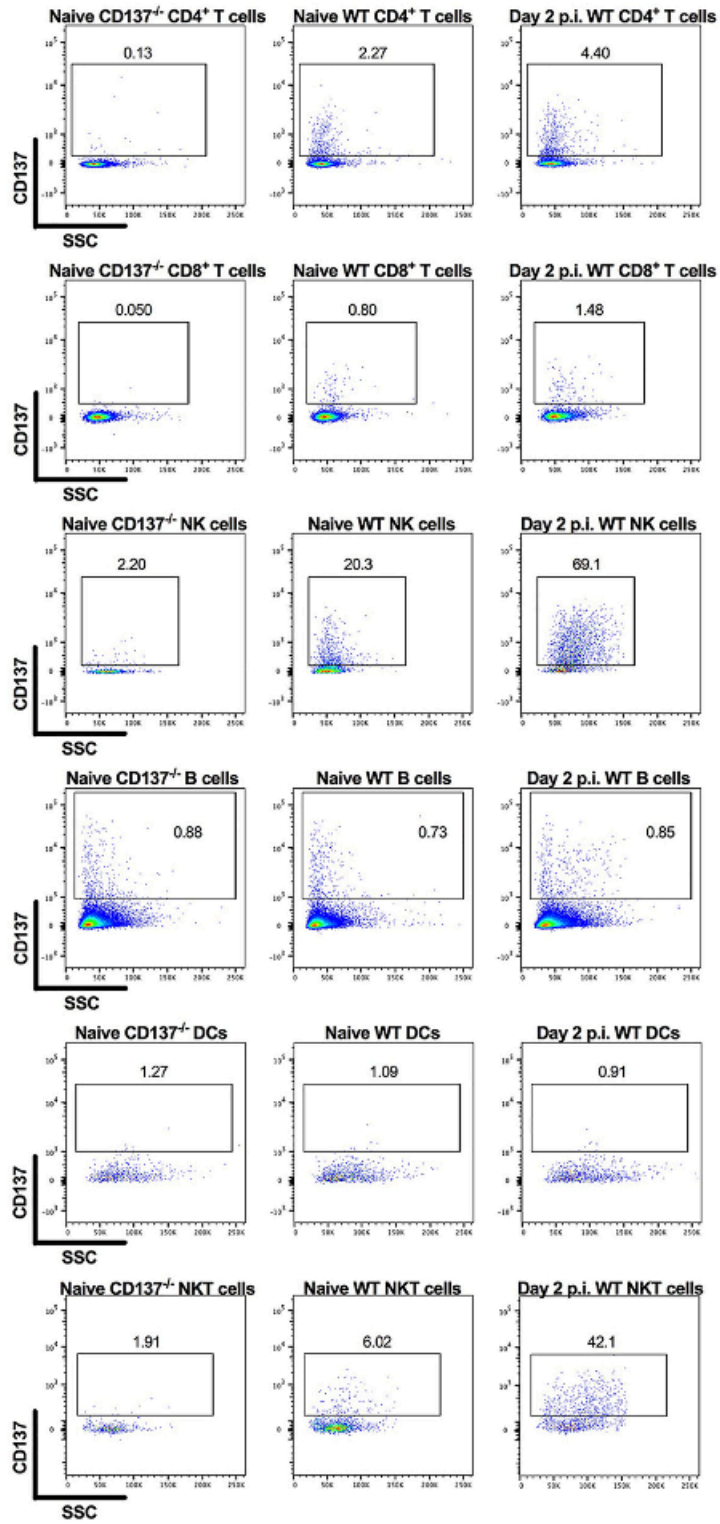
Figure 2.5. CD137 is expressed on splenic CD4$^+$ and CD8$^+$ T cells, NK cells, and NKT cells in CHIKV-infected mice at 2 dpi. Four-week-old WT C57BL/6 mice were inoculated with 10^3 FFU of CHIKV-LR strain at day 0. At 2 dpi, spleens were harvested and processed for flow cytometry. Flow cytometry dot plots showing CD137 expression levels on CD4$^+$ and CD8$^+$ T cells, CD3$^-$NK1.1$^+$ NK cells, CD19$^+$ B cells, MHC-II$^+$CD11c$^+$ DCs and CD3$^+$NK1.1$^+$ NKT cells. Data are representative of 2 experiments.

Figure 2.6
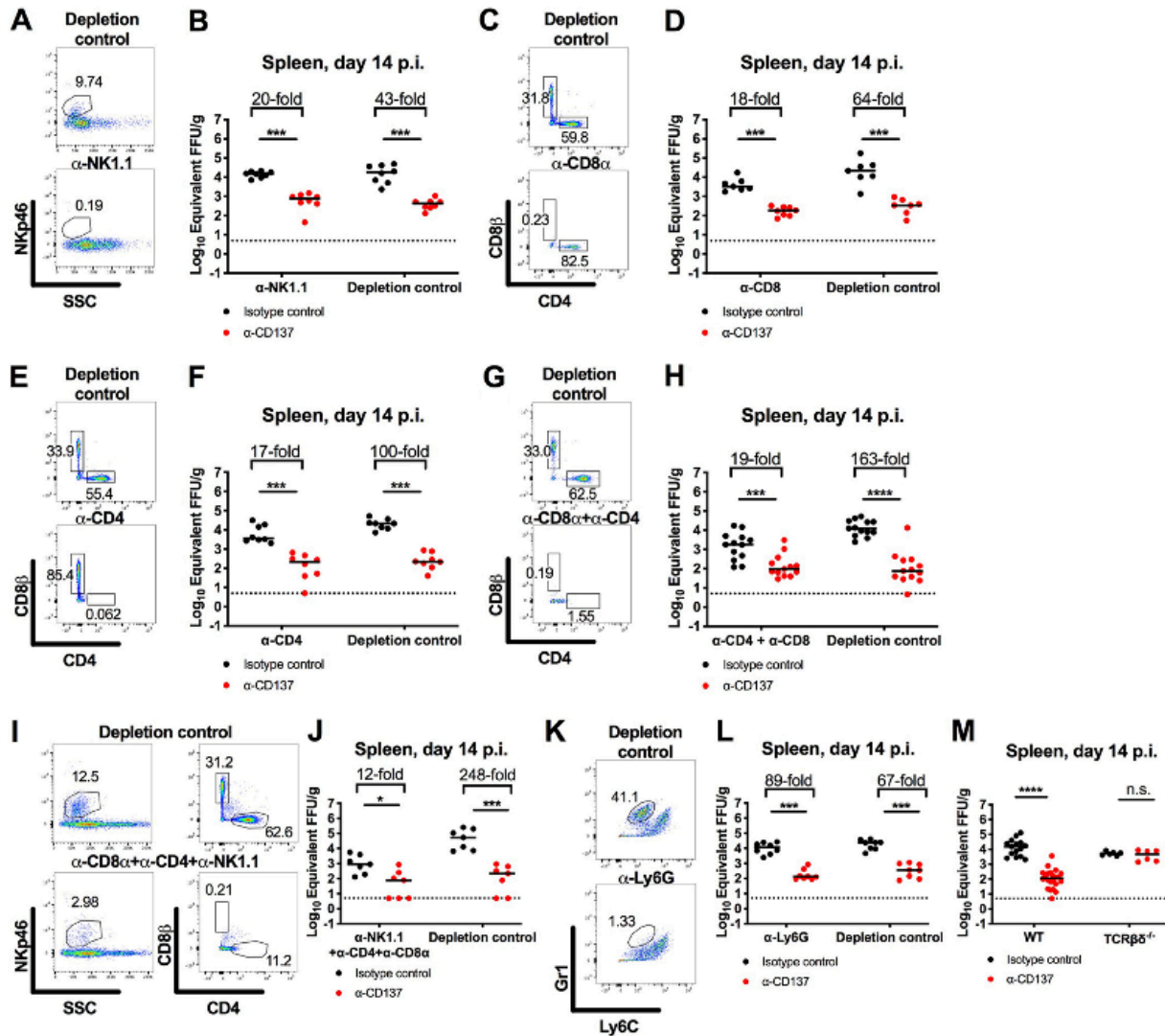
Figure 2.6. Anti-CD137 mAb-mediated clearance of CHIKV RNA in the spleen is abolished in mice lacking T cells. Four-week-old WT (**A-L**) or TCRbd^{-/-} C57BL/6 (**M**) mice were inoculated with 10^3 FFU of CHIKV-LR. At 2 dpi, 400 mg of agonistic anti-CD137 or isotype control mAb in combination with anti-NK1.1 depleting or depletion isotype control mAb (**A-B**), anti-CD8α depleting or depletion isotype control mAb (**C-D**), anti-CD4 depleting or depletion isotype control mAb (**E-F**), anti-CD8α and anti-CD4 depleting or depletion isotype control mAbs (**G-H**), anti-CD8α, anti-CD4 and anti-NK1.1 depleting or depletion isotype control mAb

(**I-J**) or anti-Ly6G depleting or depletion isotype control mAb (**K-L**) was administered via an i.p.

route. All depleting and depletion isotype control mAbs were administered every 4 days, except

for anti-Ly6G and isotype control mAbs, which were administered every 2 days. Spleens were

harvested at 14 dpi, and viral RNA was measured from tissue homogenate by qRT-PCR. Data

are pooled from 2 or 3 experiments. Each symbol represents an individual mouse, and bars

indicate median values (Mann-Whitney test: *******, $P < 0.001$; ********, $P < 0.0001$). Representative

flow cytometry dot plots confirming cell depletions are shown (**A, C, E, G, I, and K**).

Figure 2.7
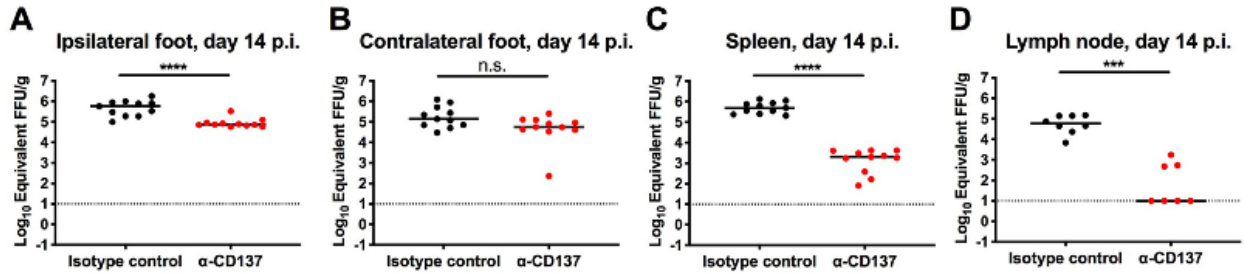
Figure 2.7. Anti-CD137 mAb treatment reduces levels of MAYV RNA in the spleen, DLN and ipsilateral foot. Four-week-old WT C57BL/6 male mice were inoculated with 10^3 FFU of MAYV-BeH407. At 2 dpi, 400 mg of agonistic anti-CD137 or isotype control mAb was administered via an i.p. route. Ipsilateral (**A**) and contralateral (**B**) feet, spleen (**C**), and DLN (**D**) were harvested at 14 dpi. Viral RNA was measured from tissue homogenates by qRT-PCR. Each symbol represents an individual mouse, and bars indicates median values. Data are pooled from 3 experiments (Mann-Whitney test: ***, $P < 0.001$; ****, $P < 0.0001$; n.s., not significant).

Chapter 3: An agonistic anti-CD137 antibody disrupts lymphoid follicle structure and T cell-dependent antibody responses

ABSTRACT

CD137 is a costimulatory receptor expressed on natural killer cells, T cells, and subsets of dendritic cells. An agonistic monoclonal antibody (mAb) against CD137 has been used to reduce tumor burden or reverse autoimmunity in animal models and clinical trials. Here, we show that mice treated with an agonistic anti-CD137 mAb have reduced numbers of germinal center B (GC B) cells and follicular dendritic cells (FDCs) in lymphoid tissues. As a result, agonistic anti-CD137 mAb treatment impairs antibody responses to multiple T cell-dependent antigens including infectious virus, recombinant viral proteins, and conjugated haptens but not to a T cell-independent antigen or at homeostasis. These effects were not due to enhanced apoptosis or impaired proliferation of B cells but instead correlated with changes in lymphoid follicle structure and GC B cell dispersal, and were mediated by CD137 signaling in CD4$^+$ and CD8$^+$ T cells. Our experiments in mice suggest that agonistic anti-CD137 mAbs used in cancer and autoimmunity therapy may cause GC collapse and impair long-term antibody and B cell memory responses.

INTRODUCTION

Agonistic monoclonal antibodies (mAbs) targeting the costimulatory receptor CD137 enhance antibody-dependent cell-mediated cytotoxicity by NK cells and proliferation, functional activity, and survival of T cells (Yonezawa et al., 2015). Because of these functions, anti-CD137 mAbs have been combined with chemotherapeutic and immunotherapeutic agents in human cancer clinical trials (Yonezawa et al., 2015). Anti-CD137 mAbs also have been evaluated in autoimmune disease animal models based on their ability to induce tolerogenic DCs and regulatory T cells (Lee et al., 2012; Seo et al., 2004).

Germinal centers (GCs) in lymphoid tissues are complex anatomical sites where somatic hypermutation and antibody isotype switching occurs. GC B cells proliferate extensively and traffic through the light and dark zones as part of an antigen-driven affinity-based clonal selection process (reviewed in (Mesin et al., 2016)). In the light zone, GC B cells recognize cognate antigens and undergo selection with the cytokine-directed input of follicular helper T cells (Tfh), which themselves are modulated by follicular regulatory T cells (Tfr) (Linterman et al., 2011). GC B cells without strong affinity for antigens or without T cell help undergo apoptosis. The GC reaction culminates in the generation of the two arms of humoral immune memory, high-affinity memory B cells (MBCs) and terminally differentiated long-lived plasma cells (LLPCs), the latter of which are professional antibody-secreting cells. Apart from follicular B cells, lymphoid tissues also contain marginal zone (MZ) B cells, which express polyreactive B cell receptors (BCR), produce natural IgM and IgG antibodies, and protect against blood-borne bacterial infection in a T cell-independent manner (Cerutti et al., 2013; Tanigaki et al., 2002).

While evaluating anti-CD137 mAb as a possible therapy for chronic alphavirus infection in mice, we unexpectedly observed reduced numbers of GC B cells (Hong et al., 2019). Here, we

evaluated the mechanistic basis and consequences of agonistic anti-CD137 mAb treatment on antibody and B cell responses in the context of immunization or virus infection in mice. During infection with chikungunya virus (CHIKV), an emerging arthritogenic alphavirus, anti-CD137 mAb treatment resulted in reduced numbers of GC B cells, MBCs, and LLPCs. Administration of anti-CD137 mAb also dampened the serum antibody response in mice immunized with other T cell-dependent antigens (influenza virus hemagglutinin (HA) and 4-hydroxy-3-nitrophenylacetyl hapten (NP)-conjugated keyhole limpet hemocyanin (KLH)), but not with a T cell-independent antigen (NP-Ficoll) or at homeostasis. The reduction of GC B cell numbers caused by anti-CD137 mAb was associated with altered GC architecture, attrition of stromal cells critical for GC formation and maintenance, and dispersal of GC B cells. Inhibition of GC formation by anti-CD137 required cell-intrinsic signaling of T cells. Thus, in mice, anti-CD137 mAb-treatment results in activation of T cells that impairs GC development and induction of long-lived antigen-specific antibody responses.

RESULTS

Anti-CD137 mAb treatment diminishes germinal centers, and antigen-specific memory B and long-lived plasma cells. Because we previously observed diminished GC numbers in CHIKV-infected mice treated with anti-CD137 mAb (Hong et al., 2019), we evaluated the effect on long-term memory B cell responses. Four-week-old C57BL/6 male mice were inoculated subcutaneously (s.c.) in the foot with CHIKV (day 0) and then injected via an intraperitoneal (i.p.) route with anti-CD137 mAb at 2 days post-infection (dpi) (**Fig 3.1A**). At 14 dpi, mice treated with anti-CD137 mAb had slightly reduced numbers of $CD19^+$ B cells in the spleen compared to isotype control mAb-treated animals (1.4-fold, $P < 0.01$; **Fig 3.1B**). However, the number of GC B cells (as determined by either peanut agglutinin lectin $(PNA)^+CD95^+$ or $GL7^+CD95^+$ staining) in the spleen at 14 dpi was reduced to a greater extent (33.3 to 43.3-fold, $P \leq 0.0001$; **Fig 3.1C-D**). To assess the long-term consequence on the antibody response, serum was obtained at 7, 14, 30, 50, 65 and 90 dpi, and the spleen and bone marrow were harvested at 90 dpi to profile antigen-specific MBCs and LLPCs (**Fig 3.1A**). Anti-CD137 mAb-treated mice had lower numbers of CHIKV-specific MBCs in the spleen (20.6-fold, $P < 0.001$) and LLPCs in the bone marrow (43.5-fold, $P < 0.001$) than isotype control mAb-treated animals (**Fig 3.1E-F**). Serum anti-CHIKV IgG levels also were reduced in anti-CD137 mAb-treated mice compared to isotype control mAb-treated animals beginning at 14 dpi (4.9 to 33.1-fold, $P \leq 0.0001$; **Fig 3.1G**).

To test the effect of anti-CD137 mAb on a later stage of the GC reaction, we treated CHIKV-infected mice with anti-CD137 mAb at 14 dpi and analyzed cell numbers at 28 dpi (**Fig 3.1H**). Although the number of total $CD19^+$ B cells did not change (**Fig 3.1I**), the number of PNA^+CD95^+ GC B cells in anti-CD137 mAb-treated mice was decreased (142-fold, $P \leq 0.0001$)

compared to isotype control mAb-treated animals (**Fig 3.1J**). We then evaluated the effect of anti-CD137 mAb on an established memory B cell response. CHIKV-infected mice were treated with anti-CD137 mAb at 56 dpi, a time when the GC reaction should be fully established (Bachmann et al., 1996; Mesin et al., 2016), and spleen and bone marrow were harvested at 90 dpi for analysis (**Fig 3.1K**). Anti-CD137 mAb-treated mice showed similar number of CHIKV-specific MBCs and only slightly reduced numbers (2-fold, *P* < 0.01) of CHIKV-specific LLPCs compared to isotype control mAb-treated animals (**Fig 3.1L-M**). Correspondingly, serum anti-CHIKV IgG levels at 90 dpi were similar between mice treated at 56 dpi with anti-CD137 or isotype control mAb (**Fig 3.1N**). These data suggest that anti-CD137 mAb treatment inhibits the development of MBCs and LLPCs but has minimal effect on the maintenance of established memory B cell compartments. However, in naïve pathogen-free mice, anti-CD137 mAb treatment did not substantially alter the relatively low number of GC B cells seen at homeostasis (**Fig 3.1O**).

Anti-CD137 mAb treatment reduces T cell-dependent but not -independent antibody responses. We evaluated the effect of anti-CD137 mAb treatment after immunization with model T cell-dependent (NP-KLH, TD) and T cell-independent (NP-Ficoll, TI) antigens (Mond et al., 1995). Four-week-old C57BL/6 male mice were immunized via i.p. route with NP-KLH or NP-Ficoll and then treated with anti-CD137 mAb two days later. Sera were obtained at multiple time points post-immunization, and at the last time point bone marrow was harvested to profile LLPCs (**Fig 3.2A and F**). Spleens from a separate cohort of mice were harvested at 30 days post-immunization to quantify MBCs. Anti-CD137 mAb treatment reduced the number of GC B cells (18-fold, *P* < 0.01) and antigen-specific LLPCs (12-fold, *P* < 0.0001) at 14 and 130 days post-immunization, respectively, in mice administered NP-KLH (**Fig 3.2B-C**). The number

of NP-specific IgG$^+$ MBCs also was reduced (7-fold, $P < 0.001$) at 30 days post-immunization (**Fig 3.2D**). Correspondingly, serum anti-NP IgG levels were diminished in anti-CD137 mAb-treated mice beginning at 28 days post-immunization (**Fig 3.2E**). In NP-Ficoll-immunized mice, the number of NP-specific LLPCs at day 130 and NP-specific IgM$^+$ MBCs at day 30 were equivalent between anti-CD137 and isotype control mAb-treated groups (**Fig 3.2G-H**), and serum anti-NP IgM and IgG levels generally were similar whether animals received anti-CD137 or not (**Fig 3.2I-J**). Thus, anti-CD137 treatment impacts B cell responses that require T cell-dependent help.

Apoptosis and proliferation of GC B cells are minimally affected by anti-CD137 mAb treatment. As reductions in GC B cells associated with anti-CD137 mAb treatment might be due to increased cell death, we stained GC B cells with annexin V, which recognizes phosphatidylserine on the plasma membrane of apoptotic cells. In this experiment, CHIKV-infected mice were treated with anti-CD137 mAb at 2 dpi. The total number of CD86^{hi}CXCR4^{lo} light zone and CD86^{lo}CXCR4^{hi} dark zone B cells were reduced slightly at 5 dpi (1.7-fold, $P < 0.01$; 1.5-fold, $P < 0.01$, respectively) but more so at 7 dpi (2.2-fold, $P < 0.0001$; 5.8-fold, $P < 0.0001$, respectively) in anti-CD137 mAb-treated mice compared to isotype control mAb-treated animals (**Fig 3.3A-C**). However, the percentage of annexin V$^+$ Viability dye$^-$ early-stage apoptotic GC B cells in light or dark zone was similar between anti-CD137 and isotype control mAb-treated animals (**Fig 3.3D, E and G**). Anti-CD137 mAb treatment also did not alter the percentage of annexin V$^+$ Viability dye$^+$ late-stage apoptotic/necrotic GC B cells in the light or dark zones (**Fig 3.3F and H**). Thus, anti-CD137 mAb treatment does not appear to cause GC B cell deficits by promoting cell death.

To determine the effect of anti-CD137 treatment on GC B cell proliferation, we injected 5-bromo-2'-deoxyuridine (Brdu) into CHIKV-infected mice and measured incorporation by GC B cells. The percentage of Brdu$^+$ proliferating GC B cells was similar between animals treated with anti-CD137 and isotype control mAb except for small differences at 4 and 5 dpi (**Fig 3.3I-K**). We also assessed whether there was any bias towards reducing the percentage of antigen-specific GC B cells by incubating cells with chikungunya virus-like particles (CHIK VLP). The percentage of CHIKV-specific GC B cells was comparable between anti-CD137 mAb-treated and isotype control mAb-treated mice except for small differences at 5 dpi (**Fig 3.4A-B**).

Anti-CD137 mAb treatment alters B cell follicle architecture. To examine whether anti-CD137 mAb affects the anatomic structures of the spleen, we performed immunofluorescence staining at 6 (**Fig 3.5A-D**), 7 (**Fig 3.5E-F**) and 14 (**Fig 3.5I**) dpi. At 6 dpi, we observed IgD$^+$ B cells surrounding CD21/35$^+$ FDCs, and some IgD$^+$ B cells at the border of the CCL21$^+$ T cell zone in isotype control mAb-treated mice (**Fig 3.5A-B**). However, in anti-CD137 mAb-treated animals, the localization of IgD$^+$ B cells at the T cell zone border was altered (**Fig 3.5C-D**). At 7 dpi, IgD$^+$ B cells surrounded FDCs in the light zone in isotype control mAb-treated mice (**Fig 3.5E**), whereas in anti-CD137 mAb-treated animals, IgD$^+$ B cells covered the FDC area (**Fig 3.5F**).

We next determined whether anti-CD137 mAb treatment altered the number of FDCs in the spleen. Flow cytometry analysis revealed that in anti-CD137 mAb-treated mice the number of FDCs was comparable at 7 dpi but reduced at 14 dpi (17-fold, $P < 0.0001$; **Fig 3.5G-H**). Immunofluorescence microscopy confirmed that at 14 dpi the numbers of FDCs and GC B cells were decreased and/or dispersed in anti-CD137 mAb-treated mice compared to isotype control mAb-treated animals (**Fig 3.5I-L**).

Anti-CD137 mAb inhibition of GC formation requires T cell-intrinsic signaling. We first evaluated a possible role of CD137 signaling on stromal cells including FDCs, by transplanting WT or CD137$^{-/-}$ bone marrow into irradiated CD137$^{-/-}$ mice (**Fig 3.6A**) and confirming reconstitution (**Fig 3.6B**). Anti-CD137 mAb treatment reduced the number of GC B cells in mice receiving WT but not CD137$^{-/-}$ bone marrow (**Fig 3.6C**). For the reciprocal experiment, TCRβδ$^{-/-}$ mice were used as recipients because some T cell subsets (*e.g.*, NKT and memory T cells) in WT recipients are radio-resistant (Yao et al., 2011), and we wanted to deplete endogenous T cells completely (**Fig 3.6D**). Anti-CD137 mAb treatment reduced the number of GC B cells in TCRβδ$^{-/-}$ mice receiving WT but not CD137$^{-/-}$ bone marrow (**Fig 3.6E**). These experiments suggest that CD137-mediated signaling in radio-sensitive, hematopoietic cells is required to reduce the number of GC B cells.

To test whether anti-CD137 mAb treatment reduced the number of GC B cells through CD137 signaling in T cells, we adoptively transferred into recipient TCRβδ$^{-/-}$ mice combinations of CD4^{+} and CD8^{+} T cells isolated from WT or CD137$^{-/-}$ mice (**Fig 3.6F**). Anti-CD137 mAb treatment reduced the number of GC B cells in mice receiving WT CD4^{+} T cells + WT CD8^{+} T cells, CD137$^{-/-}$ CD4^{+} T cells + WT CD8^{+} T cells, or WT CD4^{+} T cells + CD137$^{-/-}$ CD8^{+} T cells (15.0 to 20.5-fold, $P < 0.001$), but not in mice receiving CD137$^{-/-}$ CD4^{+} + CD137$^{-/-}$ CD8^{+} T cells (**Fig 3.6G**). Thus, CD137-mediated signaling in either CD4^{+} or CD8^{+} T cells is sufficient to inhibit GC B cell production.

Anti-CD137 mAb treatment promotes pro-inflammatory signatures in cycling CD8^{+} T cells, neutrophils, and differentiating monocytes. To define global transcriptional changes in lymphoid tissues of mice treated with anti-CD137 mAb, we performed single cell RNA sequencing (scRNAseq) on splenocytes harvested from CHIKV-infected mice during the acute

phase of infection (3 and 7 dpi). Immune cell subsets were identified by their cell type-specific gene expression: *CD3e* (T cells), *Ncr1* (NK cells), *CD79a* (B cells), *Flt3* (DCs), *Sdc1* (plasmablasts), *Adgre1* (macrophages), *S100a8* (neutrophils), and *Ccr2/Ly6c2* (monocytes) (**Fig 3.7A**).

The majority of cells expressing *Tnfrsf9*, the gene encoding CD137, were NK and T cells (**Fig 3.7B**), which were re-clustered to identify different cell subsets (*e.g.* NK cells, NKT cells, CD4$^+$ and CD8$^+$ T cells, and activated T cells) (**Fig 3.7C-D**). Among activated T cells, the frequency of cycling CD8$^+$ T cells, characterized by expression of *Ccnb2*, *Ccna2*, *Cdca3* and *Mki67* (**Fig 3.8A**), was increased in anti-CD137 mAb-treated mice compared to isotype control mAb-treated animals at 7 dpi. The cycling CD8$^+$ T cells and NK cells showed a pro-inflammatory and cytolytic signature with high transcript levels of *Gzma*, *Gzmb* and *Ccl5* (**Fig 3.8B**). The cycling CD8$^+$ T cells uniquely expressed *Gzmk* (**Fig 3.8C**). We also observed expansion of myeloid cell subsets with pro-inflammatory signatures in anti-CD137 mAb-treated mice. For example, the chemokine receptors *Ccrl2*, *Ccr1* and *Cxcr2* and *Ly6i* were expressed in the subset of *S100a8/Mmp9*-expressing neutrophils (**Fig 3.9A-F**) at higher levels at 7 dpi in anti-CD137 mAb treated mice; these cells also expressed *Cxcl2*, *Il1b*, *Ccl6*, *Csf1*, *Tnf*, *Tnfsf14*, and *Il15* (**Fig 3.9G-H**). This neutrophil subset also expressed *Irg1*, which produces itaconate, a regulator of immune cell metabolism and inflammation (Lampropoulou et al., 2016) (**Fig 3.9I-J**). Monocytes were identified by expression of *Ccr2* and *Ly6c2* (**Fig 3.7A and S4A**). Clustered with the *Ccr2*-expressing monocytes were differentiating monocytes expressing *Spic*, a marker of red pulp macrophages (**Fig 3.10B-C**). Heme moieties released from senescent or damaged erythrocytes can induce *Spic* expression in differentiating monocytes (Haldar et al., 2014), and *Hba-a1*, *Rhd* and *Tfrc* expressing reticulocytes were transiently depleted at 3 dpi, which

correlated with *Spic* induction in the monocytes (**Fig 3.10D**). Differentiating monocytes persisted in anti-CD137 but not isotype control mAb-treated mice at 7 dpi and expressed higher levels of *Cxcl10*, *Cxcl9*, *Ccl2*, *Cxcl16* and *Ccr5* (**Fig 3.10E-H**). Thus, scRNAseq analysis revealed expansion of several lymphoid and myeloid cell populations with pro-inflammatory signatures in anti-CD137 mAb-treated mice.

Anti-CD137 mAb treatment alters the number of follicular helper, regulatory, and follicular regulatory T cells. scRNAseq analysis revealed an activated CD4$^+$ T cell subset expressing genes (*Cxcr5* and *Il21*) characteristic of follicular helper T (Tfh) cells (**Fig 3.11A**) (Kuchen et al., 2007). Both RNAseq and flow cytometric data showed that at 7 dpi anti-CD137 mAb treatment resulted in a reduced frequency and number of CXCR5^{hi}PD-1^{hi} Tfh cells (2.1-fold, *P* < 0.0001) (**Fig 3.11B-C**); these T cells provide pro-survival and differentiation signals to GC B cells (Baumjohann et al., 2013). We assessed whether the decreased number of Tfh cells in anti-CD137 mAb-treated mice was linked to the reduction of GC B cells. We administered IL-2-depleting and CTLA-4-blocking mAbs: IL-2 regulates Tfh cell differentiation by negatively modulating Bcl6 expression (Ballesteros-Tato et al., 2012), and CTLA-4 regulates Tfh cell differentiation by controlling the strength of CD28 signaling (Wang et al., 2015). Combination treatment with IL-2-depleting and CTLA-4-blocking mAbs increased the number of Tfh cells in mice treated with anti-CD137 mAb to levels similar to those treated with isotype control mAb without treatment (**Fig 3.11D**). However, this treatment did not restore the number of GC B cells in anti-CD137 mAb treated mice (**Fig 3.11E**). Thus, anti-CD137 mAb-mediated reduction in GC B cells did not require reductions in Tfh cells.

By scRNAseq analysis, anti-CD137 mAb treatment increased the proportion of CD4$^+$ and CD8$^+$ T cells expressing *Foxp3* (**Fig 3.12A-C**). FoxP3 reportedly increases the expression of

Tnfrsf9 (Marson et al., 2007). Flow cytometric analysis showed that the majority of CD4$^+$ T cells expressing CD137 also expressed FoxP3 at 2 dpi (**Fig 3.12D**). Anti-CD137 mAb treatment increased the number and frequency of CD4$^+$FoxP3$^+$ Tregs (**Fig 3.12E-G**), CD4$^+$CXCR5^{hi}PD-1^{hi}FoxP3$^+$ T follicular regulatory cells (Tfr) (**Fig 3.12H-I**), and CD8$^+$FoxP3$^+$ T cells (**Fig 3.12J-K**). Because Tfr cells can modulate GC responses (Linterman et al., 2011), we used an adoptive transfer approach to assess whether the increased number of Tfr cells in anti-CD137 mAb-treated mice caused the reduction in GC B cells. T cells from CD137$^{-/-}$ mice and FoxP3$^+$ T cells sorted from FoxP3-GFP reporter mice were mixed and transferred into recipient TCRβδ$^{-/-}$ mice (**Fig 3.12L**). Although Treg and Tfr cells were reconstituted in recipient mice (**Fig 3.12M**), anti-CD137 mAb treatment failed to reduce the number of GC B cells at 14 dpi (**Fig 3.12N**). Thus, CD137 signaling exclusively on Treg and Tfr cells was not sufficient for anti-CD137 mAb-mediated reduction of GC B cells.

Anti-CD137 mAb reduces the GC B cell population defined by transcriptional signature. B cells were re-clustered to identify different cell subsets (*e.g.* follicular B cells, MZ B cells, plasmablasts, cycling B cells) (**Fig 3.7C-D**). Myc is expressed transiently in GC B precursors and establishes a cyclin D2-dependent proliferation program (Calado et al., 2012). Single cell analysis indicated that Myc-induced gene targets were expressed equivalently between anti-CD137 and isotype control mAb-treated animals (**Fig 3.13A**), suggesting that the Myc-dependent program in initiating GC precursors is not altered by anti-CD137 mAb treatment. Some of the B cell subsets were cycling based on expression of *Cdc6*, *Cdc45*, *Cdc123*, *Cdc20*, *Cdc25b*, *Cdc37* and *Mki67* (**Fig 3.13B**). A subset of the cycling B cells expressed *Ezh2* and *Dnmt1*, which silence genes inhibiting proliferation (Shaknovich et al., 2011; Velichutina et al., 2010) (**Fig 3.13C**). In this subset, we observed cells expressing *S1pr2* and *Aicda,* markers of

GC B cells (**Fig 3.13D-E**). Consistent with flow cytometry data (**Fig 3.1D**), single cell RNAseq analysis showed a lower fraction of cells with a GC B cell transcriptional signature in anti-CD137 mAb-treated animals (**Fig 3.13F**). Because CCR7 facilitates B cell migration and interaction with cognate T cells prior to the formation of GCs (Okada et al., 2005), we evaluated effects of anti-CD137 mAb treatment on *Ccr7* expression in B cells. The frequency of B cells expressing *Ccr7* was reduced in anti-CD137 mAb-treated mice compared to isotype control mAb-treated animals at 7 dpi (**Fig 3.13G**).

Anti-CD137 mAb treatment reduces the number of MZ B cells and their expression of CD21/35. The frequency of MZ B cells, characterized by expression of *Cd9*, *Dtx1*, *Fcrl5* and *Cr2*, was increased in both anti-CD137 and isotype-control mAb-treated mice at 3 dpi compared to naïve animals (**Fig 3.14A**). MZ B cell development requires Notch-RBP-J signaling (Tanigaki et al., 2002). At 7 dpi, the frequency of cells showing high expression levels of Notch signaling target genes (*e.g.*, *Dtx1* (Deltex-1, regulator of Notch signaling) and *Cr2* (Complement receptor 2)) in MZ B cells of anti-CD137 mAb-treated mice was less than in isotype control mAb-treated animals (**Fig 3.14B**). Consistently, flow cytometric analysis showed that anti-CD137 mAb treatment reduced the number of MZ B cells (2.0-fold, $P < 0.05$), but not follicular B cells at 7 dpi (**Fig 3.14C-E**). By 14 dpi, the numbers of both follicular and MZ B cells were reduced in anti-CD137 mAb treated mice compared to isotype control mAb treated animals (1.9-fold, $P < 0.01$; 3.7-fold, $P < 0.01$, respectively). B cell expression of CD21 and CD35, which encode for complement receptors, is critical for GC formation and response to T cell-dependent antigens (Carroll, 1998). Both follicular and MZ B cells showed reduced expression of CD21/CD35 at 7 dpi (1.8-fold, $P < 0.0001$; 1.7-fold, $P < 0.0001$, respectively) (**Fig 3.14F**).

Anti-CD137 mAb treatment increases the number of antigen non-specific plasmablasts and minimally alters BCR usage. Transcriptional analysis suggested that plasmablasts genes (*Xbp1*, *Irf4* and *Prdm1*) were more abundant in anti-CD137 and isotype mAb-treated mice at 7 dpi compared to naïve animals, but more so in anti-CD137 mAb-treated animals (**Fig 3.14G-H**). Indeed, flow cytometry of splenocytes showed that in anti-CD137 mAb-treated mice the total number of plasmablasts was increased at 7 dpi (2.1-fold, $P \leq 0.05$) but reduced at 14 dpi (2.9-fold, $P \leq 0.01$) (**Fig 3.14I-J**). In naïve mice, anti-CD137 mAb treatment did not alter the number of plasmablasts in the spleen (**Fig 3.14K**).

Antigen binding by BCR and subsequent signaling promotes differentiation of B cell subsets. During a primary GC reaction, germline B cells that bind to antigens undergo somatic hypermutation and clonal selection, which biases the usage of particular BCR genes in the pool of responding cells (Kuraoka et al., 2016). We evaluated whether anti-CD137 mAb treatment altered VDJ recombination and clonality of B cells by analyzing the scRNAseq data at 0 and 7 dpi. Overall, the BCR gene usage was similar between anti-CD137 mAb- and isotype control mAb-treated mice. Among the IgG clonotypes, *Igh2c* was dominantly used (**Fig 3.15A-C**). There was bias in usage of *Ighv1-80* heavy chains joined with *Igkv5-39* and *Igkv5-43* light chains in both anti-CD137 and isotype control mAb-treated CHIKV-infected mice, but not in naïve animals (**Fig 3.15A**), suggesting that these genes were selected during acute infection. There were minimal differences in V-gene usage of lambda light chains or J gene usage among anti-CD137 and isotype control mAb-treated CHIKV-infected mice and naïve animals (**Fig 3.15A-B**). Thus, the BCR usage seems minimally altered by anti-CD137 mAb treatment.

Even though there was an expansion of plasmablasts in anti-CD137 mAb-treated mice compared to isotype control mAb-treated animals, this did not occur at a clonal level (**Fig**

58

3.15C). The number of CHIKV-specific plasmablasts was similar between anti-CD137 mAb- and isotype control mAb-treated mice (**Fig 3.14L**). Thus, it appears that B cells with low or no affinity for CHIKV antigens prematurely differentiated into plasmablasts in anti-CD137 mAb-treated animals.

Anti-CD137 mAb-mediated increase in plasmablasts is abrogated by a type 2 immune response. At early stages of the immune response, B cells can differentiate into plasmablasts through T cell-dependent or -independent programs (Saito et al., 2007). We tested whether the expansion of plasmablasts in the anti-CD137 mAb-treated mice required CD40L interaction on T cells using a blocking mAb. Anti-CD137 mAb treatment increased the number of plasmablasts regardless of whether anti-CD40L blocking mAb was administered (**Fig 3.14M**), suggesting that anti-CD137 mAb treatment results in expansion of early plasmablast compartment in the spleen at 7 dpi through a pathway that at least is partially independent of CD40/CD40L signaling.

Because anti-CD137 mAb treatment drives a type 1, pro-inflammatory immune response (Sun et al., 2002), we tested whether skewing towards a type 2 immune response program would reverse the plasmablast phenotype. Indeed, the number of plasmablasts was not increased in mice given anti-CD137 mAb and the IL-4-anti-IL-4 antibody complexes (Reese et al., 2014) (**Fig 3.14N**). Thus, the type 1 immune response induced by anti-CD137 mAb that is disrupted by exogenous IL-4 treatment appears to contribute the expanded number of plasmablasts after CHIKV infection.

Anti-CD137 mAb treatment effects on GC B cells, antigen-specific MBCs, and antigen-specific plasmablasts in the context of viral vaccine immunization or boosting. Tfh and FDCs within secondary lymphoid follicles promote rapid activation and differentiation of

MBCs upon antigen re-encounter. Since we observed that anti-CD137 mAb treatment disrupted secondary lymphoid follicles, and given its possible use in humans, we tested its effect on an anamnestic response to a vaccine. Influenza virus hemagglutinin is a well-defined antigen that elicits neutralizing antibodies (Impagliazzo et al., 2015). Nine-week-old C57BL/6 female mice were injected via intramuscular route with influenza A virus H5 hemagglutinin proteins (day 0) and then injected i.p. with anti-CD137 mAb at 2 days post-immunization (**Fig 3.16A**). At 28 days post-immunization, the mice were boosted with a second dose of H5 protein. The number of GC B cells, antigen-specific MBCs and plasmablasts were reduced in anti-CD137 mAb-treated mice compared to isotype control mAb-treated animals 7 days after secondary boosting (11.6-fold, $P < 0.001$; 30.5-fold, $P < 0.001$; 281-fold, $P < 0.001$, respectively) (**Fig 3.16B-D**). In another group of mice, we administered anti-CD137 mAb the day prior to boosting to assess for effects of anti-CD137 mAb treatment on the anamnestic B cell response (**Fig 3.16E**). The numbers of GC B cells and antigen-specific MBCs but not antigen-specific plasmablasts were reduced in anti-CD137 mAb-treated mice compared to isotype control mAb-treated animals 7 days after boosting (12.9-fold, $P < 0.001$; 7.1-fold, $P < 0.001$; and not significant, respectively) (**Fig 3.16F-H**). Thus, during an anamnestic memory response, anti-CD137 mAb treatment affects the secondary GC B cell and MBC response while having a minimal effect on plasmablast differentiation from pre-existing MBCs.

DISCUSSION

In this study, we have shown that administration of anti-CD137 mAb early (day 2) but not late (day 56) after CHIKV infection dampens the durable humoral immune response as judged by marked reductions in antigen-specific MBCs, LLPCs, and serum antibody titers. Similarly, long-lasting antibody responses were impaired in response to NP-KLH, a T cell-dependent antigen, but not NP-Ficoll, a T cell-independent antigen. The inhibition of GC formation in anti-CD137 mAb-treated mice was not associated with increased cell death or decreased proliferation of GC B cells but correlated with a disorganized architecture of the B cell follicle. The anti-CD137 mAb-mediated inhibition of GC B cells required CD137 signaling on either $CD4^+$ or $CD8^+$ T cells. In addition to its effects on GC formation, anti-CD137 mAb treatment also reduced the number of MZ B cells and increased the number of antigen non-specific plasmablasts, which was reversed by IL-4-anti-IL-4 complex treatment. Administration of anti-CD137 mAb prior to boosting with an influenza virus hemagglutinin protein antigen reduced the secondary GC reaction but did not affect the differentiation of antigen-specific plasmablasts.

GCs are dynamic structures where antigen-specific B cells activated by cognate T cells ingress and egress. Upon antigen engagement, CCR7-expressing B cells migrate to the borders of T cell zones where they interact with cognate T cells before forming GCs (Okada et al., 2005). We observed that the frequency of *Ccr7*-expressing B cell subset was reduced in anti-CD137 mAb-treated mice. This was consistent with imaging experiments where we observed an altered pattern of cells at the B cell-T cell border. During GC reaction, expansion and maintenance of GC B cells requires cognate help from Tfh cells and input from stromal cells including FDCs that reside within lymphoid follicles (Endres et al., 1999). Our observations describing a

disrupted B cell follicular architecture are consistent with an earlier report, which showed that anti-CD137 mAb treatment diminished GC formation and FDC networks, although that study was limited to immunohistochemistry analysis up to 14 days after immunization with sheep red blood cells and KLH (Sun et al., 2005). Because the proportion of GC B cells undergoing apoptosis or proliferation was similar between anti-CD137 and isotype control mAb-treated mice, we hypothesize that the inflammatory environment induced by anti-CD137 mAb-activated T cells resulted in improper GC B cell priming due to altered architecture, which in turn resulted in GC collapse and dispersal of activated B cells.

V(D)J recombination establishes a diverse BCR repertoire, and subsequent somatic hypermutation and class switching after antigen encounter promote affinity maturation and effector function differentiation. In anti-CD137 mAb-treated infected mice, some B cells with low or no affinity for viral antigens may differentiate prematurely into plasmablasts. Indeed, we observed comparable numbers of CHIKV-specific plasmablasts in anti-CD137 and isotype control mAb-treated mice, even though the total number of plasmablasts was increased in anti-CD137 mAb-treated animals. Although anti-CD137 mAb treatment resulted in the expansion of the early plasmablast response, the inhibition of the GC reaction led to dampened long-term antigen-specific antibody responses.

Anti-CD137 mAb when given at 2 days after the first immunization of influenza hemagglutinin protein globally impaired anamnestic B cell responses at 7 days after the secondary booster immunization. However, when anti-CD137 mAb was given the day before secondary boosting, the number of antigen-specific plasmablasts was not reduced, suggesting that this response does not require a secondary GC reaction. After primary immunization, CXCR5-expressing memory Tfh cells accumulate at the B cell-T cell border and mediate

efficient recall antibody responses (Aiba et al., 2010; MacLeod et al., 2011). Upon encountering specific antigens during secondary infection or immunization, MBCs present antigen to cognate CD4$^+$ T cells and proliferate and differentiate rapidly into plasmablasts (Aiba et al., 2010; Kurosaki et al., 2015). Thus, when given prior to boosting, anti-CD137 mAb likely does not affect interaction between MBCs and cognate memory Tfh cells. In contrast, anti-CD137 mAb likely hinders the secondary GC reaction of pre-existing MBCs. During the recall response, exogenous antigens bound by antibodies may be transported to FDCs, which then present immune complexes to MBCs for further rounds of affinity maturation and LLPC differentiation (Hanna and Szakal, 1968). Since mice treated with anti-CD137 mAb show perturbed GC architecture, secondary MBC differentiation likely becomes compromised.

Although agonistic anti-CD137 mAb are being considered as treatments for cancer and autoimmune diseases (Foell et al., 2003; Mittler et al., 2004; Yonezawa et al., 2015), their mechanism(s) of action remain unclear, and possible collateral effects on immune responses are understudied. Ligation of CD137 in DCs was reported to enhance expression of retinal dehydrogenase, which induces differentiation of FoxP3$^+$ regulatory T cells (Lee et al., 2012). In a mouse model of collagen type II-induced arthritis, anti-CD137 mAb treatment induced expansion of CD11c$^+$CD8$^+$ T cells that produced IFNγ, which in turn induced tolerogenic DCs (Seo et al., 2004). Here, we showed that agonistic anti-CD137 mAb treatment inhibited humoral and cellular B cell responses, which could be another explanation for its utility in autoimmunity. Our data establish that T-cell-intrinsic signaling is required for CD137-dependent reduction in GC formation. This conclusion is consistent with a prior study showing that anti-CD137 mAb treatment diminished FDC networks in WT but not T cell-deficient mice (Sun et al., 2005). While the precise mechanism by which CD4$^+$ and CD8$^+$ T cells damage the FDC network

remains to be elucidated, our study establishes how anti-CD137 mAb compromises induction of memory responses in the B cell compartment. Although a corroborating analysis of human subjects is warranted, anti-CD137 mAb treatment in the context of immunotherapy could diminish or prevent antibody and memory responses to newly-administered vaccines or infection with pathogens.

Methods

Viruses and cells. The recombinant CHIKV La Reunion OPY1 strain was generated from *in vitro* transcribed cDNA as described previously (Tsetsarkin et al., 2006). The resultant virus was propagated once in C6/36 *Aedes albopictus* cells and titrated using Vero cells and a focus-forming assay as described (Pal et al., 2013).

Animal studies. All animal experiments were performed with the approval of Washington University Institutional Animal Care and Use Committee guidelines. All mouse infection studies were performed in an animal biosafety level 3 laboratory. C57BL/6J (000664), B6.129P2-Tcrb[tm1Mom] Tcrd[tm1Mom]/J (002121; abbreviated TCRβδ^{-/-}), C.Cg-Foxp3[tm2Tch]/J (006769; abbreviated FoxP3-GFP) and B6.SJL-Ptprc[a] Pepc[b]/BoyJ (002014) were purchased from Jackson Laboratories. CD137^{-/-} mice (Kwon et al., 2002) were obtained as a gift from Michael Croft (La Jolla Institute for Immunology). At 4 weeks of age, male mice were anesthetized with ketamine hydrochloride (80 mg/kg) and xylazine (15 mg/kg) and inoculated s.c. in the left rear footpad with 10^3 focus-forming units (FFU) of CHIKV in 10 μl of PBS. For immunization with NP-Ficoll (Biosearch Technologies) or NP-KLH (Biosearch Technologies), 4-week-old C57BL/6J male mice were injected via i.p. route with 5 μg of NP-Ficoll in 200 μl of PBS or 10 μg of NP-KLH in 100 μL of alum mixture (1:1 ratio of immunogen in PBS to alum (Thermo)). For administration of IL-4-anti-IL-4 antibody complexes, 5 μg of recombinant murine IL-4 (Peprotech) and 25 μg of anti-IL4 mAb (clone 11B11, Bioxcell) were mixed in 100 μl of PBS at 4°C for 30 min before injection. For immunization with influenza A virus H5 hemagglutinin, 9-week-old C57BL/6J female mice were injected via intramuscular (i.m.) route with 10 μg of recombinant H5 HA (Ellebedy et al., 2014) in 50 μL of antigen:AddaVax (1:1) (InvivoGen). At the termination of experiments, mice were euthanized and perfused via intracardiac injection

with PBS. For proliferation assays, CHIKV-infected mice were injected via intravascular route with 1 mg of Brdu in 100 μL of PBS two hours before harvest.

Antibodies and cell depletions. Anti-CD137 mAb (clone 2A, rat Ig2a) has been described previously (Wilcox et al., 2002b). Ab was purified from hybridoma supernatants by protein G affinity chromatography by a commercial vendor (BioXCell). Anti-IL-2 (clone S4B6-1), anti-CTLA-4 (clone 9D9), anti-CD40L (clone MR-1), mouse IgG2a (clone 2A3) and mouse IgG2b (clone MPC-11) served as controls for IL-2 depletion and CTLA-4 blockade, respectively. Polyclonal Armenian hamster IgG was used a control for CD40L blockade and purchased from BioXCell. Mice were administered 400 μg of anti-CD137 or rat Ig2a isotype control mAb (clone 2A3, BioXCell) via i.p. route at 2 dpi. For IL-2 depletion studies, mice were administered 500 μg of anti-IL-2 mAb on 2, 4 and 6 dpi. For CTLA-4 blockade, mice were administered 500 μg of anti-CTLA-4 mAb on 2 dpi and 250 μg on 5 dpi. For CD40L blocking experiments, mice were administered 500 μg of anti-CD40L mAb on 2 dpi and every 3 days thereafter until 7 dpi.

Immune cell analysis. Spleens were minced and incubated for 30 min at 37°C in 2 ml digestion buffer (1 mg/ml collagenase (Sigma) and 100 mg/mL DNase I (Sigma) in Dulbecco's Modified Eagle's medium (DMEM) containing 2% FBS in a 24-well plate. Cell suspensions were passed through a 100 μm cell strainer. After rinsing with 10% FBS, 5 mM EDTA in DMEM, erythrocytes were lysed with 1 mL of ACK Lysing Buffer (Gibco) per spleen for 2 min. Cells were washed with DMEM and centrifuged, followed by rinsing with washing buffer (2% FBS, 5 mM EDTA in PBS). After centrifugation, cells were resuspended in washing buffer at 5 x 10^8 cells/ml and incubated with 2.5 mg of anti-mouse CD16/32 antibody (101302, Biolegend) per 10^8 cells for 20 min on ice. Then, cells were stained with BV605-conjugated anti-CD45 (103140, Biolegend), PE-Cy7-conjugated anti-CD3 (100320, Biolegend), APC-Cy7-conjugated

anti-CD19 (115530, Biolegend), FITC-conjugated anti-CD21/35 (553818, BD Biosciences), PE-conjugated anti-CD95 (554258, BD Biosciences), Alexa647-conjugated anti-FoxP3 (126408, Biolegend), biotinylated anti-CXCR5 (145510, BIolegend), BV421-conjugated anti-CD4 (100438, Biolegend), PerCP/Cy5.5-conjugated anti-CD8α (100734, Biolegend), Alexa647-conjugated anti-CD86 (105019, Biolegend), PE-conjugated anti-CXCR4 (146505, Biolegend), FITC-conjugated anti-PD-1 (135214, Biolegend), BV510-conjugated anti-CD45.1 (110741, Biolegend), Alexa700-conjugated anti-CD45.2 (56-0454-82, eBioscience), PE-conjugated anti-CD23 (101608, Biolegend), Alexa647-conjugated anti-CD138 (142526, Biolegend), BV421-conjugated anti-TACI (742840, BD Biosciences), biotinylated anti-IgG (B7022, Sigma), BV421-conjugated anti-IgM (406517, Biolegend), Alexa647-conjugated anti-CD38 (102716, Biolegend), BV510-conjugated anti-IgD (405723, Biolegend), PerCP/Cy5.5-conjugated anti-GL7 (144609, Biolegend) antibody, biotinylated PNA (B-1075, Vector), Alexa647-conjugated streptavidin (S32357, Invitrogen) and eFluor506 fixable viability dye (65-0866-14, eBioscience). For detection of apoptosis, an annexin V detection kit eFluor450 (88-8006-72, eBioscience) was used according to the manufacturer's instructions. For proliferation detection, the Brdu flow kit (559619, BD) was used according to the manufacturer's instructions. To confirm CD137 expression, cells were stained with biotinylated anti-CD137 (106104, Biolegend). For detection of NP-specific and hemaglutinin-specific memory B cells, cells were stained sequentially with PE-conjugated NP (N-5070-1, LGC Biosearch Technologies) or biotinylated H5 (IT-003-0052ΔTMp, Immune Technology). Subsequently, cells were fixed with BD FACS Lysing Solution, processed on a LSR Fortessa X-20 (BD Biosciences) flow cytometer, and analyzed using BD FACSDiva and FlowJo software.

Single cell RNA sequencing. Isolated single cell suspensions were subjected to droplet-based massively parallel single cell RNA sequencing using Chromium Single Cell 5' Reagent Kit in a BSL-3 level laboratory as per manufacturer's instructions (10x Genomics). Briefly, cell suspensions were loaded at 1,000 cells/μL with the aim to capture 10,000 cells/well. The 10x Chromium Controller generated GEM droplets, where each cell was labeled with a specific barcode, and each transcript labeled with a unique molecular identifier (UMI) during reverse transcription. The barcoded cDNA was isolated via a Dynabeads MyOne SILANE bead cleanup mixture and amplified 13 cycles. Amplified cDNA was purified via SPRI bead cleanup and removed from the BSL-3 space for library generation.   For gene expression libraries, 50 ng of amplified cDNA was used for library preparation, consisting of fragmentation, end repair, A-tailing, adapter ligation and sample index PCR as per the manufacturer's instructions. Libraries were sequenced on a NovaSeq S4 (200 cycle) flow cell, targeting 45,000 read pairs/cell. For B Cell repertoire libraries, 2 μl of amplified cDNA underwent two rounds of Target Enrichment using nested primer pairs specific for mouse B cell Ig constant regions. 50 ng of the target enrichment PCR product was used for library preparation, consisting of fragmentation, end repair, A-tailing, adapter ligation and sample index PCR as per the manufacturer's instructions. Enriched libraries were sequenced on a NovaSeq S4 (200 cycle) flow cell, targeting 5,000 read pairs/cell. All sequencing data have been submitted to the GEO database (GSE accession number assignment pending).

scRNAseq analysis. Sample demultiplexing, barcode processing, and single-cell 5' counting was performed using the Cell Ranger Single-Cell Software Suite (10x Genomics). Cellranger count was used to align samples to the mm10 reference genome, quantify reads, and filter reads with a quality score below 30. The resultant files were input into Seurat for

normalization across all samples and merging. The Seurat package in R was used for subsequent analysis (Butler et al., 2018). Cells with mitochondrial content greater than 5 percent were removed for downstream analysis. Data were normalized using a scaling factor of 10,000, and number of Unique Molecular Identifiers was regressed with a negative binomial model. Principal component analysis was performed using the top 3,000 most variable genes and t-SNE analysis was performed with the top 10 PCAs. Clustering was performed using the FindClusters function which works on K-nearest neighbor graph model with the granularity ranging from 0.1-0.9 and selected 0.6 for the downstream clustering. For identifying the markers for each cluster, we performed differential expression of each cluster against all other clusters identifying negative and positive markers for that cluster. Nuclei from different cell types (*e.g.*, NK cells/T cells and B cells) were re-clustered to further analyze transcripts in each cell type.

B cell clonal analysis. The sequencing reads were preprocessed using 10X Genomics' cellranger vdj package. The B cell receptor (BCR) sequences were assembled using the mouse IMGT database and variable V, J, and constant chain alleles were called for both heavy and light chain. BCRs with identical CDR3 nucleotide sequences were assigned to the same clonal family irrespective of their V, J, and constant region calls, which are the standard parameters. Among all sequenced cells, B cells were identified by transcriptome analysis. Briefly, reads were mapped against the *Mus musculus* genome (mm10-3.0.0) using cellranger count, which included STAR aligner (Dobin et al., 2013) and HTSeq (Anders et al., 2015). The gene expression table was restricted to the 500 genes with the highest Fano factor and log transformed. PCA with 30 components was then used to reduce dimensionality, pairwise correlation distances were then used to construct a k-nearest neighbor graph with k=15 and a threshold for edge calling of ≥0.2. Unsupervised clustering on the graph was performed using Leiden (Traag et al., 2019), constant

Potts model optimization, and a resolution parameter of 0.001. Clonal analysis was performed for heavy and light chains separately. Clonal graph plots were restricted to families with ≥ 2 members. All plots were generated via custom Python 3.7 scripts. The code for the whole B cell clonal analysis is available at https://github.com/iosonofabio/BCR_Zanini_Diamond.

Immunofluorescence imaging. Spleens were fixed in periodate-lysine-paraformaldehyde buffer for 48 h, and moved to 30% sucrose in PBS for at least 24 h before embedding. Tissues were embedded in optimal-cutting-temperature medium (Electron Microscopy Sciences) in longitudinal orientation and frozen in dry-ice-cooled isopentane. 18-μm sections were cut on a Lecia cryostat (Leica Microsystems), blocked with 10% bovine and donkey serum, and then stained with combinations of the following antibodies: anti-ERTR7 (51824, Abcam), anti-CD21/35 (2033272, Invitrogen), anti-CD4 (ab183685, Abcam), Alexa555-conjugated anti-rabbit IgG (A21428, Invitrogen), Alexa700-conjugated anti-B220 (103232, Biolegend), Alexa647-conjugated anti-GL7 (144606, Biolegend), Alexa647-conjugated anti-goat IgG (A21447, Invitrogen), biotinylated anti-IgD (1120-08, Southern Biotech) antibody and Alexa555-conjugated streptavidin (S32355, Invitrogen). Images were acquired on a Leica SP8 confocal microscope equipped with acousto-optical tunable filters, HyD hybrid detectors, and a 700 nm wavelength laser (Leica Microsystems). Images were merged from tilescans acquired with a 40X objective. Images were processed and analyzed using Imaris (Bitplane). FDC area was calculated using the "Surfaces" function of Imaris and measured only FDCs networks in follicles that contained FDCs. GC B cells were marked using the automated "Spots" function of Imaris. The percentage of GC B cells far away from FDCs were calculated using the Imaris XT module "Spots and Surfaces Distance." GC B cells were considered far away from FDCs if they

were greater than 10 μm from the closest FDC surface. The distance between GC B cells was calculated using the Imaris XT module "Spots to Spots Closest Distance."

Adoptive transfer experiments. Minced spleens from naïve WT or CD137$^{-/-}$ mice were passed through a 70 μm cell strainer to generate single cell splenocyte suspensions. After lysis of erythrocytes, CD4$^+$ and CD8$^+$ T cells were isolated using the CD4$^+$ or CD8α$^+$ T Cell Isolation Kits (130-104-454 and 130-104-075, respectively, Miltenyi Biotec) according to the manufacturer's instructions. 4.3 x 10^6 CD4$^+$ T cells and 2.8 x 10^6 CD8$^+$ T cells were mixed and adoptively transferred into TCRβδ$^{-/-}$ mice. After 5 days, the recipient mice were inoculated with 10^3 FFU of CHIKV. For adoptive transfer of FoxP3$^+$ T cells, spleens from naïve CD137$^{-/-}$ mice and FoxP3-GFP reporter mice were processed as described above. T cells were isolated using the Pan T Cell Isolation Kit (130-090-130, Miltenyi Biotec). The isolated T cells were sorted using a BD FACS Aria II. 1.3 x 10^5 sorted FoxP3$^+$ T cells and 7.1 x 10^6 CD137$^{-/-}$ T cells were adoptively transferred into TCRβδ$^{-/-}$ mice.

ELISA. MaxiSorp 96-well flat-bottom ELISA plates (44-2404-21, Thermo) were coated with 2 μg/ml of CHIKV E2 protein (Pal et al., 2013) or 20 μg/ml of NP-conjugated chicken gamma globulin (NP-CGG, Biosearch Technologies) overnight at 4°C. Plates were washed with ELISA wash buffer (PBS, 0.05% Tween-20) and then incubated with blocking buffer (PBS, 5% FBS) for 4 h at 37°C. Sera from CHIKV-infected, NP-KLH- or NP-Ficoll-immunized mice were added in 3-fold dilutions starting with a 1/100 dilution. After incubating for 1 h at room temperature, plates were rinsed with ELISA wash buffer and then incubated with biotinylated anti-IgG (115-065-062, Jackson ImmunoResearch) for 1 h at room temperature. After washing, plates were incubated with streptavidin-conjugated HRP (SA-5004, Vector Laboratories) for 30 min at room temperature. After final rinses with ELISA wash buffer and PBS, substrate solution

(34029, Thermo) was added. The reaction was quenched with 2N H_2SO_4, and the plates were read using a Synergy H1 Hybrid Reader (BioTek). The optical density (OD) value of naïve serum was subtracted from OD values of CHIKV-infected or NP-Ficoll- or NP-KLH-immunized samples, and non-linear regression curves were calculated. The titer of anti-CHIKV or anti-NP was defined as the dilution of serum yielding a half-maximal OD value after background and naïve value subtraction.

MBC limiting dilution assay. 96-well flat-bottom feeder cell plates were seeded with BAFF- and CD40L-expressing feeder cells the day before B cell isolation and were incubated with 5 μg/ml of mitomycin C at 37°C and 5% humidified CO2 for 3 h, as described before (Purtha et al., 2011). Splenocyte suspensions from CHIKV-infected mice were centrifuged and resuspended in washing buffer (1% FBS, 2 mM EDTA in PBS). $CD19^+$ B cells were isolated using CD19 MicroBeads (130-052-201, Miltenyi Biotec) according to the manufacturer's protocol. The isolated B cells were cultured (RPMI, 10% FBS, 1X penicillin-streptomycin, 1 mM sodium pyruvate, 0.1 mM non-essential amino acids, 10 mM HEPES, 50 μM β-mercaptoethanol) in 5-fold dilutions starting at 1,000,000 cells per well in the feeder cell plates sealed with an adhesive film at 37°C and 5% humidified CO_2 for 6 days. To calculate the frequency of CHIKV-specific MBCs that produced IgG, MaxiSorp 96-well flat-bottom ELISA plates (44-2404-21, Thermo) were coated with 2 μg/ml of CHIKV E2 protein (Pal et al., 2013) overnight at 4°C. Plates were washed with ELISA wash buffer (PBS, 0.05% Tween-20) and blocked with blocking buffer (PBS, 5% FBS) for 4 h at 37°C. Supernatants from B cell culture were added to the ELISA plates (50 μl per well) and processed as described above for serum antibodies. Positive wells were defined as wells that scored 2-fold over the mean OD of negative control wells (wells containing feeder cells and naïve B cells). The frequency of CHIKV-specific

MBCs was calculated as one cell per the number of cells plated where 63.2% of wells were positive.

ELISpot assay. Mixed cellulose filter 96-well plates (Millipore) plates were pre-coated with 50 μg/ml of CHIKV E2 protein (Pal et al., 2013), 20 μg/ml of NP-CGG (Biosearch Technologies) or 2 μg/ml of H5 (Ellebedy et al., 2014) overnight at 4°C. After rinsing with ELISA wash buffer and PBS, plates were blocked for 4 h at 37°C with culture medium (RPMI, 10% FBS, penicillin-streptomycin, 1mM sodium pyruvate, 0.1 mM non-essential amino acids, 10 mM HEPES, and 50 μM β-mercaptoethanol). For LLPC assays, bone marrow from the tibia and femur was filtered through 40 μm cell strainer. For plasmablast assays, single cell splenocyte suspensions were generated as detailed above. Erythrocytes were lysed, and CD138$^+$ cells were isolated using CD138 MicroBeads (130-098-257, Miltenyi Biotec). The isolated cells were incubated (RPMI 1640, 10% FBS, penicillin-streptomycin, 1 mM sodium pyruvate, 0.1 mM non-essential amino acids, 10 mM HEPES, 50 μM β-mercaptoethanol) on the antigen-coated filter plates at 37°C and 5% humidified CO_2 overnight, except for H5-specific plasmablasts which were incubated for 4 h. After washing with PBS, plates were incubated with 1% NP40 (Sigma) for 20 min at room temperature. Plates were washed with ELISA wash buffer and incubated sequentially with biotinylated anti-IgG (B7022, Sigma) and streptavidin-conjugated horseradish peroxidase (HRP; SA-5004, Vector Laboratories), each for 1 h at room temperature. After additional washes with PBS, substrate solution (5510-0050, SeraCare) was added. The reaction was quenched by washing with water. Spots were enumerated using a Biospot plate reader (Cellular Technology).

Bone marrow transplantation. Four-week-old CD137$^{-/-}$ mice were irradiated with 900 Rads and reconstituted via intravenous injection with 3 x 10^7 bone marrow cells isolated from

the femur and tibia of WT (CD45.1) or CD137$^{-/-}$ mice (CD45.2). After 8 weeks, immune cell reconstitution was confirmed by flow cytometry.

Statistical analysis. All data were analyzed with GraphPad Prism software. For immune cell analysis, data were analyzed by the Mann-Whitney test or Kruskal-Wallis ANOVA with Dunn's post-test. A Mann-Whitney test in lieu of an unpaired t test was used throughout for consistency, as some data did not show Gaussian distribution or had points at the level of detection. For serum antibody titer analysis, data were analyzed by two-way ANOVA with Sidak post-test. *P* values of less than 0.05 indicated statistically significant differences.

FIGURES

Figure 3.1
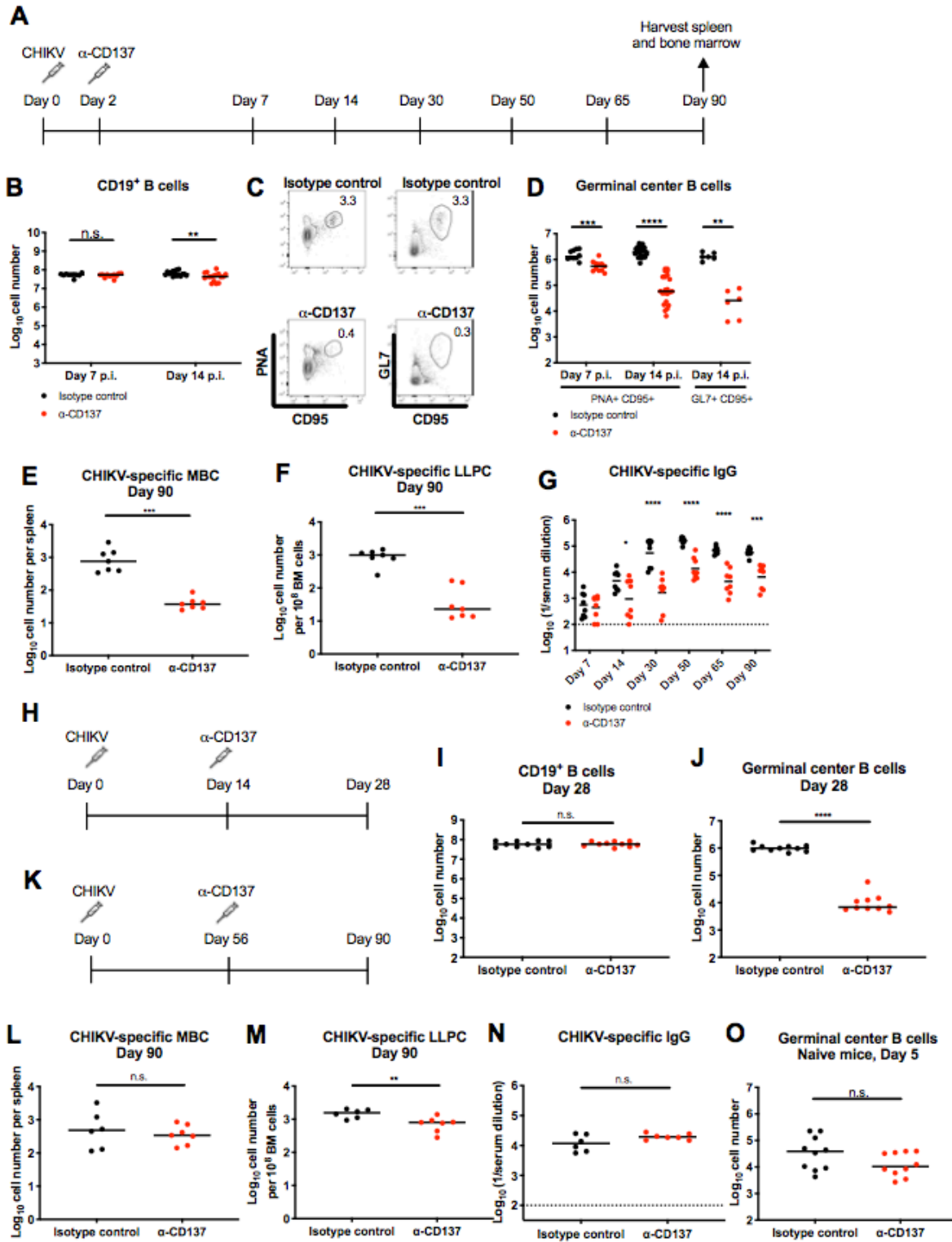
Figure 3.1 Anti-CD137 mAb treatment reduces the number of GC B cells, antigen-specific MBCs and LLPCs when given prior to GC formation. (**A-G**) Four-week-old WT C57BL/6 male mice were inoculated with 10^3 FFU of CHIKV. At 2 dpi, 400 mg of agonistic anti-CD137 or isotype control mAb was administered via an i.p. route. The number of total CD19$^+$ B cells (**B**), PNA$^+$CD95$^+$ or GL7$^+$CD95$^+$ GC B cells (**C-D**) in the spleen at 7 and 14 dpi was analyzed by flow cytometry. (**C**) Representative dot plots of GC B cells are shown. At day 90 dpi, spleen and bone marrow were harvested to assess antigen-specific MBCs (**E**) and LLPCs (**F**). (**G**) Serum was harvested at 7, 14, 30, 50, 65 and 90 dpi and anti-CHIKV IgG titers were measured. (**H-J**) Four-week-old WT C57BL/6 male mice were inoculated with 10^3 FFU of CHIKV. At 14 dpi, 400 mg of agonistic anti-CD137 or isotype control mAb was administered via an i.p. route. The number of total CD19$^+$ B cells (**I**) and PNA$^+$CD95$^+$ GC B cells (**J**) in the spleen at 28 dpi was analyzed by flow cytometry. (**K-N**) Four-week-old WT C57BL/6 male mice were inoculated with 10^3 FFU of CHIKV. At 56 dpi, 400 mg of agonistic anti-CD137 or isotype control mAb was administered via an i.p. route. At 90 dpi spleen and bone marrow were harvested to assess antigen-specific MBCs (**L**) and LLPCs (**M**). At this time, anti-CHIKV IgG titers (**N**) also were measured. (**O**) Four-week-old naïve WT C57BL/6 male mice were administered with 400 mg of agonistic anti-CD137 or isotype control mAb via an i.p. route. The numbers of PNA$^+$CD95$^+$ GC B cells in the spleen at 5 days after treatment were analyzed by flow cytometry. In this Figure, symbols represent individual mice, and bars indicate median values. Data are pooled from 2 to 4 experiments (Mann-Whitney test, except for serum antibody titers where two-way ANOVA with Sidak post-test was used: *, $P < 0.05$; **, $P < 0.01$; ***, $P < 0.001$; ****, $P < 0.0001$; n.s., not significant).

76
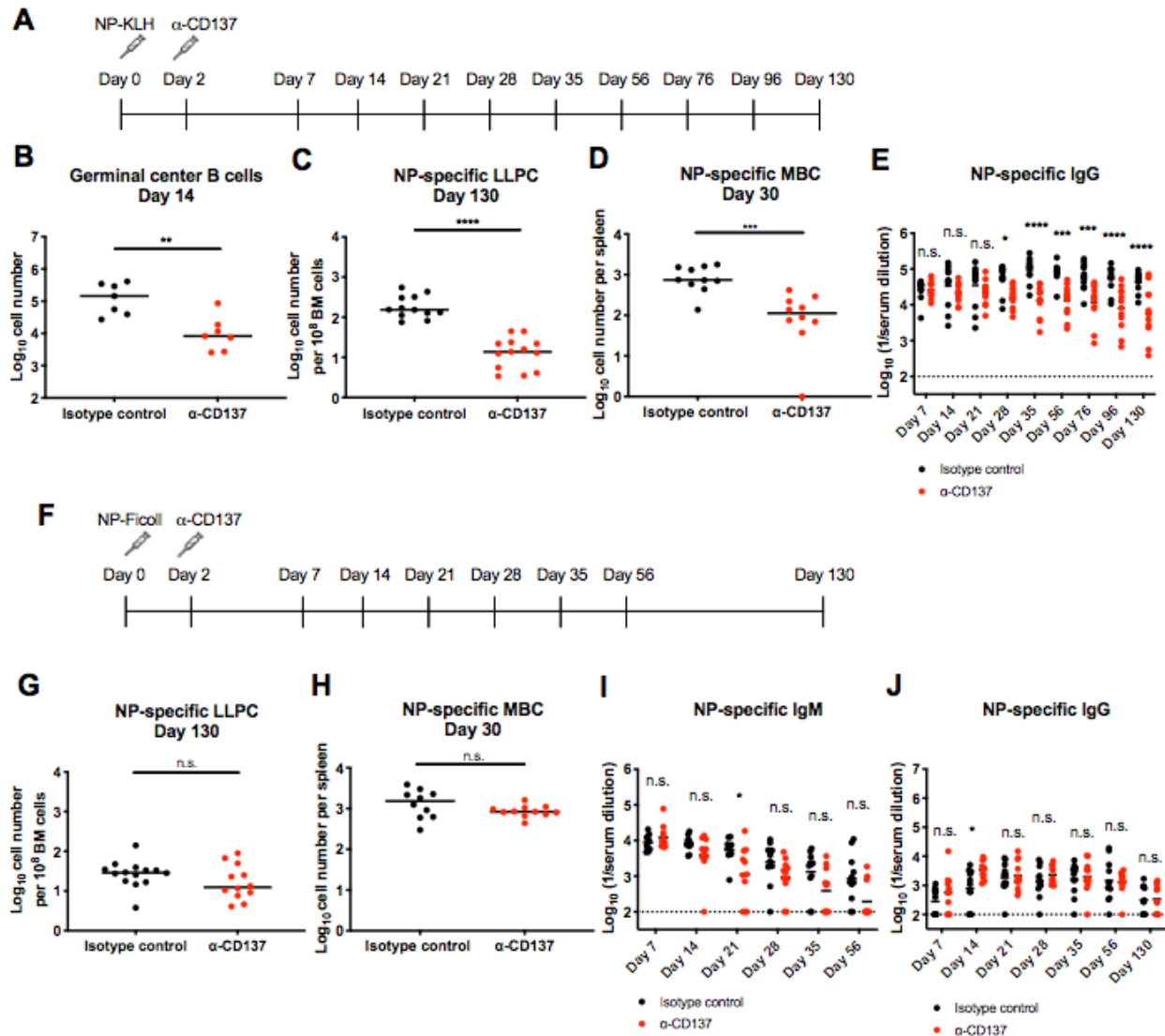
Figure 3.2

Figure 3.2. Anti-CD137 mAb treatment dampens T cell-dependent antibody responses. Four-week-old C57BL/6 male mice were injected via i.p. route with 5 µg of NP-KLH (**A**) or 10 µg of NP-Ficoll (**F**). At 2 dpi, 400 mg of agonistic anti-CD137 or isotype control mAb was administered via an i.p. route. (**B-E**) After immunization with NP-KLH, the number of PNA$^+$CD95$^+$ GC B cells (**B**) in the spleen at 14 days post-immunization was analyzed by flow cytometry. At day 130, bone marrow was harvested to profile antigen-specific LLPCs (**C**). At 30 days post-immunization, antigen-specific MBCs were harvested from a separate set of animals

and profiled (**D**). Serum was collected at 7, 14, 21, 28, 35, 56, 76, 96 and 130 days post-immunization, and anti-NP IgG (**E**) was measured. (**G-J**) After immunization with NP-Ficoll, bone marrow was harvested at day 130 to assess antigen-specific LLPCs (**G**). At 30 days post-immunization, antigen-specific MBCs separately were harvested from a separate set of animals and profiled (**H**). Serum was collected at 7, 14, 21, 28, 35, 56 and 130 days post-immunization, and anti-NP IgM (**I**) and IgG (**J**) were measured. Symbols represent individual mice, and bars indicate median values, except for serum antibody titers where bars indicate mean values. Data are pooled from 3 experiments (Mann-Whitney test, except for serum antibody titers where two-way ANOVA with Sidak post-test was used: *, $P < 0.05$; **, $P < 0.01$; ***, $P < 0.001$; ****, $P < 0.0001$; n.s., not significant).

Figure 3.3
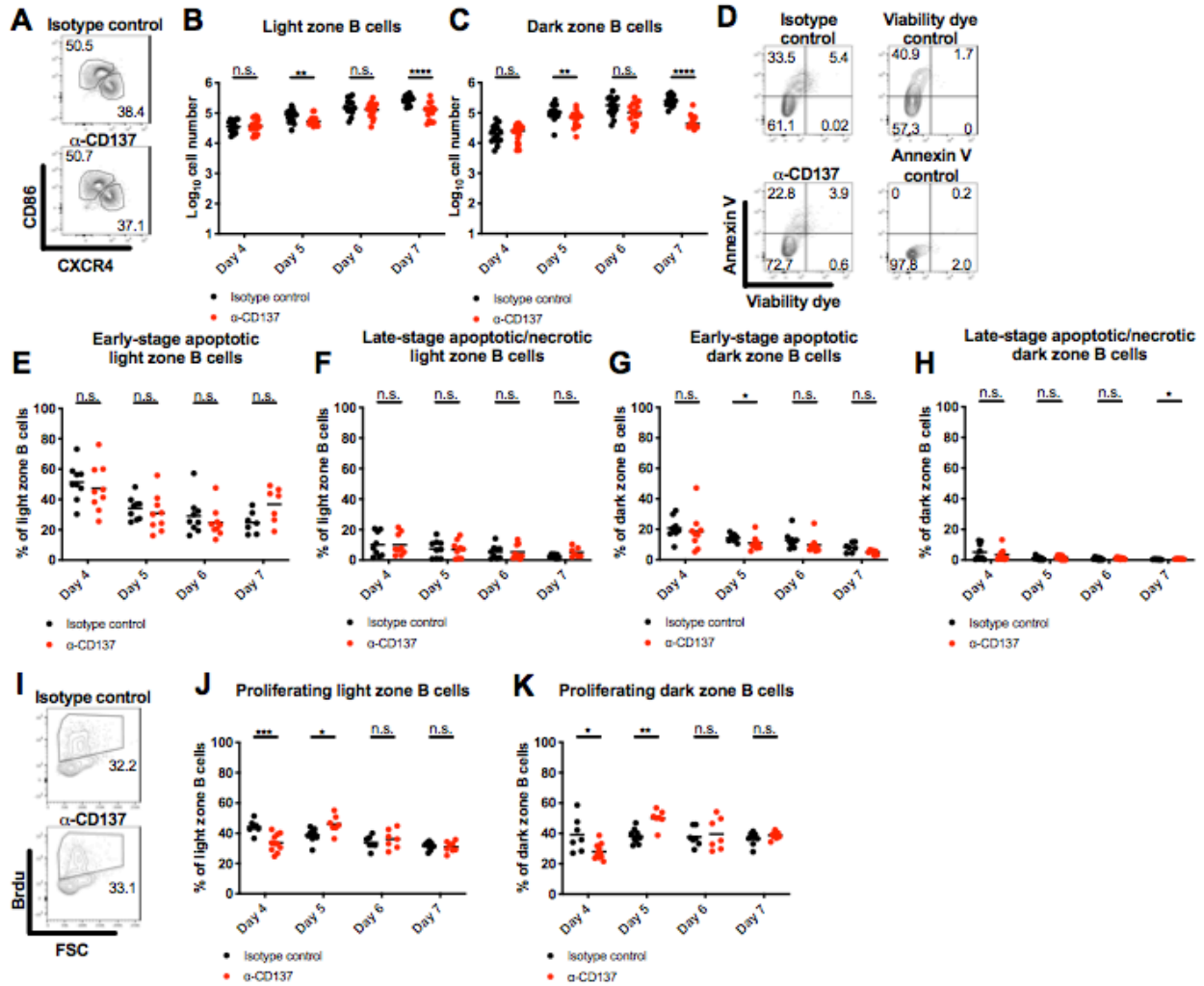
Figure 3.3. Anti-CD137 mAb treatment has a minimal effect on apoptosis and proliferation of GC B cells. Four-week-old WT C57BL/6 male mice were inoculated with 10^3 FFU of CHIKV. At 2 dpi, 400 mg of agonistic anti-CD137 or isotype control mAb was administered via an i.p. route. The number of $CD86^{hi}CXCR4^{low}$ light zone B cells (**A-B**), and $CD86^{hi}CXCR4^{low}$ dark zone B cells (**A and C**), and the percentage of annexin V^+Viability Dye$^-$ early-stage apoptotic light zone and dark zone B cells (**D-E; G,** respectively), annexin V^+Viability Dye$^+$ late-stage apoptotic light and dark zone B cells (**D and F; H,** respectively), and Brdu$^+$ proliferating light and dark zone B cells (**I-J; K**, respectively) in the spleen at 4, 5, 6 and 7

dpi was analyzed by flow cytometry. Representative dot plots of light and dark zone B cells (**A**), apoptotic light zone B cells (**D**), and proliferating light zone B cells (**I**) are shown. Symbols represent individual mice, and bars indicate median values, except for percentages where bars indicate mean values. Data are pooled from 3 experiments (Mann-Whitney test: *, $P < 0.05$; **, $P < 0.01$; ***, $P < 0.001$; ****, $P < 0.0001$; n.s., not significant).

Figure 3.4
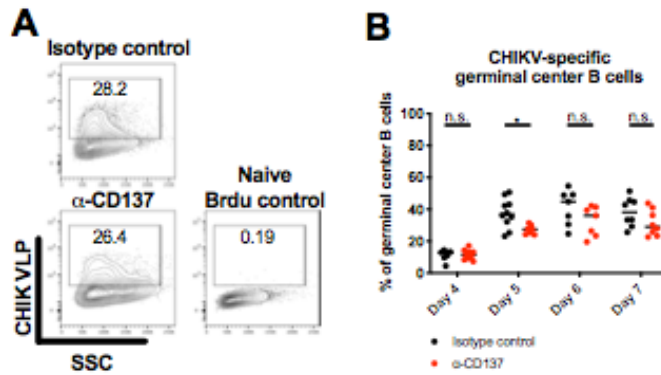
Figure 3.4. Anti-CD137 mAb treatment has a minimal effect on the percentage of antigen-specific GC B cells. Four-week-old WT C57BL/6 male mice were inoculated with 10^3 FFU of CHIKV. At 2 dpi, 400 mg of agonistic anti-CD137 or isotype control mAb was administered via an i.p. route. (**A-B**) The percentage of CHIK VLP$^+$ antigen-specific PNA$^+$CD95$^+$ GC B cells in the spleen at 4, 5, 6 and 7 dpi was analyzed by flow cytometry. (**B**) Representative flow cytometry dot plots of antigen-specific GC B cells are shown. Symbols represent individual mice, and bars indicate median values. Data are pooled from 2 experiments (Mann-Whitney test: *, $P < 0.05$; n.s., not significant).

Figure 3.5
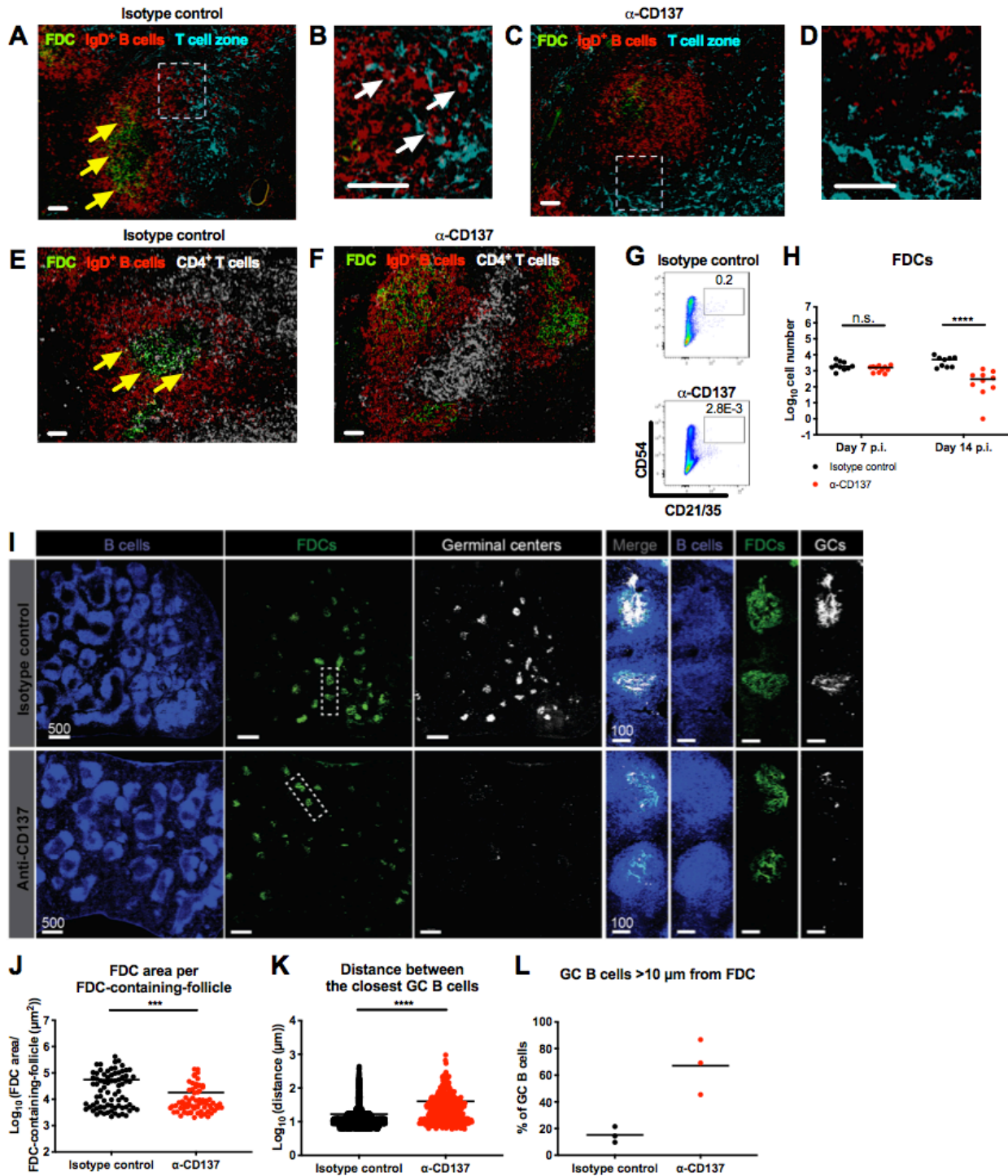
Figure 3.5. Anti-CD137 mAb results in a disorganization of B cell follicle architecture in the spleen. Four-week-old WT C57BL/6 male mice were inoculated with 10^3

FFU of CHIKV. At 2 dpi, 400 mg of agonistic anti-CD137 or isotype control mAb was administered via an i.p. route. Spleens were harvested at 6 dpi (**A-D**), 7 dpi (**E-F**) and 14 dpi (**I-L**) for imaging. (**A-D**) FDCs (green) were stained for CD21/35; IgD$^+$ B cells (red), IgD; T cell zone (turquoise), CCL21. (**B** and **D**) Insets of the respective dotted boxes. (**E-F**) FDCs (green) were stained for CD21/35; IgD$^+$ B cells (red), IgD; CD4$^+$ T cells (snow), CD4. White scale bars indicate 50 mm. Yellow arrows indicate IgD$^+$ B cells surrounding FDCs, and white arrows IgD$^+$ B cells at the CCL21$^+$ T cell zone border. (**G-H**) The number of CD21/35$^+$CD54$^+$ FDCs in the spleen at 7 and 14 dpi was analyzed by flow cytometry. (**G**) Representative flow cytometry dot plots of FDCs are shown. (**I**) B cells (blue) were stained for B220; FDCs (green), CD21/35; GC B cells (snow), GL7. White scale bars indicate 500 mm or 100 mm (*insets*). Each symbol represents individual FDC-containing follicle (**J**), GC B cell (**K**) or spleen (**L**), and bars indicate mean values. Quantification was done for: FDC area per FDC-containing-follicle (**J**), distance between the closest GC B cells (**K**), and GC B cells greater than 10 mm from an FDC (**L**). The images are representative of 3 spleens per group from 2 experiments (Mann-Whitney test: ***, *P* < 0.001; ****, *P* < 0.0001; n.s., not significant).

Figure 3.6
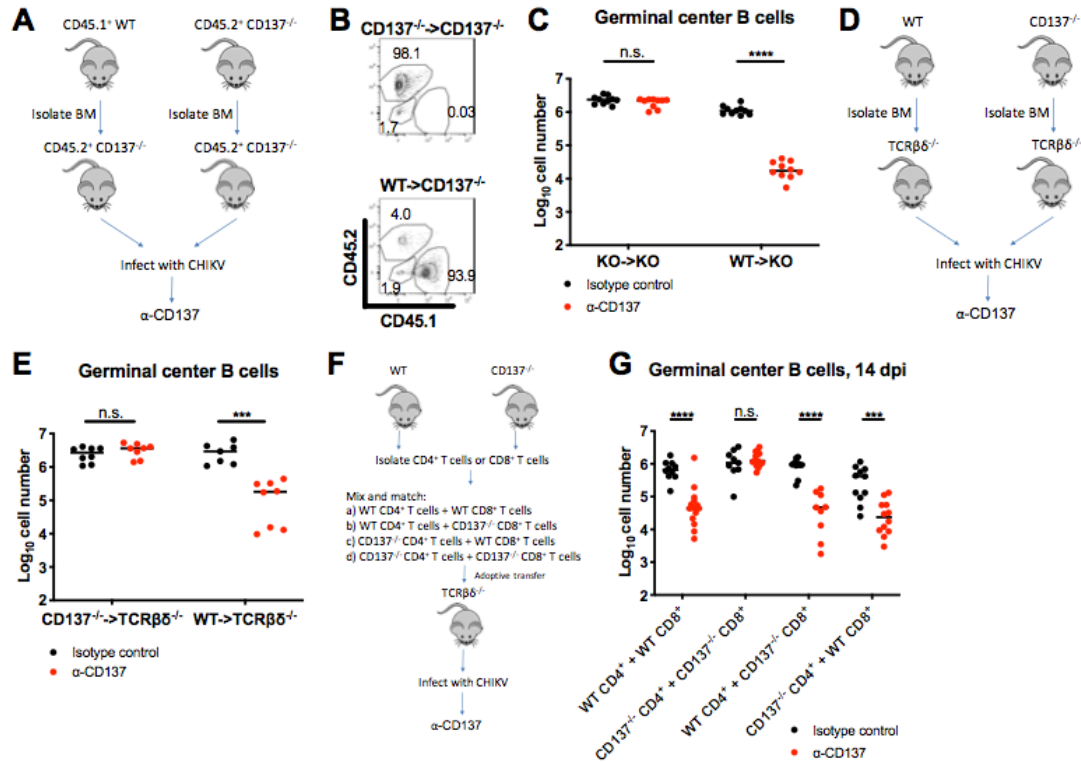
Figure 3.6. Cell-intrinsic CD137 signaling in CD4$^+$ or CD8$^+$ T cells is required for anti-CD137 mAb-mediated inhibition of GC formation. Four-week-old (**A**) CD137$^{-/-}$ or (**D**) TCRβδ$^{-/-}$ mice were irradiated and then received bone marrow cells from WT or CD137$^{-/-}$ mice. After 8 weeks, recipient mice were inoculated with 10^3 FFU of CHIKV. At 2 dpi, 400 mg of agonistic anti-CD137 or isotype control mAb was administered via an i.p. route. (**B**) Immune cell reconstitution was confirmed in recipient mice. The number of PNA$^+$CD95$^+$ GC B cells (**C, E and G**) in the spleen at 14 dpi was determined. (**F-G**) Four-week-old TCRβδ$^{-/-}$ mice were administered 7.1 x 10^6 WT CD4$^+$ T cells + WT CD8$^+$ T cells, WT CD4$^+$ T cells + CD137$^{-/-}$ CD8$^+$ T cells, CD137$^{-/-}$ CD4$^+$ T cells + WT CD8$^+$ T cells or CD137$^{-/-}$ CD4$^+$ T cells + CD137$^{-/-}$ CD8$^+$ T cells via an i.v. route. Five days later, recipient mice were inoculated with 10^3 FFU of CHIKV. At 2 dpi, 400 mg of agonistic anti-CD137 or isotype control mAb was administered via an i.p.

route. Symbols represent individual mice, and bars indicate median values. Data are pooled from

3 to 4 experiments (Mann-Whitney test: ***, $P < 0.001$; ****, $P < 0.0001$; n.s., not significant).

Figure 3.7
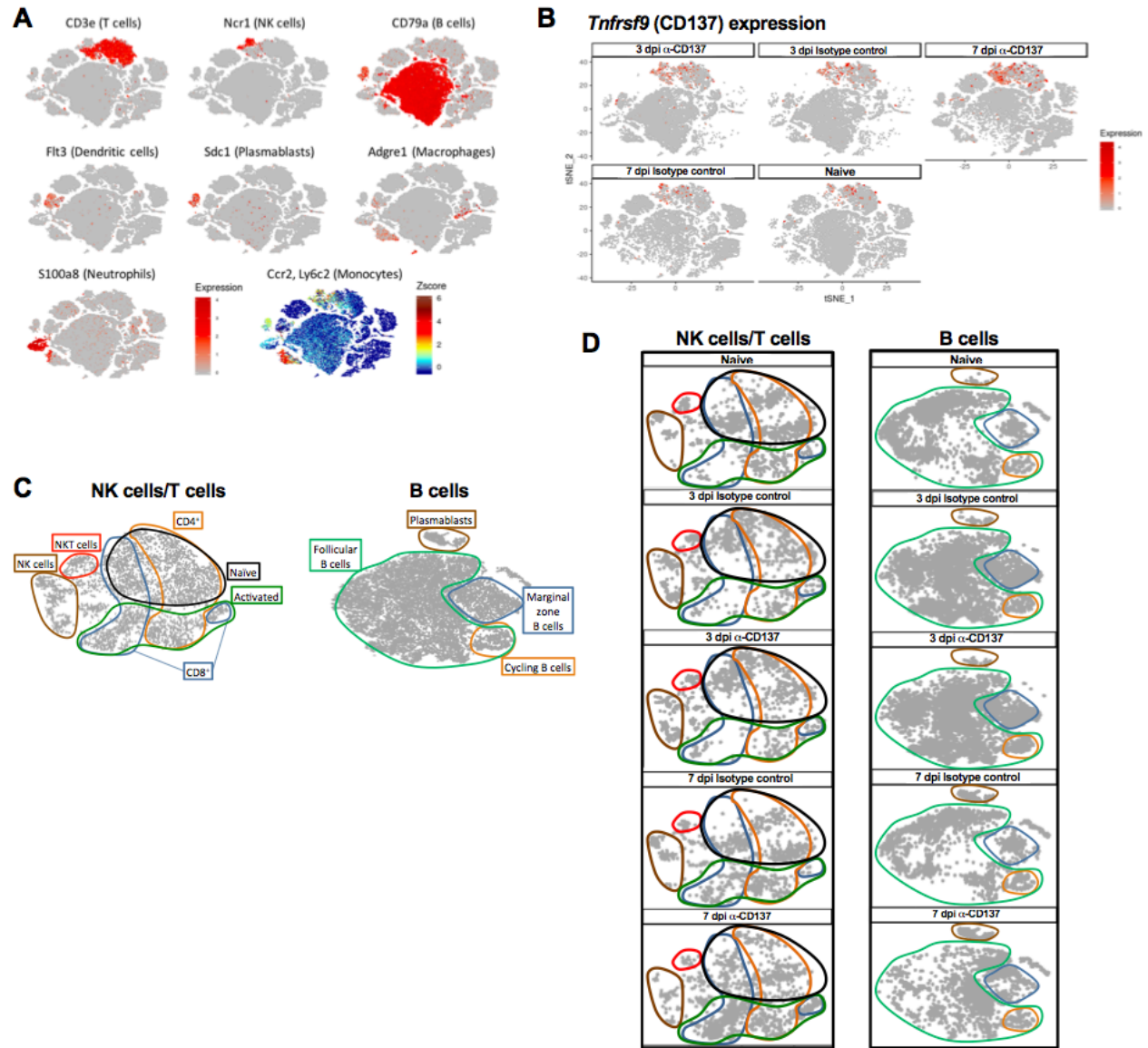
Figure 3.7. Immune cell populations identified by single cell RNA sequencing of splenocytes. Four-week-old WT C57BL/6 male mice were inoculated with 10^3 FFU of CHIKV. At 2 dpi, 400 mg of agonistic anti-CD137 or isotype control mAb was administered via an i.p. route. Single cell RNA sequencing was performed from spleens of naïve and CHIKV-infected mice at 3 and 7 dpi. Expression of *CD3e* (T cells), *Ncr1* (NK cells), *CD79a* (B cells), *Flt3* (DCs), *Sdc1* (plasmablasts), *Adgre1* (macrophages), *S100a8* (neutrophils), *Ccr2/Ly6c2* (monocytes) (**A**),

and *Tnfrsf9* (**B**) is shown in tSNE plots. (**C-D**) Cell subsets among NK cells/T cells and B cells were segregated in tSNE plots. Spleens from 3 mice were pooled for each group.

Figure 3.8
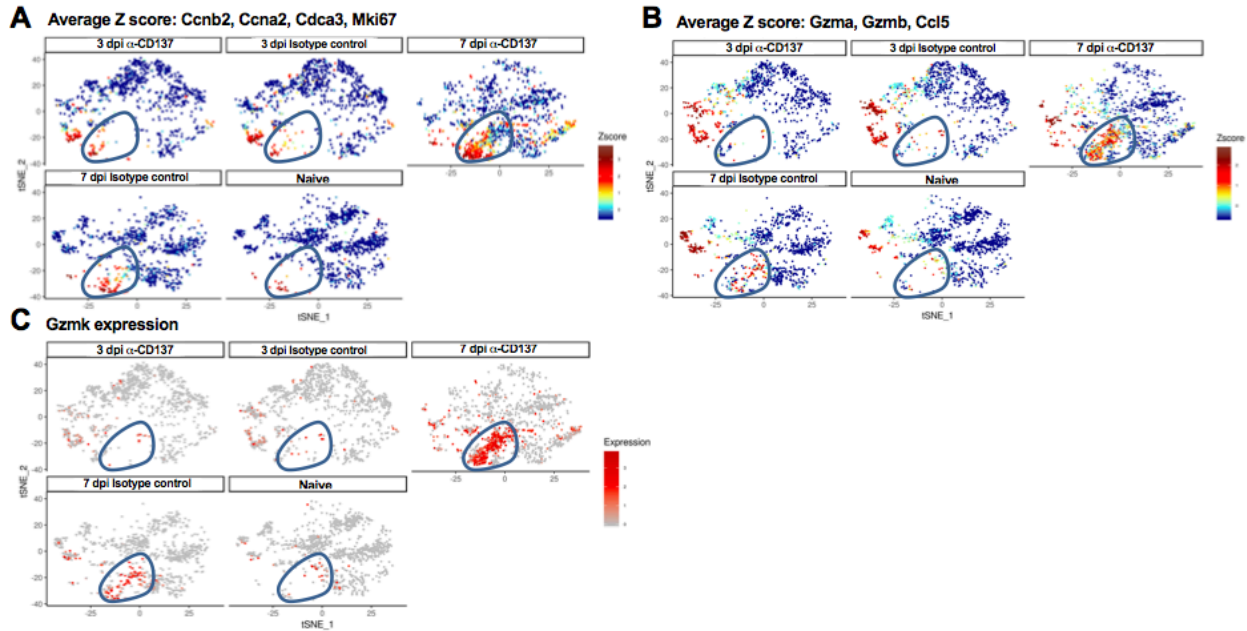
Figure 3.8. Anti-CD137 mAb treatment increases the frequency of cycling CD8⁺ T cells with pro-inflammatory signatures. Four-week-old WT C57BL/6 male mice were inoculated with 10^3 FFU of CHIKV. At 2 dpi, 400 mg of agonistic anti-CD137 or isotype control mAb was administered via an i.p. route. Single cell RNA sequencing was performed from spleens of naïve mice and CHIKV-infected mice at 3 and 7 dpi. Cycling CD8⁺ T cells (*Ccnb2*, *Ccna2*, *Cdca3* and *Mki67*; **A**) with pro-inflammatory signatures (*Gzma*, *Gzmb* and *Ccl5*; **B**) are shown in tSNE plots. (**C**) Expression of *Gzmk* in these cycling CD8⁺ T cells is shown in tSNE plots. Blue circle regions indicate cycling CD8⁺ T cells. Spleens from 3 mice were pooled for each group.

Figure 3.9
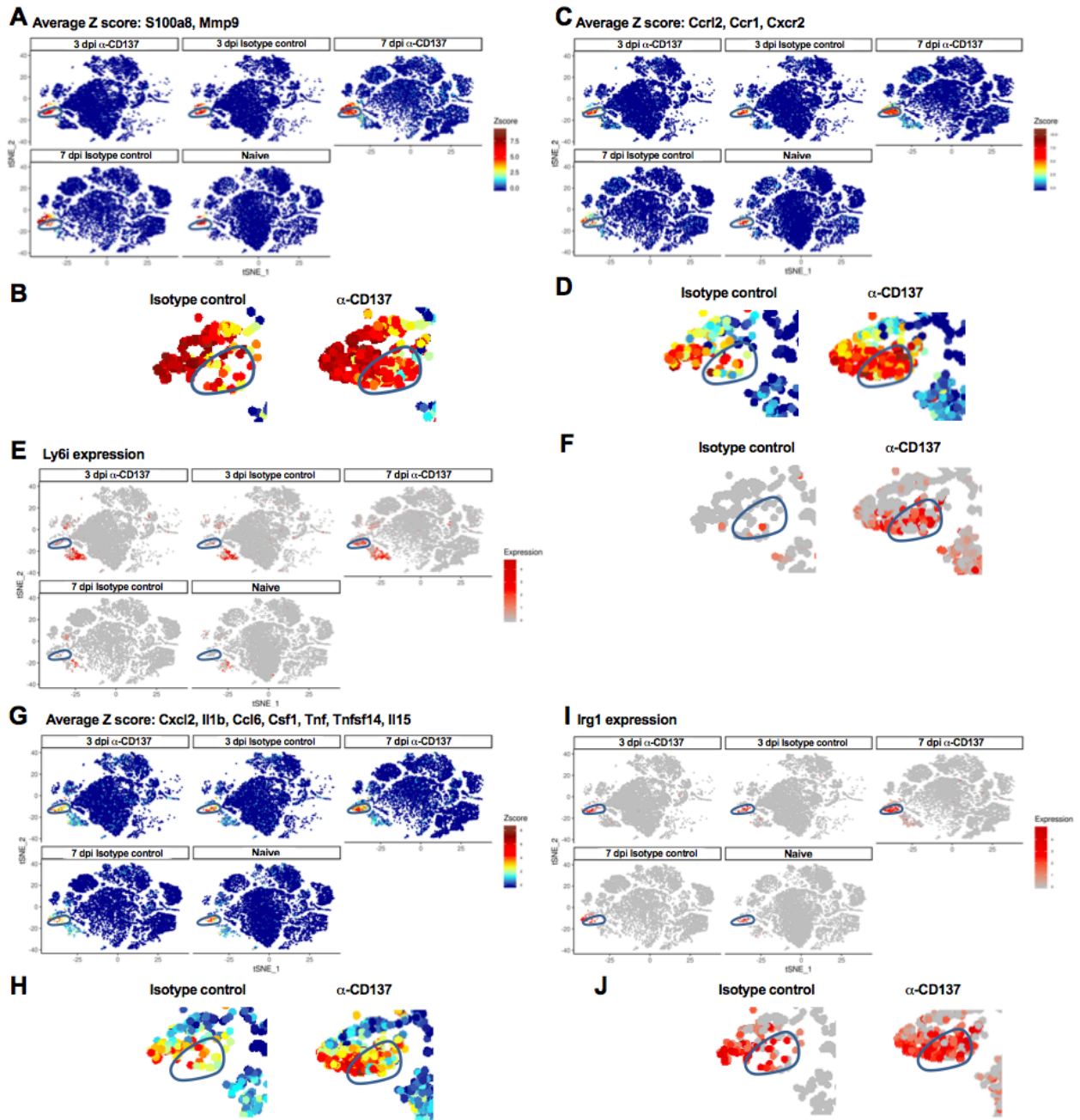
Figure 3.9. Anti-CD137 mAb treatment increases the frequency of neutrophils with pro-inflammatory signatures. Four-week-old WT C57BL/6 male mice were inoculated with 10^3 FFU of CHIKV. At 2 dpi, 400 mg of agonistic anti-CD137 or isotype control mAb was administered via an i.p. route. Single cell RNA sequencing was performed from spleens of naïve

mice and CHIKV-infected mice at 3 and 7 dpi. A subset of neutrophils (*S100a8* and *Mmp9*; **A-B**) that expressed *Ccrl2*, *Ccr1*, *Cxcr2* (**C-D**), *Ly6i* (**E-F**) and pro-inflammatory signatures (*Cxcl2*, *Il1b*, *Ccl6*, *Csf1*, *Tnf*, *Tnfsf14* and *Il15*; **G-H**) is shown in tSNE plots. (**I-J**) Expression of *Irg1* in this subset of neutrophils is shown in tSNE plots. **B, D, F, H and J** are insets of panel **A**, **C**, **E**, **G** and **I**, respectively, showing neutrophils at 7 dpi. Blue circled regions indicate neutrophils with pro-inflammatory signatures. Spleens from 3 mice were pooled for each group.

Figure 3.10
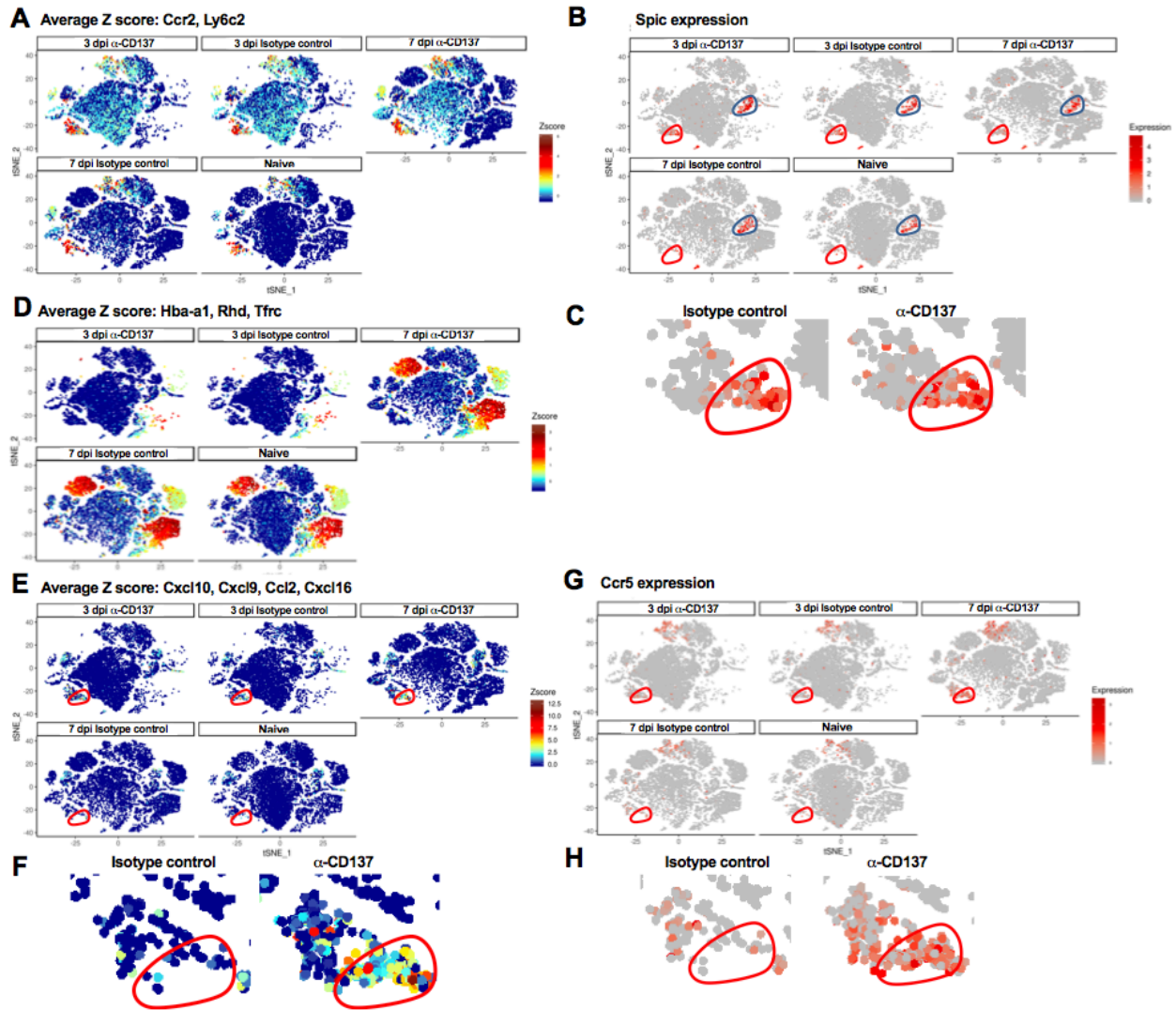
Figure 3.10. Anti-CD137 mAb treatment increases the frequency of differentiating monocytes with pro-inflammatory signatures. Four-week-old WT C57BL/6 male mice were inoculated with 10^3 FFU of CHIKV. At 2 dpi, 400 mg of agonistic anti-CD137 or isotype control mAb was administered via an i.p. route. Single cell RNA sequencing was performed from spleens of naïve mice and CHIKV-infected mice at 3 and 7 dpi. Monocytes (*Ccr2* and *Ly6c2*; **A**), *Spic*-expressing differentiating monocytes (red circles) and red pulp macrophages (blue circles) (**B-C**) and reticulocytes (*Hba-a1*, *Rhd* and *Tfrc*; **D**) are shown in tSNE plots. Expression of pro-

inflammatory signatures (*Cxcl10, Cxcl9, Ccl2* and *Cxcl16*; **E-F**) and *Ccr5* (**G-H**) in the differentiating monocytes is shown in tSNE plots. **C, F and H** are insets of panel **B**, **E** and **G**, respectively, showing differentiating monocytes at 3 dpi (**C**) or 7 dpi (**F and H**). Red circled regions indicate differentiating monocytes with pro-inflammatory signatures. Spleens from 3 mice were pooled for each group.

Figure 3.11
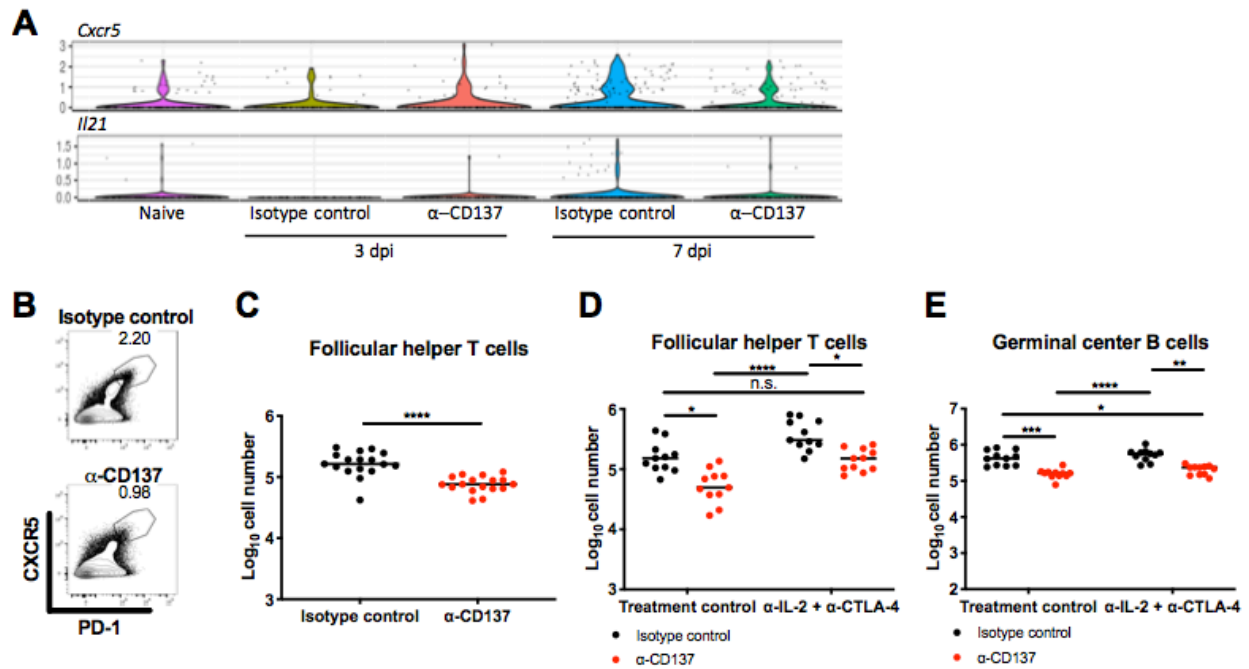
Figure 3.11. Anti-CD137 mAb treatment reduces the number of Tfh cells. Four-week-old WT C57BL/6 male mice were inoculated with 10^3 FFU of CHIKV. At 2 dpi, 400 mg of agonistic anti-CD137 or isotype control mAb was administered via an i.p. route. (**A**) Single cell RNA sequencing was performed from spleens of naïve mice and CHIKV-infected mice at 3 and 7 dpi. Expression of Tfh cell markers (*Cxcr5* and *Il21*) in activated CD4$^+$ T cells is shown in violin plots. (**B-C**) The number of CXCR5^{hi}PD-1^{hi} Tfh cells in the spleen at 7 dpi was analyzed by flow cytometry. (**B**) Representative flow cytometry dot plots of Tfh cells are shown. (**D-E**) At 2 dpi, 400 mg of agonistic anti-CD137 or isotype control mAb in combination with anti-IL-2 neutralizing or isotype (neutralizing) control mAb and anti-CTLA-4 blocking or isotype (block) control mAb was administered. IL-2 neutralizing and isotype (neutralizing) control mAb were administered again at 4 and 6 dpi. CTLA-4 blocking and isotype (blocking) control mAb were administered again at 5 dpi. Spleens were harvested at 7 dpi, and the number of CXCR5^{hi}PD-1^{hi} Tfh cells (**D**) and PNA$^+$CD95$^+$ GC B cells (**E**) was analyzed. Symbols represent individual mice,

and bars indicate median values. Data are pooled from 3 experiments (Mann-Whitney test for (**C**) and Kruskal-Wallis ANOVA with Dunn's post-test for (**D-E**): *, $P < 0.05$; **, $P < 0.01$; ***, $P < 0.001$; ****, $P < 0.0001$; n.s., not significant).

.

Figure 3.12
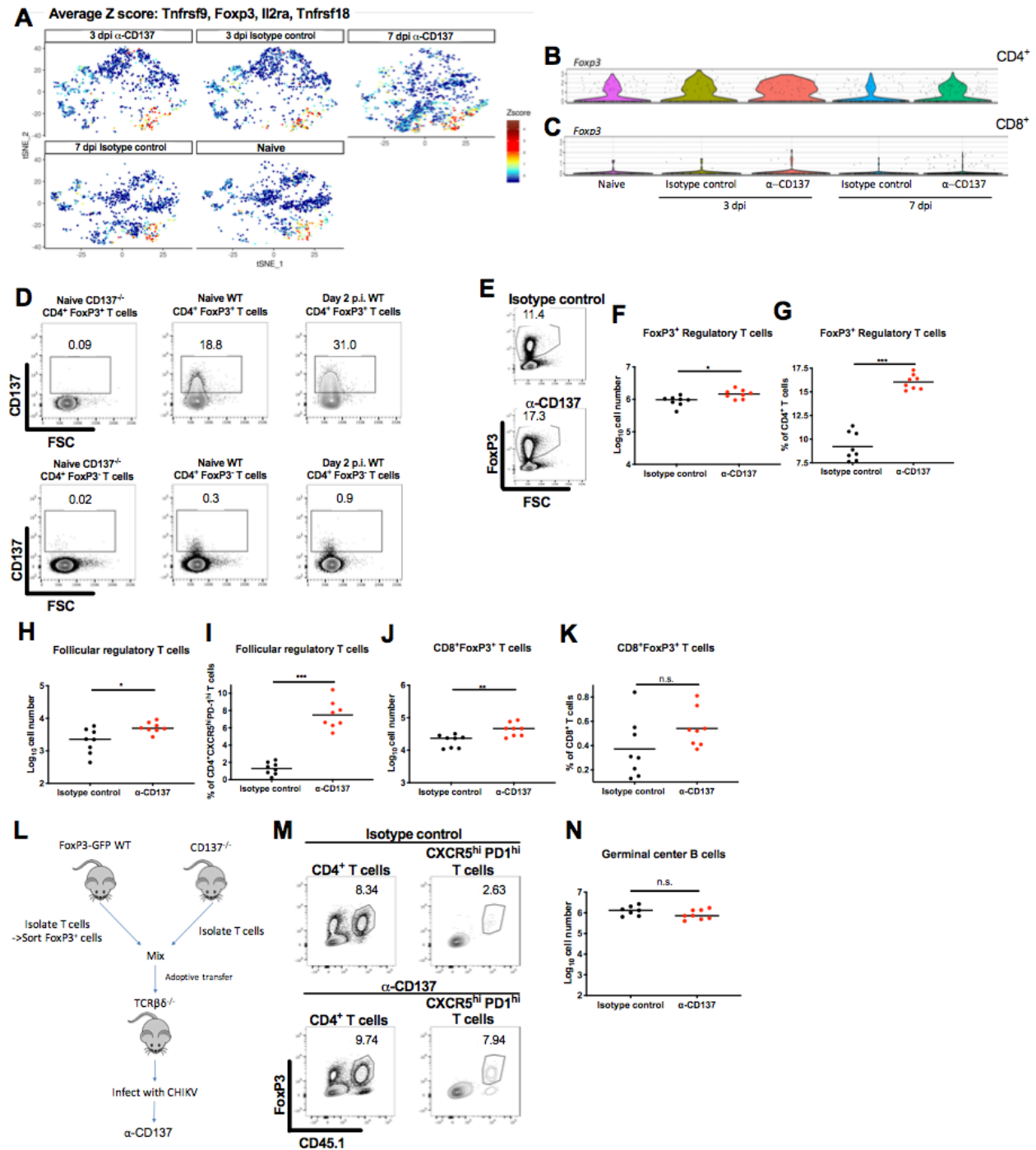
Figure 3.12. Anti-CD137 mAb treatment increases the number of Tregs, Tfrs and CD8+FoxP3+ T cells. Four-week-old WT C57BL/6 male mice were inoculated with 10^3 FFU of CHIKV. At 2 dpi, 400 mg of agonistic anti-CD137 or isotype control mAb was administered via

an i.p. route. (**A-C**) Single cell RNA sequencing was performed from spleens of naïve mice and CHIKV-infected mice at 3 and 7 dpi. (**A**) Tregs (*Tnfrsf9*, *Foxp3*, *Il2ra* and *Tnfrsf18*) are shown in tSNE plots. Expression of *Foxp3* in activated CD4$^+$ (**B**) and CD8$^+$ T cells (**C**) is shown in violin plots. (**D**) Representative flow plots of CD137 expression on CD4$^+$FoxP3$^+$ Tregs and CD4$^+$FoxP3$^-$ T cells from naïve CD137$^{-/-}$, naïve WT or CHIKV-infected WT mice at 2 dpi are shown. The number and percentage of CD4$^+$FoxP3$^+$ Tregs (**E-G**), CD4$^+$FoxP3$^+$CXCR5^{hi}PD-1^{hi} Tfr cells (**H-I**) and CD8$^+$FoxP3$^+$ T cells (**J-K**) in the spleen at 7 dpi was analyzed by flow cytometry. (**E**) Representative flow plots of Tregs are shown. (**L-N**) Four-week-old TCRβδ$^{-/-}$ mice received FoxP3-GFP WT FoxP3$^+$ T cells + CD137$^{-/-}$ T cells via i.v. route. After 5 days, the recipient mice were inoculated with 10^3 FFU of CHIKV. At 2 dpi, 400 mg of agonistic anti-CD137 or isotype control mAb was administered via an i.p. route. (**M**) Reconstitution of Tregs and Tfr cells was confirmed in the recipient mice. (**N**) The number of PNA$^+$CD95$^+$ GC B cells in the spleen at 14 dpi was analyzed by flow cytometry. Symbols represent individual mice, and bars indicate median values, except for percentages where bars indicate mean values. Data are pooled from 2 experiments (Mann-Whitney test: *, $P < 0.05$; **, $P < 0.01$; ***, $P < 0.001$; n.s., not significant).

Figure 3.13
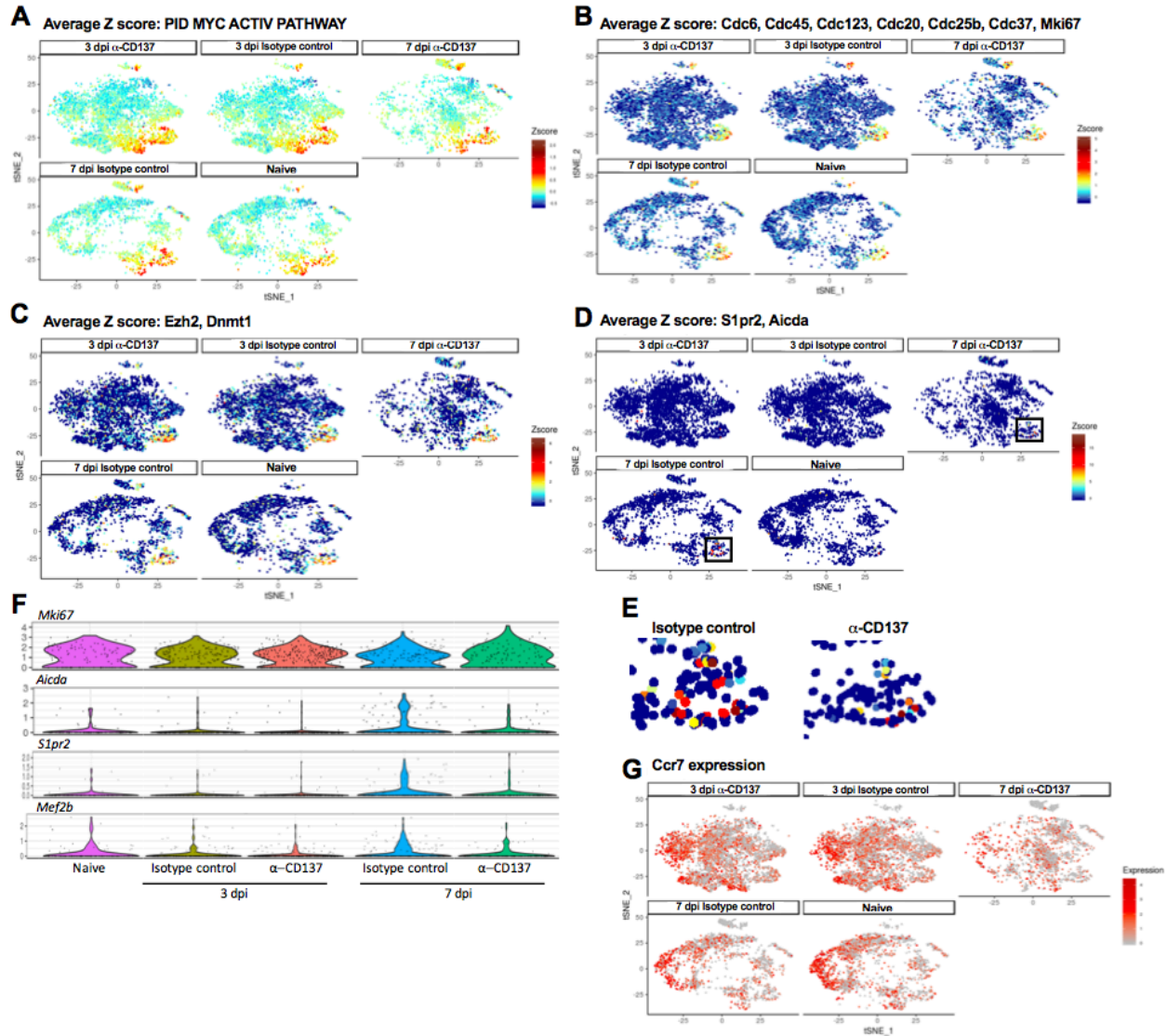
Figure 3.13. Anti-CD137 mAb treatment reduces the frequency of GC B cells. Four-week-old WT C57BL/6 male mice were inoculated with 10^3 FFU of CHIKV. At 2 dpi, 400 mg of agonistic anti-CD137 or isotype control mAb was administered via an i.p. route. Single cell RNA sequencing was performed from spleens of naïve mice and CHIKV-infected mice at 3 and 7 dpi. The tSNE plots show GC B precursors (*Myc-activated pathway*; **A**), cycling B cells (*Cdc6, Cdc45, Cdc123, Cdc20, Cdc25b, Cdc37* and *Mki67*; **B**) expressing *Ezh2* and *Dnmt1* (**C**). B cell subset expressing GC B cell markers is shown in tSNE plots (*S1pr2* and *Aicda*; **D-E**) and violin

plots (*Mki67*, *Aicda*, *S1pr2* and *Mef2b*; **F**). (**E**) Insets of panel **D** (black boxes) showing cycling

B cells at 7 dpi. (**G**) Expression of *Ccr7* in B cells is shown in tSNE plots. Spleens from 3 mice

were pooled for each group.

Figure 3.14
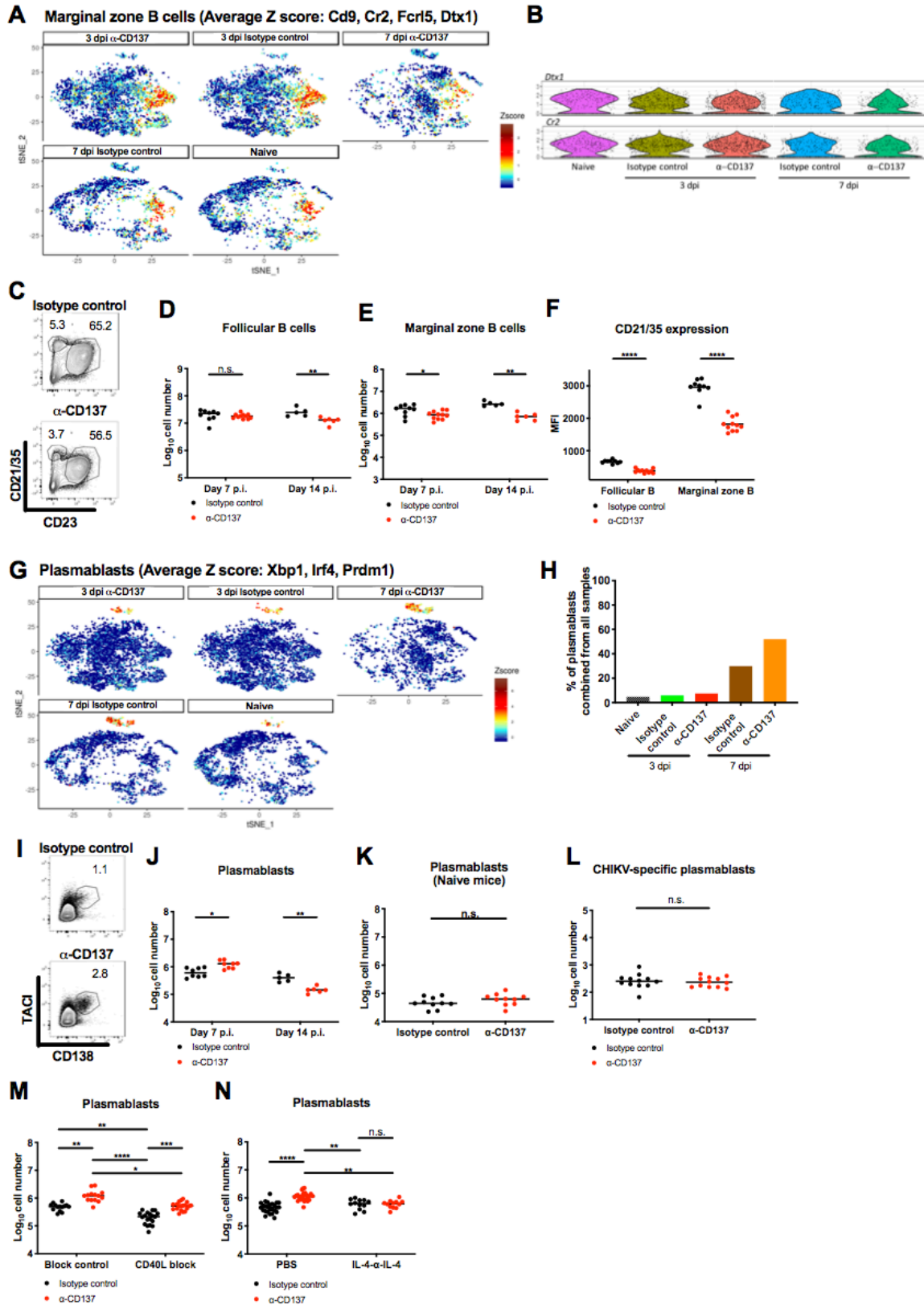
Figure 3.14. Anti-CD137 mAb treatment reduces the number of MZ B cells and increases the number of plasmablasts. Four-week-old WT C57BL/6 male mice were inoculated with 10^3 FFU of CHIKV. At 2 dpi, 400 mg of agonistic anti-CD137 or isotype control mAb was administered via an i.p. route. (**A**) Single cell RNA sequencing was performed on spleens of naïve and CHIKV-infected mice at 3 and 7 dpi. Expression of *Cd9, Cr2, Fcrl5* and *Dtx1* in MZ B cells is shown in tSNE plots. (**B**) Expression of *Dtx1* and *Cr2* in MZ B cells is shown in violin plots. The number of CD21/35^{low}CD23^{hi} follicular B cells (**C-D**) and CD21/35^{hi}CD23^{low} MZ B cells (**C and E**) in the spleen at 7 and 14 dpi was analyzed. (**C**) Representative flow cytometry dot plots of follicular and MZ B cells are shown. (**F**) The mean fluorescence intensity (MFI) of follicular and MZ B cells is shown. (**G**) Expression of *Xbp1, Irf4* and *Prdm1* in plasmablasts is shown in tSNE plots. (**H**) The fraction of plasmablasts combined from all samples is shown in bar graphs. (**I-J**) The number of TACI$^+$CD138$^+$ plasmablasts in the spleen at 7 dpi was analyzed by flow cytometry. (**I**) Representative flow cytometry dot plots of plasmablasts are shown. (**K**) Four-week-old naive (uninfected) WT C57BL/6 male mice were administered 400 mg of agonistic anti-CD137 or isotype control mAb via an i.p. route. The numbers of TACI$^+$CD138$^+$ plasmablasts in the spleen at 5 days after treatment were analyzed by flow cytometry. (**L**) Four-week-old WT C57BL/6 male mice were inoculated with 10^3 FFU of CHIKV. At 2 dpi, 400 mg of agonistic anti-CD137 or isotype control mAb was administered via an i.p. route. The number of antigen-specific plasmablasts in the spleen at 7 dpi was analyzed by ELISPOT. (**M**) Four-week-old WT C57BL/6 male mice were inoculated with 10^3 FFU of CHIKV. At 2 dpi, 400 mg of agonistic anti-CD137 or isotype control mAb in combination with anti-CD40L blocking or isotype (block) control mAb was administered. Blocking and isotype (block) control mAb were administered again at 5 dpi. Spleens were harvested at 7 dpi, and the

number of TACI$^+$CD138$^+$ plasmablasts was analyzed by flow cytometry. (**N**) Immediately prior to CHIKV infection, IL-4-anti-IL-4 complex was administered via an i.p. route. IL-4-anti-IL-4 complex was administered again at 1 and 2 dpi. At 2 dpi, 400 mg of agonistic anti-CD137 or isotype control mAb was administered via an i.p. route. Spleens were harvested at 7 dpi, and the number of plasmablasts was analyzed by flow cytometry. Symbols represent individual mice, and bars indicate median values, except for MFI where bars indicate mean values. Data are pooled from 3 experiments (Mann-Whitney test, except for (**M-N**) where Kruskal-Wallis ANOVA with Dunn's post-test was used: *, $P < 0.05$; **, $P < 0.01$; ***, $P < 0.001$; ****, $P < 0.0001$; n.s., not significant).

Figure 3.15
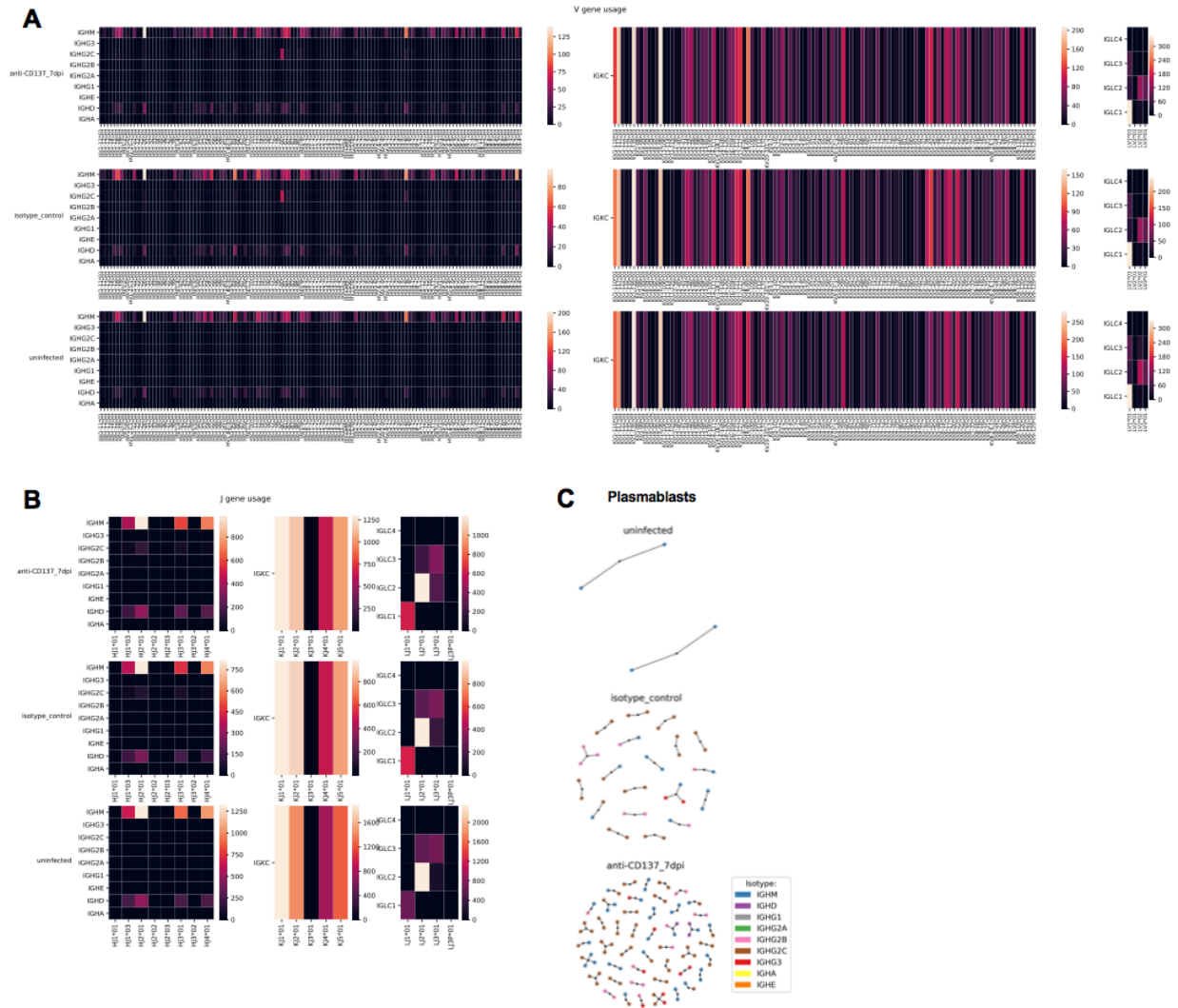
Figure 3.15. Anti-CD137 mAb treatment has a minimal effect on BCR usage or clonal expansion. Four-week-old WT C57BL/6 male mice were inoculated with 10^3 FFU of CHIKV. At 2 dpi, 400 mg of agonistic anti-CD137 or isotype control mAb was administered via an i.p. route. Single cell RNA sequencing was performed from spleens of naïve mice and CHIKV-infected mice at 3 and 7 dpi. V gene (**A**) and J gene (**B**) usage of heavy and light chains is shown. (**C**) The ball graph plots show heavy chain CDR3 clonality and extent of clonal

expansion with color-coded isotypes among plasmablasts. Each dot indicates a unique BCR sequence. Spleens from 3 mice were pooled for each group.

Figure 3.16
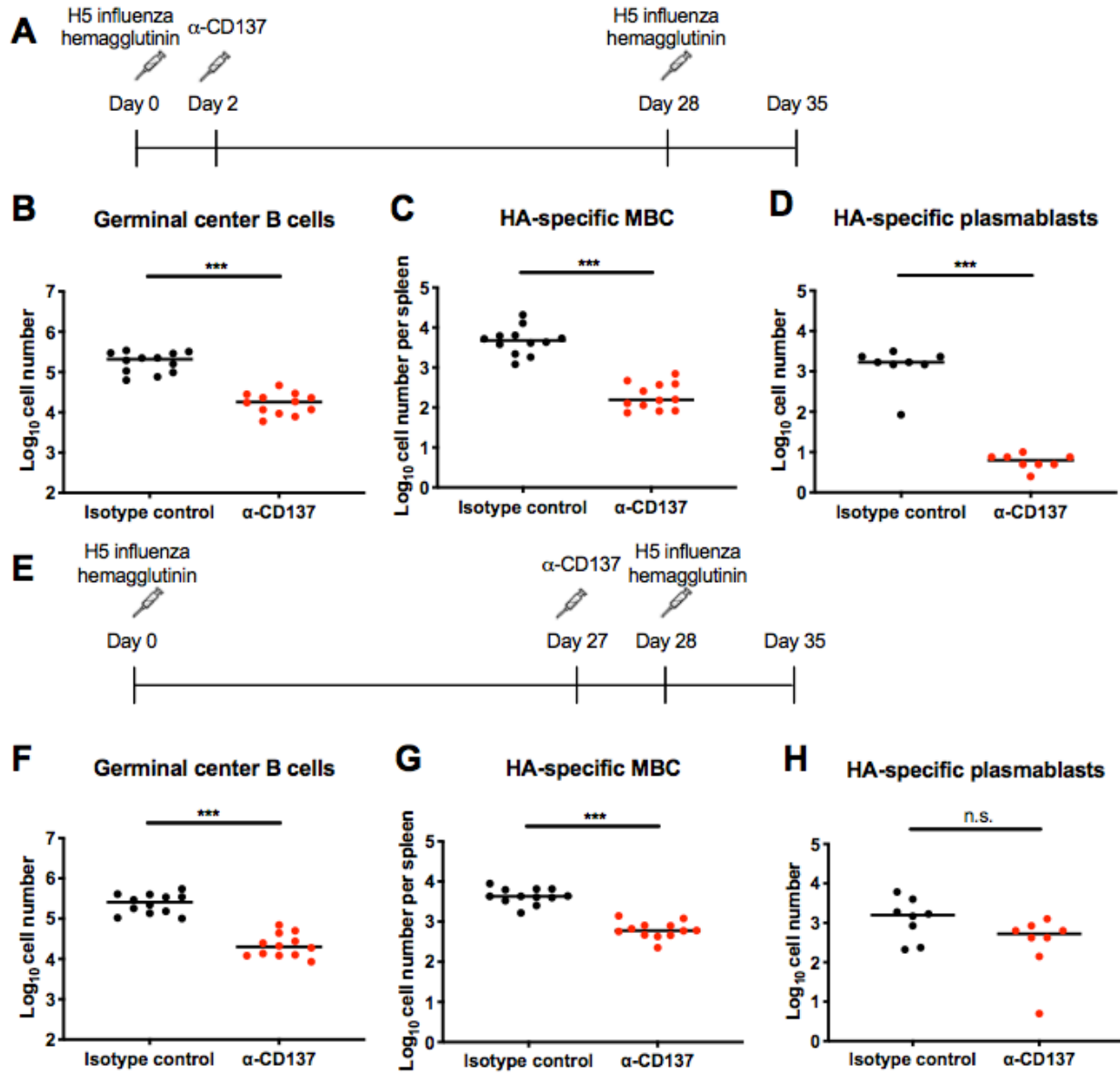
Figure 3.16. Effect of Anti-CD137 mAb treatment on antigen-specific B cell populations when administered before viral vaccine boosting. Nine-week-old WT C57BL/6J female mice were injected via an i.m. route with recombinant influenza A virus H5 hemagglutinin proteins. 400 mg of agonistic anti-CD137 or isotype control mAb was administered via an i.p. route at either 2 days post-immunization (**A**) or 27 days post-immunization (**E**) before secondary immunization with another dose of H5 at 28 days post-

immunization. Spleens were harvested 7 days after the secondary booster immunization, and the numbers of GC B cells (**B and F**) and antigen-specific MBCs (**C and G**) were analyzed by flow cytometry. (**D and H**) The number of antigen-specific plasmablasts was analyzed by ELISPOT. Symbols represent individual mice, and bars indicate median values. Data are pooled from 2 experiments (Mann-Whitney test: ***, $P < 0.001$; n.s., not significant).

Chapter 4: Conclusion and Future Directions

Reduced chikungunya infection by agonistic anti-CD137 monoclonal antibody

B cell/FDC tropism of chikungunya virus

The tropism of chronic CHIKV RNA in the musculoskeletal tissues and the lymphoid tissues is not clear, although there are some reports on the sites of viral replication during the acute phase of infection (Hawman et al., 2013; Nair et al., 2017; Young et al., 2019). Even though viral RNA was readily detected in the spleen, infectious virus was not recovered, as judged by plaque- or focus-forming assays. Nonetheless, higher E1/nsP2 RNA ratios were observed, consistent with productive infection. Based on the cell-sorting and tropism data in the spleen, GC B cells and FDCs were associated with the highest levels of viral RNA, on a per-cell basis, at 7 and 14 dpi. Unlike WT mice, neither μMT mice nor MD4 transgenic mice showed chronic viral RNA in their spleens, suggesting that the antigen-specific B cells are required for the persistence of CHIKV RNA in the spleen. It is plausible that B cells capture anti-CHIKV-antibody-CHIKV immune complex on their surface CRs and/or Fcγ receptors during the active process of antigen transportation to FDCs in the lymphoid follicles (Cinamon et al., 2008; Heinen et al., 1986). FDCs reportedly can retain HIV within nondegrative cycling compartments for long periods (Heesters et al., 2015). Similar phenomenon has not been reported for B cells. Although cell culture-adapted and some clinical isolates of CHIKV are dependent on glycosaminoglycans to differing extents for attachment and efficient infection, there has not been clear reports on receptors for CHIKV until recently when Zhang *et. al.* identified Mxra8 as an entry mediator for multiple arthritogenic alphaviruses, including CHIKV, using a genome-wide CRISPR-Cas9-based screen (Silva et al., 2014; Zhang et al., 2018). Expression of Mxra8 on B cells has not been reported, and Raji, a B cell lymphoma cell line, does not express surface Mxra8 (Zhang et al.,

2018). However, the possibility of other yet unidentified CHIKV receptor on B cells cannot be excluded. B cells can engage immune complex presented by FDCs, macrophages or DCs via BCR and internalize antigen-BCR complex, which is delivered to endocytic pathways. Whether CHIKV internalized through BCR contributes to chronic viral RNA is not clear. B cell tropism has been reported with PBMCs from dengue virus (DENV)-infected patients (King et al., 1999; Zanini et al., 2018). DENV may reside both on the surface and in intracellular compartments of B cells (King et al., 1999). Experiments involving protease digestion of splenic B cells from CHIKV-infected mice may provide insights into the localization of CHIKV RNA. Additionally, high-resolution imaging technique such as cryogenic electron microscopy may reveal some information on the location where viral RNA may reside. To test whether CHIKV-containing immune complexes binding to surface CR- or Fcγ receptors contribute to chronic viral RNA in the spleen, one could infect WT and CR- or Fcγ receptor-deficient mixed bone marrow chimeras with CHIKV and compare viral RNA contents between WT and the mutant cells. Additionally, virus-inactivated, CHIKV-immune serum could be adoptively transferred into μMT mice or MD4 transgenic mice before CHIKV infection. If the recipient animals show increased viral RNA in the spleens, the data would support the role of immune complex for chronic CHIKV RNA in the spleen. IgM dominates early antibody responses. The pentameric form of IgM efficiently activates complement upon binding to antigens and is trapped together with antigen on FDCs through the expressed CRs. Mice deficient in secreted IgM (sIgM$^{-/-}$) show diminished antigen trapping on FDCs and germinal center reaction, suggesting the role of screted IgM for immune complex formation during early antibody responses (Boes et al., 1998). Since the B cells in sIgM$^{-/-}$ mice can still express antigen-specific, membrane-bound BCRs and produce IgG responses, if these mice do not show chronic CHIKV RNA in their spleens, the data would

support the model that CHIKV-containing immune complexes contribute to chronic viral RNA in the spleen.

Agonistic anti-CD137 antibody-mediated viral clearance in lymphoid tissues

While anti-CD137 mAb treatment induced clearance of CHIKV RNA in the lymphoid tissues, it minimally affected the levels of viral RNA in the feet of the same animals. The lack of CHIKV RNA clearance in the musculoskeletal tissues after anti-CD137 mAb treatment may be due to distinct viral tropism in these tissues (Nair et al., 2017; Young et al., 2019). The clearance of CHIKV RNA in the lymphoid tissues was correlated with a reduction in B cells and FDCs that was mediated by anti-CD137 mAb treatment and T cells. I hypothesize that anti-CD137 mAb clears CHIKV RNA in the lymphoid tissues by targeting B cells and/or FDCs, major reservoirs of chronic CHIKV RNA. Whether T cells eliminate viral RNA-containing cells in antigen-specific manner is not clear. However, two sets of data do not support this scenario. Although the number of FDCs remained unchanged at 7 dpi, as judged by flow cytometry and immunofluorescence imaging, the levels of viral RNA in FDCs were significantly reduced after anti-CD137 mAb treatment at the same time point. Moreover, cell death analysis of germinal center B cells showed minimal difference in the frequencies of the cells undergoing apoptosis. Anti-CD137 mAb treatment reduced the surface expression of CRs on B cells, which may have resulted in less CHIKV-immune complexes binding to cells via CRs. This model would be supported if CR-deficient cells show decreased levels of CHIKV RNA compared to WT cells in the spleens of the CHIKV-infected mixed bone marrow chimera. It is possible that some chronic CHIKV RNA remains in intracellular compartments of B cells, which clear it after anti-CD137 mAb treatment. This is supported by the scRNAseq analysis showing that the B cells in anti-CD137 mAb-treated mice transcriptionally express higher levels of interferon stimulated genes

important in restricting CHIKV infection, such as *Ifitm3* and *Irf1*, at 7 dpi compared to those in isotype control mAb-treated animals.

Agonistic anti-CD137 antibody disrupts germinal center formation

Altered B cell differentiation after anti-CD137 antibody treatment

Anti-CD137 mAb treatment impaired GC formation and long-term antibody and B cell memory responses. Anti-CD137 mAb treatment did not enhance apoptosis or impair proliferation of B cells, nor did it significantly alter TI responses to NP-Ficoll. Although the number of Tfh was reduced after anti-CD137 mAb treatment, this effect could be due to decreased number of GC B cells as they are interdependent on each other. Boosting the number of Tfh using the combination of neutralizing anti-IL-2 and blocking anti-CTLA-4 antibodies did not restore the GC B cells. Whether or how the functions of Tfh are altered by anti-CD137 mAb treatment is not clear. scRNAseq analysis showed that anti-CD137 mAb treatment enhanced overall pro-inflammatory transcriptional program, including multiple cytokines, in T cells, neutrophils, and differentiating monocytes compared to isotype control mAb. Cytokines, including IFN-γ, IL-4, IL-10, IL-13, and IL-21, which regulate CSR and B cell maturation, signal through the activation of JAK/STAT pathways (Ding et al., 2013; Kiu and Nicholson, 2012). B cell-intrinsic IL-21 signals are required for optimal GC formation. In addition, IL-21 and CD40L synergistically promote plasma cell differentiation. This likely occurs through STAT3, activated by IL-21, and Irf4, activated by CD40L, competitively binding to shared Bcl6-binding sites within the regulatory sequences in *Prdm1* gene and, therefore, increasing the expression of Prdm1, the transcription factor important for plasma cell differentiation (Ding et al., 2013; Kwon et al., 2009). IL-21 signaling via STAT3 also sensitizes B cells to the stimulatory effects of IL-2 by inducing the expression of CD25, a component of IL-2 receptor (Berglund et al., 2013). IL-2-mediated

ERK/ELK1signaling pathway represses Bach2 and directs plasma cell lineage commitment (Hipp et al., 2017). Therefore, cytokines and their downstream STAT pathways are critical in B cell fate decisions and, if altered, may influence germinal center B cell differentiation. Adoptive transfer experiments showed that inhibition of GC formation required cell-intrinsic signaling of T cells. It is possible that anti-CD137 mAb-induced cytokines from T cells cause dysregulated differentiation of B cells. While the number of GC B cells was reduced in anti-CD137 mAb-treated mice, the number of plasmablasts was increased compared to isotype control mAb-treated animals. Since repression of Bach2 and subsequent upregulation of Prdm1 directs plasma cell commitment, the cytokines produced by T cells in anti-CD137 mAb-treated mice may have inhibited the expression of Bach2. Ablation of Prdm1 restores GC differentiation of Bach2-deficient B cells (Shinnakasu et al., 2016). If anti-CD137 mAb-mediated inhibition of GC was due to repression of Bach2, GC B cells should be restored in Prdm1$^{-/-}$ mice.

Disrupted lymphoid follicle after anti-CD137 antibody treatment

Anti-CD137 mAb-mediated inhibition of GC was correlated with changes in lymphoid follicle structure and GC B cell dispersal. By flow cytometry, the GC reaction seems normal until 7 dpi, when the numbers of both light and dark zone B cells were significantly reduced after anti-CD137 mAb treatment. Thus, the early GC response may be minimally affected. Green *et. al.* described S1PR2, which is selectively expressed on GC B cells, as a GC confinement factor along with CXCR5 (Green et al., 2011). In S1PR2$^{-/-}$ immunized SRBCs, the boundary between the GC and mantle zone was less well defined, which was also seen in anti-CD137 mAb-treated mice (Green et al., 2011). However, the number of GC B cells was not altered in S1PR2$^{-/-}$ mice in contrast to the reduced number of GC B cells in anti-CD137 mAb-treated mice. It is possible that anti-CD137 mAb treatment induces decreased expression of S1PR2 on GC B cells or alters

the gradient of S1P, its ligand, produced by the stromal cells outside the follicles, which would result in dispersal of GC B cells, and additional factors contribute to their reduced number. This could be tested by measuring the expression of S1PR2 on GC B cells from anti-CD137 mAb-treated mice and by performing migration assays *in vitro*. Additionally, B cells constitutively expressing S1PR2 could be adoptively transferred into anti-CD137 mAb- or isotype control mAb-treated, immunized mice. If the S1P gradient were not altered after anti-CD137 mAb treatment, the transferred B cells would form clusters.

References

Aiba, Y., K. Kometani, M. Hamadate, S. Moriyama, A. Sakaue-Sawano, M. Tomura, H. Luche, H.J. Fehling, R. Casellas, O. Kanagawa, A. Miyawaki, and T. Kurosaki. 2010. Preferential localization of IgG memory B cells adjacent to contracted germinal centers. *Proc Natl Acad Sci U S A* 107:12192-12197.

Allman, D., R.C. Lindsley, W. DeMuth, K. Rudd, S.A. Shinton, and R.R. Hardy. 2001. Resolution of three nonproliferative immature splenic B cell subsets reveals multiple selection points during peripheral B cell maturation. *J Immunol* 167:6834-6840.

Anders, S., P.T. Pyl, and W. Huber. 2015. HTSeq--a Python framework to work with high-throughput sequencing data. *Bioinformatics* 31:166-169.

Arch, R.H., and C.B. Thompson. 1998. 4-1BB and Ox40 are members of a tumor necrosis factor (TNF)-nerve growth factor receptor subfamily that bind TNF receptor-associated factors and activate nuclear factor kappaB. *Mol Cell Biol* 18:558-565.

Bachmann, M.F., B. Odermatt, H. Hengartner, and R.M. Zinkernagel. 1996. Induction of long-lived germinal centers associated with persisting antigen after viral infection. *J Exp Med* 183:2259-2269.

Ballesteros-Tato, A., B. Leon, B.A. Graf, A. Moquin, P.S. Adams, F.E. Lund, and T.D. Randall. 2012. Interleukin-2 inhibits germinal center formation by limiting T follicular helper cell differentiation. *Immunity* 36:847-856.

Batista, F.D., and N.E. Harwood. 2009. The who, how and where of antigen presentation to B cells. *Nat Rev Immunol* 9:15-27.

Baumjohann, D., S. Preite, A. Reboldi, F. Ronchi, K.M. Ansel, A. Lanzavecchia, and F. Sallusto. 2013. Persistent antigen and germinal center B cells sustain T follicular helper cell responses and phenotype. *Immunity* 38:596-605.

Bellini, R., A. Medici, M. Calzolari, P. Bonilauri, F. Cavrini, V. Sambri, P. Angelini, and M. Dottori. 2012. Impact of Chikungunya virus on Aedes albopictus females and possibility of vertical transmission using the actors of the 2007 outbreak in Italy. *PLoS One* 7:e28360.

Berglund, L.J., D.T. Avery, C.S. Ma, L. Moens, E.K. Deenick, J. Bustamante, S. Boisson-Dupuis, M. Wong, S. Adelstein, P.D. Arkwright, R. Bacchetta, L. Bezrodnik, H. Dadi, C.M. Roifman, D.A. Fulcher, J.B. Ziegler, J.M. Smart, M. Kobayashi, C. Picard, A. Durandy, M.C. Cook, J.L. Casanova, G. Uzel, and S.G. Tangye. 2013. IL-21 signalling via STAT3 primes human naive B cells to respond to IL-2 to enhance their differentiation into plasmablasts. *Blood* 122:3940-3950.

Bertram, E.M., P. Lau, and T.H. Watts. 2002. Temporal segregation of 4-1BB versus CD28-mediated costimulation: 4-1BB ligand influences T cell numbers late in the primary response and regulates the size of the T cell memory response following influenza infection. *J Immunol* 168:3777-3785.

Blazar, B.R., B.S. Kwon, A. Panoskaltsis-Mortari, K.B. Kwak, J.J. Peschon, and P.A. Taylor. 2001. Ligation of 4-1BB (CDw137) regulates graft-versus-host disease, graft-versus-leukemia, and graft rejection in allogeneic bone marrow transplant recipients. *J Immunol* 166:3174-3183.

Bodmer, J.L., P. Schneider, and J. Tschopp. 2002. The molecular architecture of the TNF superfamily. *Trends Biochem Sci* 27:19-26.

Boes, M., C. Esau, M.B. Fischer, T. Schmidt, M. Carroll, and J. Chen. 1998. Enhanced B-1 cell development, but impaired IgG antibody responses in mice deficient in secreted IgM. *J Immunol* 160:4776-4787.

Botchkareva, N.V., V.A. Botchkarev, L.H. Chen, G. Lindner, and R. Paus. 1999. A role for p75 neurotrophin receptor in the control of hair follicle morphogenesis. *Dev Biol* 216:135-153.

Butler, A., P. Hoffman, P. Smibert, E. Papalexi, and R. Satija. 2018. Integrating single-cell transcriptomic data across different conditions, technologies, and species. *Nat Biotechnol* 36:411-420.

Calado, D.P., Y. Sasaki, S.A. Godinho, A. Pellerin, K. Kochert, B.P. Sleckman, I.M. de Alboran, M. Janz, S. Rodig, and K. Rajewsky. 2012. The cell-cycle regulator c-Myc is essential for the formation and maintenance of germinal centers. *Nat Immunol* 13:1092-1100.

Cancro, M.P. 2009. Signalling crosstalk in B cells: managing worth and need. *Nat Rev Immunol* 9:657-661.

Cannons, J.L., Y. Choi, and T.H. Watts. 2000. Role of TNF receptor-associated factor 2 and p38 mitogen-activated protein kinase activation during 4-1BB-dependent immune response. *J Immunol* 165:6193-6204.

Cannons, J.L., K.P. Hoeflich, J.R. Woodgett, and T.H. Watts. 1999. Role of the stress kinase pathway in signaling via the T cell costimulatory receptor 4-1BB. *J Immunol* 163:2990-2998.

Cannons, J.L., S.G. Tangye, and P.L. Schwartzberg. 2011. SLAM family receptors and SAP adaptors in immunity. *Annu Rev Immunol* 29:665-705.

Cariappa, A., H.C. Liou, B.H. Horwitz, and S. Pillai. 2000. Nuclear factor kappa B is required for the development of marginal zone B lymphocytes. *J Exp Med* 192:1175-1182.

Cariappa, A., M. Tang, C. Parng, E. Nebelitskiy, M. Carroll, K. Georgopoulos, and S. Pillai. 2001. The follicular versus marginal zone B lymphocyte cell fate decision is regulated by Aiolos, Btk, and CD21. *Immunity* 14:603-615.

Carrasco, L., M.A. Sanz, and E. Gonzalez-Almela. 2018. The Regulation of Translation in Alphavirus-Infected Cells. *Viruses* 10:

Carroll, M.C. 1998. CD21/CD35 in B cell activation. *Semin Immunol* 10:279-286.

Cerutti, A., M. Cols, and I. Puga. 2013. Marginal zone B cells: virtues of innate-like antibody-producing lymphocytes. *Nat Rev Immunol* 13:118-132.

Chen, W., S.S. Foo, A. Taylor, A. Lulla, A. Merits, L. Hueston, M.R. Forwood, N.C. Walsh, N.A. Sims, L.J. Herrero, and S. Mahalingam. 2015. Bindarit, an inhibitor of monocyte chemotactic protein synthesis, protects against bone loss induced by chikungunya virus infection. *J Virol* 89:581-593.

Choi, B.K., J.S. Bae, E.M. Choi, W.J. Kang, S. Sakaguchi, D.S. Vinay, and B.S. Kwon. 2004. 4-1BB-dependent inhibition of immunosuppression by activated CD4+CD25+ T cells. *J Leukoc Biol* 75:785-791.

Choi, B.K., Y.H. Kim, W.J. Kang, S.K. Lee, K.H. Kim, S.M. Shin, W.M. Yokoyama, T.Y. Kim, and B.S. Kwon. 2007. Mechanisms involved in synergistic anticancer immunity of anti-4-1BB and anti-CD4 therapy. *Cancer Res* 67:8891-8899.

Cinamon, G., M.A. Zachariah, O.M. Lam, F.W. Foss, Jr., and J.G. Cyster. 2008. Follicular shuttling of marginal zone B cells facilitates antigen transport. *Nat Immunol* 9:54-62.

Couderc, T., F. Chretien, C. Schilte, O. Disson, M. Brigitte, F. Guivel-Benhassine, Y. Touret, G. Barau, N. Cayet, I. Schuffenecker, P. Despres, F. Arenzana-Seisdedos, A. Michault, M.L. Albert, and M. Lecuit. 2008. A mouse model for Chikungunya: young age and inefficient type-I interferon signaling are risk factors for severe disease. *PLoS Pathog* 4:e29.

Cuadros, C., A.L. Dominguez, P.L. Lollini, M. Croft, R.S. Mittler, P. Borgstrom, and J. Lustgarten. 2005. Vaccination with dendritic cells pulsed with apoptotic tumors in combination with anti-OX40 and anti-4-1BB monoclonal antibodies induces T cell-mediated protective immunity in Her-2/neu transgenic mice. *Int J Cancer* 116:934-943.

Curran, M.A., T.L. Geiger, W. Montalvo, M. Kim, S.L. Reiner, A. Al-Shamkhani, J.C. Sun, and J.P. Allison. 2013. Systemic 4-1BB activation induces a novel T cell phenotype driven by high expression of Eomesodermin. *J Exp Med* 210:743-755.

Curran, M.A., M. Kim, W. Montalvo, A. Al-Shamkhani, and J.P. Allison. 2011. Combination CTLA-4 blockade and 4-1BB activation enhances tumor rejection by increasing T-cell infiltration, proliferation, and cytokine production. *PLoS One* 6:e19499.

Cyster, J.G., E.V. Dang, A. Reboldi, and T. Yi. 2014. 25-Hydroxycholesterols in innate and adaptive immunity. *Nat Rev Immunol* 14:731-743.

Dawicki, W., and T.H. Watts. 2004. Expression and function of 4-1BB during CD4 versus CD8 T cell responses in vivo. *Eur J Immunol* 34:743-751.

De Silva, N.S., and U. Klein. 2015. Dynamics of B cells in germinal centres. *Nat Rev Immunol* 15:137-148.

Ding, B.B., E. Bi, H. Chen, J.J. Yu, and B.H. Ye. 2013. IL-21 and CD40L synergistically promote plasma cell differentiation through upregulation of Blimp-1 in human B cells. *J Immunol* 190:1827-1836.

Dobin, A., C.A. Davis, F. Schlesinger, J. Drenkow, C. Zaleski, S. Jha, P. Batut, M. Chaisson, and T.R. Gingeras. 2013. STAR: ultrafast universal RNA-seq aligner. *Bioinformatics* 29:15-21.

Ellebedy, A.H., F. Krammer, G.M. Li, M.S. Miller, C. Chiu, J. Wrammert, C.Y. Chang, C.W. Davis, M. McCausland, R. Elbein, S. Edupuganti, P. Spearman, S.F. Andrews, P.C. Wilson, A. Garcia-Sastre, M.J. Mulligan, A.K. Mehta, P. Palese, and R. Ahmed. 2014. Induction of broadly cross-reactive antibody responses to the influenza HA stem region following H5N1 vaccination in humans. *Proc Natl Acad Sci U S A* 111:13133-13138.

Endres, R., M.B. Alimzhanov, T. Plitz, A. Futterer, M.H. Kosco-Vilbois, S.A. Nedospasov, K. Rajewsky, and K. Pfeffer. 1999. Mature follicular dendritic cell networks depend on expression of lymphotoxin beta receptor by radioresistant stromal cells and of lymphotoxin beta and tumor necrosis factor by B cells. *J Exp Med* 189:159-168.

Fisher, T.S., C. Kamperschroer, T. Oliphant, V.A. Love, P.D. Lira, R. Doyonnas, S. Bergqvist, S.M. Baxi, A. Rohner, A.C. Shen, C. Huang, S.A. Sokolowski, and L.L. Sharp. 2012. Targeting of 4-1BB by monoclonal antibody PF-05082566 enhances T-cell function and promotes anti-tumor activity. *Cancer Immunol Immunother* 61:1721-1733.

Foell, J., S. Strahotin, S.P. O'Neil, M.M. McCausland, C. Suwyn, M. Haber, P.N. Chander, A.S. Bapat, X.J. Yan, N. Chiorazzi, M.K. Hoffmann, and R.S. Mittler. 2003. CD137 costimulatory T cell receptor engagement reverses acute disease in lupus-prone NZB x NZW F1 mice. *J Clin Invest* 111:1505-1518.

Gardner, J., I. Anraku, T.T. Le, T. Larcher, L. Major, P. Roques, W.A. Schroder, S. Higgs, and A. Suhrbier. 2010. Chikungunya virus arthritis in adult wild-type mice. *J Virol* 84:8021-8032.

Gardner, T.S., C.R. Cantor, and J.J. Collins. 2000. Construction of a genetic toggle switch in Escherichia coli. *Nature* 403:339-342.

Gauttier, V., J.P. Judor, V. Le Guen, J. Cany, N. Ferry, and S. Conchon. 2014. Agonistic anti-CD137 antibody treatment leads to antitumor response in mice with liver cancer. *Int J Cancer* 135:2857-2867.

Goodwin, R.G., W.S. Din, T. Davis-Smith, D.M. Anderson, S.D. Gimpel, T.A. Sato, C.R. Maliszewski, C.I. Brannan, N.G. Copeland, N.A. Jenkins, and et al. 1993. Molecular cloning of a ligand for the inducible T cell gene 4-1BB: a member of an emerging family of cytokines with homology to tumor necrosis factor. *Eur J Immunol* 23:2631-2641.

Green, J.A., K. Suzuki, B. Cho, L.D. Willison, D. Palmer, C.D. Allen, T.H. Schmidt, Y. Xu, R.L. Proia, S.R. Coughlin, and J.G. Cyster. 2011. The sphingosine 1-phosphate receptor S1P(2) maintains the homeostasis of germinal center B cells and promotes niche confinement. *Nat Immunol* 12:672-680.

Guo, Z., D. Cheng, Z. Xia, M. Luan, L. Wu, G. Wang, and S. Zhang. 2013. Combined TIM-3 blockade and CD137 activation affords the long-term protection in a murine model of ovarian cancer. *J Transl Med* 11:215.

Haldar, M., M. Kohyama, A.Y. So, W. Kc, X. Wu, C.G. Briseno, A.T. Satpathy, N.M. Kretzer, H. Arase, N.S. Rajasekaran, L. Wang, T. Egawa, K. Igarashi, D. Baltimore, T.L. Murphy, and K.M. Murphy. 2014. Heme-mediated SPI-C induction promotes monocyte differentiation into iron-recycling macrophages. *Cell* 156:1223-1234.

Hanna, M.G., Jr., and A.K. Szakal. 1968. Localization of 125I-labeled antigen in germinal centers of mouse spleen: histologic and ultrastructural autoradiographic studies of the secondary immune reaction. *J Immunol* 101:949-962.

Hawman, D.W., J.M. Fox, A.W. Ashbrook, N.A. May, K.M.S. Schroeder, R.M. Torres, J.E. Crowe, Jr., T.S. Dermody, M.S. Diamond, and T.E. Morrison. 2016. Pathogenic Chikungunya Virus Evades B Cell Responses to Establish Persistence. *Cell Rep* 16:1326-1338.

Hawman, D.W., K.A. Stoermer, S.A. Montgomery, P. Pal, L. Oko, M.S. Diamond, and T.E. Morrison. 2013. Chronic joint disease caused by persistent Chikungunya virus infection is controlled by the adaptive immune response. *J Virol* 87:13878-13888.

Heesters, B.A., M. Lindqvist, P.A. Vagefi, E.P. Scully, F.A. Schildberg, M. Altfeld, B.D. Walker, D.E. Kaufmann, and M.C. Carroll. 2015. Follicular Dendritic Cells Retain Infectious HIV in Cycling Endosomes. *PLoS Pathog* 11:e1005285.

Heinen, E., M. Braun, P.G. Coulie, J. Van Snick, M. Moeremans, N. Cormann, C. Kinet-Denoel, and L.J. Simar. 1986. Transfer of immune complexes from lymphocytes to follicular dendritic cells. *Eur J Immunol* 16:167-172.

Heinisch, I.V., C. Bizer, W. Volgger, and H.U. Simon. 2001. Functional CD137 receptors are expressed by eosinophils from patients with IgE-mediated allergic responses but not by eosinophils from patients with non-IgE-mediated eosinophilic disorders. *J Allergy Clin Immunol* 108:21-28.

Hipp, N., H. Symington, C. Pastoret, G. Caron, C. Monvoisin, K. Tarte, T. Fest, and C. Delaloy. 2017. IL-2 imprints human naive B cell fate towards plasma cell through ERK/ELK1-mediated BACH2 repression. *Nat Commun* 8:1443.

Hoarau, J.J., M.C. Jaffar Bandjee, P. Krejbich Trotot, T. Das, G. Li-Pat-Yuen, B. Dassa, M. Denizot, E. Guichard, A. Ribera, T. Henni, F. Tallet, M.P. Moiton, B.A. Gauzere, S. Bruniquet, Z.

Jaffar Bandjee, P. Morbidelli, G. Martigny, M. Jolivet, F. Gay, M. Grandadam, H. Tolou, V. Vieillard, P. Debre, B. Autran, and P. Gasque. 2010. Persistent chronic inflammation and infection by Chikungunya arthritogenic alphavirus in spite of a robust host immune response. *J Immunol* 184:5914-5927.

Hong, J.P., M.K. McCarthy, B.J. Davenport, T.E. Morrison, and M.S. Diamond. 2019. Clearance of Chikungunya virus infection in lymphoid tissues is promoted by treatment with an agonistic anti-CD137 antibody. *J Virol*

Houot, R., M.J. Goldstein, H.E. Kohrt, J.H. Myklebust, A.A. Alizadeh, J.T. Lin, J.M. Irish, J.A. Torchia, A. Kolstad, L. Chen, and R. Levy. 2009. Therapeutic effect of CD137 immunomodulation in lymphoma and its enhancement by Treg depletion. *Blood* 114:3431-3438.

Hsieh, E.H., X. Fernandez, J. Wang, M. Hamer, S. Calvillo, M. Croft, B.S. Kwon, and D.D. Lo. 2010. CD137 is required for M cell functional maturation but not lineage commitment. *Am J Pathol* 177:666-676.

Impagliazzo, A., F. Milder, H. Kuipers, M.V. Wagner, X. Zhu, R.M. Hoffman, R. van Meersbergen, J. Huizingh, P. Wanningen, J. Verspuij, M. de Man, Z. Ding, A. Apetri, B. Kukrer, E. Sneekes-Vriese, D. Tomkiewicz, N.S. Laursen, P.S. Lee, A. Zakrzewska, L. Dekking, J. Tolboom, L. Tettero, S. van Meerten, W. Yu, W. Koudstaal, J. Goudsmit, A.B. Ward, W. Meijberg, I.A. Wilson, and K. Radosevic. 2015. A stable trimeric influenza hemagglutinin stem as a broadly protective immunogen. *Science* 349:1301-1306.

Ise, W., K. Fujii, K. Shiroguchi, A. Ito, K. Kometani, K. Takeda, E. Kawakami, K. Yamashita, K. Suzuki, T. Okada, and T. Kurosaki. 2018. T Follicular Helper Cell-Germinal Center B Cell Interaction Strength Regulates Entry into Plasma Cell or Recycling Germinal Center Cell Fate. *Immunity* 48:702-715 e704.

Ito, F., Q. Li, A.B. Shreiner, R. Okuyama, M.N. Jure-Kunkel, S. Teitz-Tennenbaum, and A.E. Chang. 2004. Anti-CD137 monoclonal antibody administration augments the antitumor efficacy of dendritic cell-based vaccines. *Cancer Res* 64:8411-8419.

Jang, I.K., Z.H. Lee, Y.J. Kim, S.H. Kim, and B.S. Kwon. 1998. Human 4-1BB (CD137) signals are mediated by TRAF2 and activate nuclear factor-kappa B. *Biochem Biophys Res Commun* 242:613-620.

John, L.B., L.J. Howland, J.K. Flynn, A.C. West, C. Devaud, C.P. Duong, T.J. Stewart, J.A. Westwood, Z.S. Guo, D.L. Bartlett, M.J. Smyth, M.H. Kershaw, and P.K. Darcy. 2012. Oncolytic virus and anti-4-1BB combination therapy elicits strong antitumor immunity against established cancer. *Cancer Res* 72:1651-1660.

Kienzle, G., and J. von Kempis. 2000. CD137 (ILA/4-1BB), expressed by primary human monocytes, induces monocyte activation and apoptosis of B lymphocytes. *Int Immunol* 12:73-82.

King, A.D., A. Nisalak, S. Kalayanrooj, K.S. Myint, K. Pattanapanyasat, S. Nimmannitya, and B.L. Innis. 1999. B cells are the principal circulating mononuclear cells infected by dengue virus. *Southeast Asian J Trop Med Public Health* 30:718-728.

Kiu, H., and S.E. Nicholson. 2012. Biology and significance of the JAK/STAT signalling pathways. *Growth Factors* 30:88-106.

Knight, D.A., S.F. Ngiow, M. Li, T. Parmenter, S. Mok, A. Cass, N.M. Haynes, K. Kinross, H. Yagita, R.C. Koya, T.G. Graeber, A. Ribas, G.A. McArthur, and M.J. Smyth. 2013. Host immunity

contributes to the anti-melanoma activity of BRAF inhibitors. *J Clin Invest* 123:1371-1381.

Ko, E., W. Luo, L. Peng, X. Wang, and S. Ferrone. 2007. Mouse dendritic-endothelial cell hybrids and 4-1BB costimulation elicit antitumor effects mediated by broad antiangiogenic immunity. *Cancer Res* 67:7875-7884.

Kocak, E., K. Lute, X. Chang, K.F. May, Jr., K.R. Exten, H. Zhang, S.F. Abdessalam, A.M. Lehman, D. Jarjoura, P. Zheng, and Y. Liu. 2006. Combination therapy with anti-CTL antigen-4 and anti-4-1BB antibodies enhances cancer immunity and reduces autoimmunity. *Cancer Res* 66:7276-7284.

Kohrt, H.E., A.D. Colevas, R. Houot, K. Weiskopf, M.J. Goldstein, P. Lund, A. Mueller, I. Sagiv-Barfi, A. Marabelle, R. Lira, E. Troutner, L. Richards, A. Rajapaska, J. Hebb, C. Chester, E. Waller, A. Ostashko, W.K. Weng, L. Chen, D. Czerwinski, Y.X. Fu, J. Sunwoo, and R. Levy. 2014. Targeting CD137 enhances the efficacy of cetuximab. *J Clin Invest* 124:2668-2682.

Kohrt, H.E., R. Houot, M.J. Goldstein, K. Weiskopf, A.A. Alizadeh, J. Brody, A. Muller, R. Pachynski, D. Czerwinski, S. Coutre, M.P. Chao, L. Chen, T.F. Tedder, and R. Levy. 2011. CD137 stimulation enhances the antilymphoma activity of anti-CD20 antibodies. *Blood* 117:2423-2432.

Koike, T., K. Harada, S. Horiuchi, and D. Kitamura. 2019. The quantity of CD40 signaling determines the differentiation of B cells into functionally distinct memory cell subsets. *Elife* 8:

Kong, Y.Y., H. Yoshida, I. Sarosi, H.L. Tan, E. Timms, C. Capparelli, S. Morony, A.J. Oliveira-dos-Santos, G. Van, A. Itie, W. Khoo, A. Wakeham, C.R. Dunstan, D.L. Lacey, T.W. Mak, W.J. Boyle, and J.M. Penninger. 1999. OPGL is a key regulator of osteoclastogenesis, lymphocyte development and lymph-node organogenesis. *Nature* 397:315-323.

Kraus, M., L.I. Pao, A. Reichlin, Y. Hu, B. Canono, J.C. Cambier, M.C. Nussenzweig, and K. Rajewsky. 2001. Interference with immunoglobulin (Ig)alpha immunoreceptor tyrosine-based activation motif (ITAM) phosphorylation modulates or blocks B cell development, depending on the availability of an Igbeta cytoplasmic tail. *J Exp Med* 194:455-469.

Kuchen, S., R. Robbins, G.P. Sims, C. Sheng, T.M. Phillips, P.E. Lipsky, and R. Ettinger. 2007. Essential role of IL-21 in B cell activation, expansion, and plasma cell generation during CD4+ T cell-B cell collaboration. *J Immunol* 179:5886-5896.

Kuraoka, M., A.G. Schmidt, T. Nojima, F. Feng, A. Watanabe, D. Kitamura, S.C. Harrison, T.B. Kepler, and G. Kelsoe. 2016. Complex Antigens Drive Permissive Clonal Selection in Germinal Centers. *Immunity* 44:542-552.

Kurosaki, T., K. Kometani, and W. Ise. 2015. Memory B cells. *Nat Rev Immunol* 15:149-159.

Kwon, B.S., J.C. Hurtado, Z.H. Lee, K.B. Kwack, S.K. Seo, B.K. Choi, B.H. Koller, G. Wolisi, H.E. Broxmeyer, and D.S. Vinay. 2002. Immune responses in 4-1BB (CD137)-deficient mice. *J Immunol* 168:5483-5490.

Kwon, B.S., and S.M. Weissman. 1989. cDNA sequences of two inducible T-cell genes. *Proc Natl Acad Sci U S A* 86:1963-1967.

Kwon, H., D. Thierry-Mieg, J. Thierry-Mieg, H.P. Kim, J. Oh, C. Tunyaplin, S. Carotta, C.E. Donovan, M.L. Goldman, P. Tailor, K. Ozato, D.E. Levy, S.L. Nutt, K. Calame, and W.J. Leonard. 2009. Analysis of interleukin-21-induced Prdm1 gene regulation reveals functional cooperation of STAT3 and IRF4 transcription factors. *Immunity* 31:941-952.

Labadie, K., T. Larcher, C. Joubert, A. Mannioui, B. Delache, P. Brochard, L. Guigand, L. Dubreil, P. Lebon, B. Verrier, X. de Lamballerie, A. Suhrbier, Y. Cherel, R. Le Grand, and P. Roques. 2010. Chikungunya disease in nonhuman primates involves long-term viral persistence in macrophages. *J Clin Invest* 120:894-906.

Lampropoulou, V., A. Sergushichev, M. Bambouskova, S. Nair, E.E. Vincent, E. Loginicheva, L. Cervantes-Barragan, X. Ma, S.C. Huang, T. Griss, C.J. Weinheimer, S. Khader, G.J. Randolph, E.J. Pearce, R.G. Jones, A. Diwan, M.S. Diamond, and M.N. Artyomov. 2016. Itaconate Links Inhibition of Succinate Dehydrogenase with Macrophage Metabolic Remodeling and Regulation of Inflammation. *Cell Metab* 24:158-166.

Lee, H., H.J. Park, H.J. Sohn, J.M. Kim, and S.J. Kim. 2011. Combinatorial therapy for liver metastatic colon cancer: dendritic cell vaccine and low-dose agonistic anti-4-1BB antibody co-stimulatory signal. *J Surg Res* 169:e43-50.

Lee, S.J., L. Myers, G. Muralimohan, J. Dai, Y. Qiao, Z. Li, R.S. Mittler, and A.T. Vella. 2004. 4-1BB and OX40 dual costimulation synergistically stimulate primary specific CD8 T cells for robust effector function. *J Immunol* 173:3002-3012.

Lee, S.W., Y. Park, S.Y. Eun, S. Madireddi, H. Cheroutre, and M. Croft. 2012. Cutting edge: 4-1BB controls regulatory activity in dendritic cells through promoting optimal expression of retinal dehydrogenase. *J Immunol* 189:2697-2701.

Lee, S.W., Y. Park, T. So, B.S. Kwon, H. Cheroutre, R.S. Mittler, and M. Croft. 2008. Identification of regulatory functions for 4-1BB and 4-1BBL in myelopoiesis and the development of dendritic cells. *Nat Immunol* 9:917-926.

Lee, S.W., A.T. Vella, B.S. Kwon, and M. Croft. 2005. Enhanced CD4 T cell responsiveness in the absence of 4-1BB. *J Immunol* 174:6803-6808.

Li, G., J.C. Boucher, H. Kotani, K. Park, Y. Zhang, B. Shrestha, X. Wang, L. Guan, N. Beatty, D. Abate-Daga, and M.L. Davila. 2018. 4-1BB enhancement of CAR T function requires NF-kappaB and TRAFs. *JCI Insight* 3:

Li, J., E. Lu, T. Yi, and J.G. Cyster. 2016. EBI2 augments Tfh cell fate by promoting interaction with IL-2-quenching dendritic cells. *Nature* 533:110-114.

Linterman, M.A., W. Pierson, S.K. Lee, A. Kallies, S. Kawamoto, T.F. Rayner, M. Srivastava, D.P. Divekar, L. Beaton, J.J. Hogan, S. Fagarasan, A. Liston, K.G. Smith, and C.G. Vinuesa. 2011. Foxp3+ follicular regulatory T cells control the germinal center response. *Nat Med* 17:975-982.

Long, K.C., S.A. Ziegler, S. Thangamani, N.L. Hausser, T.J. Kochel, S. Higgs, and R.B. Tesh. 2011. Experimental transmission of Mayaro virus by Aedes aegypti. *Am J Trop Med Hyg* 85:750-757.

Long, K.M., M.T. Ferris, A.C. Whitmore, S.A. Montgomery, L.R. Thurlow, C.E. McGee, C.A. Rodriguez, J.K. Lim, and M.T. Heise. 2016. gammadelta T Cells Play a Protective Role in Chikungunya Virus-Induced Disease. *J Virol* 90:433-443.

Lu, T.T., and J.G. Cyster. 2002. Integrin-mediated long-term B cell retention in the splenic marginal zone. *Science* 297:409-412.

Luo, W., F. Weisel, and M.J. Shlomchik. 2018. B Cell Receptor and CD40 Signaling Are Rewired for Synergistic Induction of the c-Myc Transcription Factor in Germinal Center B Cells. *Immunity* 48:313-326 e315.

MacLeod, M.K., A. David, A.S. McKee, F. Crawford, J.W. Kappler, and P. Marrack. 2011. Memory CD4 T cells that express CXCR5 provide accelerated help to B cells. *J Immunol* 186:2889-2896.

Magnusson, M., F. Zare, and A. Tarkowski. 2006. Requirement of type I interferon signaling for arthritis triggered by double-stranded RNA. *Arthritis Rheum* 54:148-157.

Marson, A., K. Kretschmer, G.M. Frampton, E.S. Jacobsen, J.K. Polansky, K.D. MacIsaac, S.S. Levine, E. Fraenkel, H. von Boehmer, and R.A. Young. 2007. Foxp3 occupancy and regulation of key target genes during T-cell stimulation. *Nature* 445:931-935.

Mason, D.Y., M. Jones, and C.C. Goodnow. 1992. Development and follicular localization of tolerant B lymphocytes in lysozyme/anti-lysozyme IgM/IgD transgenic mice. *Int Immunol* 4:163-175.

McCarthy, M.K., and T.E. Morrison. 2017. Persistent RNA virus infections: do PAMPS drive chronic disease? *Curr Opin Virol* 23:8-15.

McKee, S.J., B.L. Doff, M.S. Soon, and S.R. Mattarollo. 2017. Therapeutic Efficacy of 4-1BB Costimulation Is Abrogated by PD-1 Blockade in a Model of Spontaneous B-cell Lymphoma. *Cancer Immunol Res* 5:191-197.

Melero, I., O. Murillo, J. Dubrot, S. Hervas-Stubbs, and J.L. Perez-Gracia. 2008. Multi-layered action mechanisms of CD137 (4-1BB)-targeted immunotherapies. *Trends Pharmacol Sci* 29:383-390.

Melero, I., W.W. Shuford, S.A. Newby, A. Aruffo, J.A. Ledbetter, K.E. Hellstrom, R.S. Mittler, and L. Chen. 1997. Monoclonal antibodies against the 4-1BB T-cell activation molecule eradicate established tumors. *Nat Med* 3:682-685.

Mesin, L., J. Ersching, and G.D. Victora. 2016. Germinal Center B Cell Dynamics. *Immunity* 45:471-482.

Miner, J.J., L.E. Cook, J.P. Hong, A.M. Smith, J.M. Richner, R.M. Shimak, A.R. Young, K. Monte, S. Poddar, J.E. Crowe, Jr., D.J. Lenschow, and M.S. Diamond. 2017. Therapy with CTLA4-Ig and an antiviral monoclonal antibody controls chikungunya virus arthritis. *Sci Transl Med* 9:

Mittler, R.S., J. Foell, M. McCausland, S. Strahotin, L. Niu, A. Bapat, and L.B. Hewes. 2004. Anti-CD137 antibodies in the treatment of autoimmune disease and cancer. *Immunol Res* 29:197-208.

Moens, L., and S.G. Tangye. 2014. Cytokine-Mediated Regulation of Plasma Cell Generation: IL-21 Takes Center Stage. *Front Immunol* 5:65.

Mond, J.J., A. Lees, and C.M. Snapper. 1995. T cell-independent antigens type 2. *Annu Rev Immunol* 13:655-692.

Morales-Kastresana, A., E. Catalan, S. Hervas-Stubbs, A. Palazon, A. Azpilikueta, E. Bolanos, A. Anel, J. Pardo, and I. Melero. 2013a. Essential complicity of perforin-granzyme and FAS-L mechanisms to achieve tumor rejection following treatment with anti-CD137 mAb. *J Immunother Cancer* 1:3.

Morales-Kastresana, A., M.F. Sanmamed, I. Rodriguez, A. Palazon, I. Martinez-Forero, S. Labiano, S. Hervas-Stubbs, B. Sangro, C. Ochoa, A. Rouzaut, A. Azpilikueta, E. Bolanos, M. Jure-Kunkel, I. Gutgemann, and I. Melero. 2013b. Combined immunostimulatory monoclonal antibodies extend survival in an aggressive transgenic hepatocellular carcinoma mouse model. *Clin Cancer Res* 19:6151-6162.

Moriyama, S., N. Takahashi, J.A. Green, S. Hori, M. Kubo, J.G. Cyster, and T. Okada. 2014. Sphingosine-1-phosphate receptor 2 is critical for follicular helper T cell retention in germinal centers. *J Exp Med* 211:1297-1305.

Morrison, T.E., L. Oko, S.A. Montgomery, A.C. Whitmore, A.R. Lotstein, B.M. Gunn, S.A. Elmore, and M.T. Heise. 2011. A mouse model of chikungunya virus-induced musculoskeletal inflammatory disease: evidence of arthritis, tenosynovitis, myositis, and persistence. *Am J Pathol* 178:32-40.

Muppidi, J.R., R. Schmitz, J.A. Green, W. Xiao, A.B. Larsen, S.E. Braun, J. An, Y. Xu, A. Rosenwald, G. Ott, R.D. Gascoyne, L.M. Rimsza, E. Campo, E.S. Jaffe, J. Delabie, E.B. Smeland, R.M. Braziel, R.R. Tubbs, J.R. Cook, D.D. Weisenburger, W.C. Chan, N. Vaidehi, L.M. Staudt, and J.G. Cyster. 2014. Loss of signalling via Galpha13 in germinal centre B-cell-derived lymphoma. *Nature* 516:254-258.

Muto, A., K. Ochiai, Y. Kimura, A. Itoh-Nakadai, K.L. Calame, D. Ikebe, S. Tashiro, and K. Igarashi. 2010. Bach2 represses plasma cell gene regulatory network in B cells to promote antibody class switch. *EMBO J* 29:4048-4061.

Muto, A., S. Tashiro, O. Nakajima, H. Hoshino, S. Takahashi, E. Sakoda, D. Ikebe, M. Yamamoto, and K. Igarashi. 2004. The transcriptional programme of antibody class switching involves the repressor Bach2. *Nature* 429:566-571.

Nair, S., S. Poddar, R.M. Shimak, and M.S. Diamond. 2017. Interferon regulatory factor-1 (IRF-1) protects against chikungunya virus induced immunopathology by restricting infection in muscle cells. *J Virol*

Narazaki, H., Y. Zhu, L. Luo, G. Zhu, and L. Chen. 2010. CD137 agonist antibody prevents cancer recurrence: contribution of CD137 on both hematopoietic and nonhematopoietic cells. *Blood* 115:1941-1948.

Nutt, S.L., P.D. Hodgkin, D.M. Tarlinton, and L.M. Corcoran. 2015. The generation of antibody-secreting plasma cells. *Nat Rev Immunol* 15:160-171.

Ochiai, K., A. Muto, H. Tanaka, S. Takahashi, and K. Igarashi. 2008. Regulation of the plasma cell transcription factor Blimp-1 gene by Bach2 and Bcl6. *Int Immunol* 20:453-460.

Okada, T., M.J. Miller, I. Parker, M.F. Krummel, M. Neighbors, S.B. Hartley, A. O'Garra, M.D. Cahalan, and J.G. Cyster. 2005. Antigen-engaged B cells undergo chemotaxis toward the T zone and form motile conjugates with helper T cells. *PLoS Biol* 3:e150.

Pal, P., K.A. Dowd, J.D. Brien, M.A. Edeling, S. Gorlatov, S. Johnson, I. Lee, W. Akahata, G.J. Nabel, M.K. Richter, J.M. Smit, D.H. Fremont, T.C. Pierson, M.T. Heise, and M.S. Diamond. 2013. Development of a highly protective combination monoclonal antibody therapy against Chikungunya virus. *PLoS Pathog* 9:e1003312.

Palazon, A., I. Martinez-Forero, A. Teijeira, A. Morales-Kastresana, C. Alfaro, M.F. Sanmamed, J.L. Perez-Gracia, I. Penuelas, S. Hervas-Stubbs, A. Rouzaut, M.O. de Landazuri, M. Jure-Kunkel, J. Aragones, and I. Melero. 2012. The HIF-1alpha hypoxia response in tumor-infiltrating T lymphocytes induces functional CD137 (4-1BB) for immunotherapy. *Cancer Discov* 2:608-623.

Park, J.J., S. Anand, Y. Zhao, Y. Matsumura, Y. Sakoda, A. Kuramasu, S.E. Strome, L. Chen, and K. Tamada. 2012. Expression of anti-HVEM single-chain antibody on tumor cells induces tumor-specific immunity with long-term memory. *Cancer Immunol Immunother* 61:203-214.

Petersen, L.R., and A.M. Powers. 2016. Chikungunya: epidemiology. *F1000Res* 5:

Phan, T.G., D. Paus, T.D. Chan, M.L. Turner, S.L. Nutt, A. Basten, and R. Brink. 2006. High affinity germinal center B cells are actively selected into the plasma cell compartment. *J Exp Med* 203:2419-2424.

Pollok, K.E., Y.J. Kim, J. Hurtado, Z. Zhou, K.K. Kim, and B.S. Kwon. 1994. 4-1BB T-cell antigen binds to mature B cells and macrophages, and costimulates anti-mu-primed splenic B cells. *Eur J Immunol* 24:367-374.

Poo, Y.S., H. Nakaya, J. Gardner, T. Larcher, W.A. Schroder, T.T. Le, L.D. Major, and A. Suhrbier. 2014a. CCR2 deficiency promotes exacerbated chronic erosive neutrophil-dominated chikungunya virus arthritis. *J Virol* 88:6862-6872.

Poo, Y.S., P.A. Rudd, J. Gardner, J.A. Wilson, T. Larcher, M.A. Colle, T.T. Le, H.I. Nakaya, D. Warrilow, R. Allcock, H. Bielefeldt-Ohmann, W.A. Schroder, A.A. Khromykh, J.A. Lopez, and A. Suhrbier. 2014b. Multiple immune factors are involved in controlling acute and chronic chikungunya virus infection. *PLoS Negl Trop Dis* 8:e3354.

Purtha, W.E., T.F. Tedder, S. Johnson, D. Bhattacharya, and M.S. Diamond. 2011. Memory B cells, but not long-lived plasma cells, possess antigen specificities for viral escape mutants. *J Exp Med* 208:2599-2606.

Reese, T.A., B.S. Wakeman, H.S. Choi, M.M. Hufford, S.C. Huang, X. Zhang, M.D. Buck, A. Jezewski, A. Kambal, C.Y. Liu, G. Goel, P.J. Murray, R.J. Xavier, M.H. Kaplan, R. Renne, S.H. Speck, M.N. Artyomov, E.J. Pearce, and H.W. Virgin. 2014. Helminth infection reactivates latent gamma-herpesvirus via cytokine competition at a viral promoter. *Science* 345:573-577.

Robinson, M.C. 1955. An epidemic of virus disease in Southern Province, Tanganyika Territory, in 1952-53. I. Clinical features. *Trans R Soc Trop Med Hyg* 49:28-32.

Rodriguez-Morales, A.J., J.A. Cardona-Ospina, W. Villamil-Gomez, and A.E. Paniz-Mondolfi. 2015. How many patients with post-chikungunya chronic inflammatory rheumatism can we expect in the new endemic areas of Latin America? *Rheumatol Int* 35:2091-2094.

Rodriguez-Morales, A.J., W. Villamil-Gomez, M. Merlano-Espinosa, and L. Simone-Kleber. 2016. Post-chikungunya chronic arthralgia: a first retrospective follow-up study of 39 cases in Colombia. *Clin Rheumatol* 35:831-832.

Saito, M., J. Gao, K. Basso, Y. Kitagawa, P.M. Smith, G. Bhagat, A. Pernis, L. Pasqualucci, and R. Dalla-Favera. 2007. A signaling pathway mediating downregulation of BCL6 in germinal center B cells is blocked by BCL6 gene alterations in B cell lymphoma. *Cancer Cell* 12:280-292.

Samardzic, T., D. Marinkovic, C.P. Danzer, J. Gerlach, L. Nitschke, and T. Wirth. 2002. Reduction of marginal zone B cells in CD22-deficient mice. *Eur J Immunol* 32:561-567.

Saoulli, K., S.Y. Lee, J.L. Cannons, W.C. Yeh, A. Santana, M.D. Goldstein, N. Bangia, M.A. DeBenedette, T.W. Mak, Y. Choi, and T.H. Watts. 1998. CD28-independent, TRAF2-dependent costimulation of resting T cells by 4-1BB ligand. *J Exp Med* 187:1849-1862.

Schebesta, A., S. McManus, G. Salvagiotto, A. Delogu, G.A. Busslinger, and M. Busslinger. 2007. Transcription factor Pax5 activates the chromatin of key genes involved in B cell signaling, adhesion, migration, and immune function. *Immunity* 27:49-63.

Schilte, C., M.R. Buckwalter, M.E. Laird, M.S. Diamond, O. Schwartz, and M.L. Albert. 2012. Cutting edge: independent roles for IRF-3 and IRF-7 in hematopoietic and

nonhematopoietic cells during host response to Chikungunya infection. *J Immunol* 188:2967-2971.

Schwab, S.R., and J.G. Cyster. 2007. Finding a way out: lymphocyte egress from lymphoid organs. *Nat Immunol* 8:1295-1301.

Senftleben, U., Y. Cao, G. Xiao, F.R. Greten, G. Krahn, G. Bonizzi, Y. Chen, Y. Hu, A. Fong, S.C. Sun, and M. Karin. 2001. Activation by IKKalpha of a second, evolutionary conserved, NF-kappa B signaling pathway. *Science* 293:1495-1499.

Seo, S.K., J.H. Choi, Y.H. Kim, W.J. Kang, H.Y. Park, J.H. Suh, B.K. Choi, D.S. Vinay, and B.S. Kwon. 2004. 4-1BB-mediated immunotherapy of rheumatoid arthritis. *Nat Med* 10:1088-1094.

Shaknovich, R., L. Cerchietti, L. Tsikitas, M. Kormaksson, S. De, M.E. Figueroa, G. Ballon, S.N. Yang, N. Weinhold, M. Reimers, T. Clozel, K. Luttrop, T.J. Ekstrom, J. Frank, A. Vasanthakumar, L.A. Godley, F. Michor, O. Elemento, and A. Melnick. 2011. DNA methyltransferase 1 and DNA methylation patterning contribute to germinal center B-cell differentiation. *Blood* 118:3559-3569.

Shi, J., S. Hou, Q. Fang, X. Liu, X. Liu, and H. Qi. 2018. PD-1 Controls Follicular T Helper Cell Positioning and Function. *Immunity* 49:264-274 e264.

Shi, W., and D.W. Siemann. 2006. Augmented antitumor effects of radiation therapy by 4-1BB antibody (BMS-469492) treatment. *Anticancer Res* 26:3445-3453.

Shinnakasu, R., T. Inoue, K. Kometani, S. Moriyama, Y. Adachi, M. Nakayama, Y. Takahashi, H. Fukuyama, T. Okada, and T. Kurosaki. 2016. Regulated selection of germinal-center cells into the memory B cell compartment. *Nat Immunol* 17:861-869.

Shuford, W.W., K. Klussman, D.D. Tritchler, D.T. Loo, J. Chalupny, A.W. Siadak, T.J. Brown, J. Emswiler, H. Raecho, C.P. Larsen, T.C. Pearson, J.A. Ledbetter, A. Aruffo, and R.S. Mittler. 1997. 4-1BB costimulatory signals preferentially induce CD8+ T cell proliferation and lead to the amplification in vivo of cytotoxic T cell responses. *J Exp Med* 186:47-55.

Siebenlist, U., K. Brown, and E. Claudio. 2005. Control of lymphocyte development by nuclear factor-kappaB. *Nat Rev Immunol* 5:435-445.

Silva, L.A., S. Khomandiak, A.W. Ashbrook, R. Weller, M.T. Heise, T.E. Morrison, and T.S. Dermody. 2014. A single-amino-acid polymorphism in Chikungunya virus E2 glycoprotein influences glycosaminoglycan utilization. *J Virol* 88:2385-2397.

Simon, F., E. Javelle, M. Oliver, I. Leparc-Goffart, and C. Marimoutou. 2011. Chikungunya virus infection. *Curr Infect Dis Rep* 13:218-228.

Sissoko, D., D. Malvy, K. Ezzedine, P. Renault, F. Moscetti, M. Ledrans, and V. Pierre. 2009. Post-epidemic Chikungunya disease on Reunion Island: course of rheumatic manifestations and associated factors over a 15-month period. *PLoS Negl Trop Dis* 3:e389.

Smith, K.G., A. Light, G.J. Nossal, and D.M. Tarlinton. 1997. The extent of affinity maturation differs between the memory and antibody-forming cell compartments in the primary immune response. *EMBO J* 16:2996-3006.

Stagg, J., S. Loi, U. Divisekera, S.F. Ngiow, H. Duret, H. Yagita, M.W. Teng, and M.J. Smyth. 2011. Anti-ErbB-2 mAb therapy requires type I and II interferons and synergizes with anti-PD-1 or anti-CD137 mAb therapy. *Proc Natl Acad Sci U S A* 108:7142-7147.

Staples, J.E., R.F. Breiman, and A.M. Powers. 2009. Chikungunya fever: an epidemiological review of a re-emerging infectious disease. *Clin Infect Dis* 49:942-948.

Starck, L., C. Scholz, B. Dorken, and P.T. Daniel. 2005. Costimulation by CD137/4-1BB inhibits T cell apoptosis and induces Bcl-xL and c-FLIP(short) via phosphatidylinositol 3-kinase and AKT/protein kinase B. *Eur J Immunol* 35:1257-1266.

Suhrbier, A., and M. La Linn. 2004. Clinical and pathologic aspects of arthritis due to Ross River virus and other alphaviruses. *Curr Opin Rheumatol* 16:374-379.

Sun, Y., S.E. Blink, J.H. Chen, and Y.X. Fu. 2005. Regulation of follicular dendritic cell networks by activated T cells: the role of CD137 signaling. *J Immunol* 175:884-890.

Sun, Y., H.M. Chen, S.K. Subudhi, J. Chen, R. Koka, L. Chen, and Y.X. Fu. 2002. Costimulatory molecule-targeted antibody therapy of a spontaneous autoimmune disease. *Nat Med* 8:1405-1413.

Tan, J.B., K. Xu, K. Cretegny, I. Visan, J.S. Yuan, S.E. Egan, and C.J. Guidos. 2009. Lunatic and manic fringe cooperatively enhance marginal zone B cell precursor competition for delta-like 1 in splenic endothelial niches. *Immunity* 30:254-263.

Tanigaki, K., H. Han, N. Yamamoto, K. Tashiro, M. Ikegawa, K. Kuroda, A. Suzuki, T. Nakano, and T. Honjo. 2002. Notch-RBP-J signaling is involved in cell fate determination of marginal zone B cells. *Nat Immunol* 3:443-450.

Teo, T.H., F.M. Lum, C. Claser, V. Lulla, A. Lulla, A. Merits, L. Renia, and L.F. Ng. 2013. A pathogenic role for CD4+ T cells during Chikungunya virus infection in mice. *J Immunol* 190:259-269.

Toyama, H., S. Okada, M. Hatano, Y. Takahashi, N. Takeda, H. Ichii, T. Takemori, Y. Kuroda, and T. Tokuhisa. 2002. Memory B cells without somatic hypermutation are generated from Bcl6-deficient B cells. *Immunity* 17:329-339.

Traag, V.A., L. Waltman, and N.J. van Eck. 2019. From Louvain to Leiden: guaranteeing well-connected communities. *Sci Rep* 9:5233.

Tsetsarkin, K., S. Higgs, C.E. McGee, X. De Lamballerie, R.N. Charrel, and D.L. Vanlandingham. 2006. Infectious clones of Chikungunya virus (La Reunion isolate) for vector competence studies. *Vector Borne Zoonotic Dis* 6:325-337.

Velichutina, I., R. Shaknovich, H. Geng, N.A. Johnson, R.D. Gascoyne, A.M. Melnick, and O. Elemento. 2010. EZH2-mediated epigenetic silencing in germinal center B cells contributes to proliferation and lymphomagenesis. *Blood* 116:5247-5255.

Victora, G.D., T.A. Schwickert, D.R. Fooksman, A.O. Kamphorst, M. Meyer-Hermann, M.L. Dustin, and M.C. Nussenzweig. 2010. Germinal center dynamics revealed by multiphoton microscopy with a photoactivatable fluorescent reporter. *Cell* 143:592-605.

Vinay, D.S., B.K. Choi, J.S. Bae, W.Y. Kim, B.M. Gebhardt, and B.S. Kwon. 2004. CD137-deficient mice have reduced NK/NKT cell numbers and function, are resistant to lipopolysaccharide-induced shock syndromes, and have lower IL-4 responses. *J Immunol* 173:4218-4229.

Vinuesa, C.G., M.A. Linterman, D. Yu, and I.C. MacLennan. 2016. Follicular Helper T Cells. *Annu Rev Immunol* 34:335-368.

Wang, C., G.H. Lin, A.J. McPherson, and T.H. Watts. 2009. Immune regulation by 4-1BB and 4-1BBL: complexities and challenges. *Immunol Rev* 229:192-215.

Wang, C.J., F. Heuts, V. Ovcinnikovs, L. Wardzinski, C. Bowers, E.M. Schmidt, A. Kogimtzis, R. Kenefeck, D.M. Sansom, and L.S. Walker. 2015. CTLA-4 controls follicular helper T-cell

differentiation by regulating the strength of CD28 engagement. *Proc Natl Acad Sci U S A* 112:524-529.

Wei, H., L. Zhao, W. Li, K. Fan, W. Qian, S. Hou, H. Wang, M. Dai, I. Hellstrom, K.E. Hellstrom, and Y. Guo. 2013. Combinatorial PD-1 blockade and CD137 activation has therapeutic efficacy in murine cancer models and synergizes with cisplatin. *PLoS One* 8:e84927.

Westwood, J.A., G.M. Matthews, J. Shortt, D. Faulkner, H.J. Pegram, C.P. Duong, M. Chesi, P.L. Bergsagel, L.L. Sharp, R.D. Huhn, P.K. Darcy, R.W. Johnstone, and M.H. Kershaw. 2014. Combination anti-CD137 and anti-CD40 antibody therapy in murine myc-driven hematological cancers. *Leuk Res* 38:948-954.

Wilcox, R.A., A.I. Chapoval, K.S. Gorski, M. Otsuji, T. Shin, D.B. Flies, K. Tamada, R.S. Mittler, H. Tsuchiya, D.M. Pardoll, and L. Chen. 2002a. Cutting edge: Expression of functional CD137 receptor by dendritic cells. *J Immunol* 168:4262-4267.

Wilcox, R.A., D.B. Flies, G. Zhu, A.J. Johnson, K. Tamada, A.I. Chapoval, S.E. Strome, L.R. Pease, and L. Chen. 2002b. Provision of antigen and CD137 signaling breaks immunological ignorance, promoting regression of poorly immunogenic tumors. *J Clin Invest* 109:651-659.

Wilcox, R.A., K. Tamada, S.E. Strome, and L. Chen. 2002c. Signaling through NK cell-associated CD137 promotes both helper function for CD8+ cytolytic T cells and responsiveness to IL-2 but not cytolytic activity. *J Immunol* 169:4230-4236.

Xu, D., P. Gu, P.Y. Pan, Q. Li, A.I. Sato, and S.H. Chen. 2004. NK and CD8+ T cell-mediated eradication of poorly immunogenic B16-F10 melanoma by the combined action of IL-12 gene therapy and 4-1BB costimulation. *Int J Cancer* 109:499-506.

Yao, Z., J. Jones, H. Kohrt, and S. Strober. 2011. Selective resistance of CD44hi T cells to p53-dependent cell death results in persistence of immunologic memory after total body irradiation. *J Immunol* 187:4100-4108.

Ye, H., Y.C. Park, M. Kreishman, E. Kieff, and H. Wu. 1999. The structural basis for the recognition of diverse receptor sequences by TRAF2. *Mol Cell* 4:321-330.

Yi, T., X. Wang, L.M. Kelly, J. An, Y. Xu, A.W. Sailer, J.A. Gustafsson, D.W. Russell, and J.G. Cyster. 2012. Oxysterol gradient generation by lymphoid stromal cells guides activated B cell movement during humoral responses. *Immunity* 37:535-548.

Yonezawa, A., S. Dutt, C. Chester, J. Kim, and H.E. Kohrt. 2015. Boosting Cancer Immunotherapy with Anti-CD137 Antibody Therapy. *Clin Cancer Res* 21:3113-3120.

Young, A.R., M.C. Locke, L.E. Cook, B.E. Hiller, R. Zhang, M.L. Hedberg, K.J. Monte, D.J. Veis, M.S. Diamond, and D.J. Lenschow. 2019. Dermal and muscle fibroblasts and skeletal myofibers survive chikungunya virus infection and harbor persistent RNA. *PLoS Pathog* 15:e1007993.

Zanini, F., M.L. Robinson, D. Croote, M.K. Sahoo, A.M. Sanz, E. Ortiz-Lasso, L.L. Albornoz, F. Rosso, J.G. Montoya, L. Goo, B.A. Pinsky, S.R. Quake, and S. Einav. 2018. Virus-inclusive single-cell RNA sequencing reveals the molecular signature of progression to severe dengue. *Proc Natl Acad Sci U S A* 115:E12363-E12369.

Zare, F., M. Bokarewa, N. Nenonen, T. Bergstrom, L. Alexopoulou, R.A. Flavell, and A. Tarkowski. 2004. Arthritogenic properties of double-stranded (viral) RNA. *J Immunol* 172:5656-5663.

Zhang, R., A.S. Kim, J.M. Fox, S. Nair, K. Basore, W.B. Klimstra, R. Rimkunas, R.H. Fong, H. Lin, S. Poddar, J.E. Crowe, Jr., B.J. Doranz, D.H. Fremont, and M.S. Diamond. 2018. Mxra8 is a receptor for multiple arthritogenic alphaviruses. *Nature* 557:570-574.